Universidad Autónoma de Madrid

Programa de Doctorado en Biociencias Moleculares

Doctoral Thesis

Role of Hypoxia Inducible Factors in Alveolar Macrophage physiology

Helena María Izquierdo Fernández

Madrid, 2018

Departamento de Bioquímica

Facultad de Medicina

Universidad Autónoma de Madrid

Doctoral Thesis

Role of Hypoxia Inducible Factors in Alveolar Macrophage physiology

Memoria presentada por la Licenciada en Bioquímica:

Helena María Izquierdo Fernández

Para optar al grado de Doctor en Bioquímica, Biología Molecular, Biomedicina y Biotecnología por la Universidad Autónoma de Madrid

Director de tesis: **Dr. David Sancho Madrid**

Este trabajo se ha realizado en el laboratorio de Inmunobiología de la Fundación-Centro Nacional de Investigaciones Cardiovasculares Carlos III (CNIC).

Madrid, 2018

El Doctor David Sancho Madrid, líder del grupo de investigación “Inmunobiología” de la Fundación-Centro Nacional de Investigaciones Cardiovasculares Carlos III (CNIC),

CERTIFICA:

que **Helena María Izquierdo Fernández**, Licenciada en Bioquímica y Máster en Biomedicina Molecular, ambas titulaciones obtenidas por la Universidad Autónoma de Madrid, ha realizado bajo su supervisión el trabajo de Tesis Doctoral: **Role of Hypoxia Inducible Factors in Alveolar Macrophage physiology.**

Para la realización de esta Tesis Doctoral se contó con la financiación de: Beca para la Formación de Personal Investigador (FPI-MICINN, Referencia: BES-2011-044928), del Consejo Europeo de Investigación (ERC-2010-StG 260414), de la Fundación ACTERIA y del Ministerio de Economía y Competitividad (SAF2010-15120, SAF2013-42920R y SAF2016-79040-R).

Revisado el presente trabajo, expresa su conformidad para la presentación del mismo en el Departamento de Bioquímica de la Universidad Autónoma de Madrid, por considerar que reúne los requisitos necesarios para ser sometido a su evaluación ante el tribunal correspondiente para optar al grado de **Doctor en Bioquímica, Biología Molecular, Biomedicina y Biotecnología por la Universidad Autónoma de Madrid.**

Y para que así conste y a los efectos oportunos, firma el presente certificado en Madrid, a 24 de mayo de 2018.

Dr. David Sancho

Director de tesis

A mis padres y a mi hermano

A Agustín

Agradecimientos / Acknowledgements

A todos aquellos que han hecho posible esta tesis:

Gracias a **David Sancho**, por darme la oportunidad de desarrollar mi tesis doctoral en su laboratorio y financiarla hasta el final. Gracias por tu flexibilidad con la estancia, y por estar abierto a las colaboraciones que han permitido que mi trabajo mejore notablemente. Gracias también por impulsar mi proyecto en su fase final. Hacer el doctorado en tu laboratorio me ha obligado a desarrollarme profesionalmente a nivel individual, a dar pasos "sin red" y a superar el vértigo. Además, esta primera experiencia profesional también me ha hecho madurar mucho a nivel personal: he aprendido a perseverar y a defender mis intereses profesionales, manteniendo mis valores. El proceso ha sido arduo, pero confío en que me será útil en el futuro.

Gracias a **todos mis compañeros** del labo, los que siguen y los que cambiaron de etapa, porque lo cierto es que todos, de un modo u otro, y al menos en alguna ocasión, me habéis ayudado. Gracias especialmente a **Elena**, por tu entusiasmo inagotable, tu predisposición y seriedad en el trabajo. Muchas gracias a **Ruth**, por tu gran ayuda los últimos años y por tu capacidad de adaptación a cada uno de nosotros. Trabajar contigo me ha dado la calma que necesitaba en momentos críticos. Ha sido un placer trabajar mano a mano con vosotras, lo he disfrutado mucho. Gracias a mi murcianico **Joaquín**, por hacerme reír tanto chantageándome con las PCRs y los caldericos en Cartagena…muy hábil! Gracias a **Sofía**, por tu gran ayuda con el GSEA, y por las risas y fotos inéditas en el labo a altas horas de la noche. Thank you **Steffi**, for the good chats from time to time, for your experimental help, and for standing my "long breathings" this last time period.

Muchas gracias a todos los que leísteis el paper y la tesis, y me ayudasteis a mejorarlos: gracias por vuestro tiempo y vuestro interés.

Thanks to **Johan Garaude**, for helping me to get the short-stage at Institut Curie: thanks for sharing your ideas and your time with me. The stage gave me the space that I needed to recover my professional self-esteem, which was essential to reset, go back and really develop my PhD.

Gracias a **Candelas Carreiro**, por ayudarme tanto y más en la gestión de la estancia, por tu amabilidad y sabiduría en "cosas de laboratorio". Gracias por compartir tu visión experimentada de las cosas, por escuchar y entender y por tus buenos consejos, que tanto me han ayudado.

Thanks to **Nicolas Manel**, for giving me the opportunity of being in such an excellent lab. Special thanks to my great friend **Silvia Cerboni**, I love you amiga! and also to **Matteo** and **Xavier**. Thanks to all of you for treating me so well in the lab, for the jokes about my "Es-panglish", and for that goodbye party that I will never forget. Thank you to all the other members (Marine, Phillippe, Laurent, Florence, Cecile, Esther, Nicolas, …) because all of you made me feel very comfortable and happy in the lab…it was definitely the best experience of my PhD.

Gracias a **Iria**, por hacer tan divertidos los intratraqueales y dejarme claro, con humor, que no estoy hecha para la costura. Gracias **Francesca** por tu buen humor, que se contagia. Gracias a la gente del animalario: **Iván**, **John**, **Antonio**, por ser siempre tan amables y hacerme la vida más fácil…y a **Rebeca**, por revivirme a tantos ratones y tener tanta paciencia. Gracias a la gente de la cafetería, por vuestra dedicación: **Elena**, por tu amabilidad y templanza, me encanta! a **Ángel**, por meter tanta caña, … Gracias a la gente de citometría: **Elena**, por tu interés y empeño

en el trabajo, siempre con esa calma… ¿cómo lo haces? Y qué conversaciones y risas más buenas! Gracias por escuchar. A **Ligos**, por estar siempre ahí para todo: dudas, compensaciones, y tantos otros líos a deshora. Gracias a **Mariano** y a **Raquel**, por vuestra predisposición a ayudar y por vuestra paciencia. Gracias a **Maria Laura** y a **Olga**, por esas tardes de cotilleos y risas, y las cenitas por el centro, qué buenos ratos hemos pasado! A **Anita**, por ser siempre tan dulce e interesarte por cómo me van las cosas. A **Ángel Álvarez**, por darme tanta seguridad cada vez que hablamos! Gracias a **Pablo Pérez Durán**, por el buen vino y los mejores ratos. Aún no he visto Blade runner…no tengo perdón! Gracias a **Silvia Martín Puig**, por todo el entusiasmo que muestras cada vez que discutimos los datos, por tu curiosidad, que siempre logra motivarme. Thanks to **Martin Guilliams**, for his great work, which definitely inspired mine in a hostile "DC environment" :), thanks for being so open scientifically and help us pushing the story.

Gracias a **Elisa**, por darte cuenta de todo sin necesidad de hablar, por tu entereza y por tantas buenas conversaciones, qué te puedo decir! Me encantas…A **Edgar**, y su "señora" para arriba y para abajo, qué bueno ha sido conocerte, un día menos para la jubilación! A **Ivana**, mi serbia favorita, por ser como eres, por apoyarme tanto y siempre, por tus seguridad y tu firmeza. A mi **Luis**, qué bueno eres! Por hacerme reír constantemente con tus piropos descarados y por los paseos en moto para despejar la cabeza. Gracias a **Magda** y a **Noelia Alonso**, por compartir conmigo vuestra sabiduría, que es mucha. Gracias a **Toñi**, por estar siempre dispuesta a conversar y compartir tu tiempo, por tu sonrisa. A **Carlos López**, gracias por contestar a todos mis emails pidiendo reactivos! gracias por tu generosidad.

Gracias a **Juan Miguel Redondo**, por tu cercanía, y por darme la primera oportunidad de trabajar en el CNIC, y a todo tu grupo de aquel momento, por tantos buenos ratos. Gracias a **Amelia Escolano**, mi primera supervisora oficial, por tu paciencia y firmeza, y por ser un ejemplo inspirador de perseverancia y de lucha individual por un objetivo profesional. Gracias a **Almudena** y a **Laura Grau**, por vuestra actitud afable, contra viento y marea, por resolverme papeletas varias, siempre de buena gana.

Gracias a mis amigos **Lucía**, **Adela** y **Sylvain**, por estar siempre ahí sin condiciones, por animarme cada vez, os quiero. Gracias a **Leyre** y a **Silvia**, las mejores compañeras de piso del mundo, gracias por tantas risas viendo programas que no mencionaré, y por tantos buenos ratos.

Gracias a **mi madre**, por apoyarme siempre en todo lo que he hecho, por confiar plenamente en mi, por tranquilizarme y ocuparte de mí con infinita paciencia. Gracias a **mi padre**, por tu templanza, y por las conversaciones cortas y concisas, como a mí me gustan. Gracias a los dos por ayudarme y quererme tanto, por dármelo todo. Gracias a **mi hermano**, por ser tan pragmático, por escucharme siempre y hacer tantos esfuerzos por mantener el contacto, sé que no lo pongo fácil. Gracias a **mis primas** y a mi **madrina**, por creer que merezco lo mejor y echarme una mano en esta última etapa en la que se ha juntado todo!

Y por último y muy especialmente, gracias a **Agustín**, por tu apoyo incondicional todos estos años, por tu paciencia. Gracias por hacerme ver siempre las cosas desde otro ángulo. Y porque sin ti a mi lado, esta tesis no existiría y nada de esto estaría ocurriendo.

Summary

Summary

The rapid transit from hypoxia to normoxia in the lung that follows the first breath in newborn mice coincides with alveolar macrophage (AM) terminal differentiation. Indeed, *in silico* analysis showed that the expression of genes involved in glycolysis and adaptation to hypoxia is gradually downregulated during AM maturation after birth, suggesting an adaptation to increased oxygen concentrations. However, whether sensing of oxygen fluctuations contributes to post-birth AM maturation and function has not been previously explored. For this purpose, we generated mice whose AMs show a deficient ability to sense oxygen after birth by deleting von Hippel-Lindau (*Vhl*) gene, which codifies for the master negative regulator of hypoxia inducible factors (HIF), under the control of the CD11c promoter (CD11cΔ*Vhl* mice).

VHL-deficient AMs were more glycolytic and showed a decreased oxygen consumption, compared to control WT AMs in steady state. We found that VHL-deficient AMs showed an immature-like phenotype and an altered transcriptional identity. In addition, the absence of VHL impaired AM self-renewal capacity *in vivo*, and also upon growth factor stimulation *ex vivo*. Unlike AMs transplanted from control $Vhl^{fl/fl}$ mice, AMs from CD11cΔ*Vhl* mice did not reverse pulmonary alveolar proteinosis when transplanted into $Csf2rb^{-/-}$ mice, which spontaneously develop lung proteinosis. This result correlated with the increased lipid accumulation found in AMs lacking VHL, which also showed a decreased lipid oxidation capacity.

In order to demonstrate how all these AM features are regulated by HIF, we generated mice with a deletion in *Hif1*α, *Hif2*α or both in addition to the *Vhl* deletion, all under the control of the CD11c promoter. HIF-1 and HIF-2 depletion differentially affected AM phenotypic maturation. However, both isoforms similarly restrain AM self-renewal. HIF-1 was essential for the glycolytic shift in VHL-deficient AMs. Finally, we found that HIF-2 depletion rescued the ability of AMs to remove the surfactant excess *in vivo*, pointing to its specific role regulating lipid metabolism in AMs.

Thus, these results highlight the relevance of HIF regulation for AM maturation and function and contribute to clarify the molecular requirements for the adaptation of AMs to its evolving niche during maturation.

Resumen

Resumen

El nacimiento supone el tránsito desde un ambiente relativamente hipóxico a otro con niveles más elevados de oxígeno en el pulmón, y en ratones, coincide con la última etapa de diferenciación de los macrófagos alveolares (MAs). El análisis de datos computacionales demostró que la expresión de genes implicados en glicolisis y en adaptación a hipoxia disminuye de forma gradual en MAs tras el nacimiento, sugiriendo que éstos se adaptan a concentraciones más altas de oxígeno durante su proceso de maduración. Sin embargo, se desconoce si la detección de fluctuaciones en los niveles de oxígeno contribuye a la maduración y función de MAs tras el nacimiento. Para investigar esta hipótesis, se generó un modelo de ratón con una deleción condicional del gen von Hippel-Lindau (*Vhl*), controlada por el promotor del gen *Cd11c* (ratones CD11cΔ*Vhl*). VHL regula negativamente la estabilidad de los factores de transcripción inducidos por hipoxia (HIF), de modo que este modelo genético nos permitió estudiar la fisiología de MAs con una menor capacidad de detectar el oxígeno tras el nacimiento.

Comparando con MAs control de cepa salvaje (WT, del inglés “wild type”), se encontró que los MAs deficientes en VHL eran más glicolíticos y consumían menos oxígeno en condiciones basales. Además, en ausencia de VHL, los MAs tenían un fenotipo inmaduro y su capacidad proliferativa estaba disminuida, tanto *in vivo*, como bajo condiciones de estimulación *ex vivo*. A nivel funcional, los MAs deficientes en VHL no eran capaces de eliminar el exceso de surfactante presente en los pulmones de ratones *Csf2rb*$^{-/-}$, que desarrollan proteinosis pulmonar espontaneamente. Este resultado correlacionó con la mayor acumulación de lípidos observada en MAs deficientes en VHL, y con su menor capacidad de oxidar lípidos, comparando con MAs WT.

Para demostrar si HIF regulaba las diferencias encontradas en MA deficientes en VHL, se generaron ratones con deleciones condicionales en los genes *Hif1*α, *Hif2*α o ambos, además de la deleción de *Vhl*, todas ellas bajo el control del promotor del gen *Cd11c*. La depleción de HIF-1 y HIF-2 afectó la maduración fenotípica de MAs de forma diferencial. Sin embargo, ambas isoformas disminuían por igual su capacidad proliferativa. A nivel metabólico, HIF-1 era esencial para la inducción de glicolisis en los MAs deficientes en VHL. Finalmente, se encontró que la depleción de HIF-2 restauraba la capacidad de los MAs deficientes en VHL de eliminar el exceso de surfactante *in vivo*, lo que sugiere el papel específico de este factor en la regulación del metabolismo lipídico de los MAs.

En conclusión, estos resultados ponen de manifiesto la relevancia de la regulación de HIF en la adaptación de los MAs al nicho alveolar durante su maduración tras el nacimiento.

Index

Index

AGRADECIMIENTOS / ACKNOWLEDGEMENTS **1**

SUMMARY **5**

RESUMEN **9**

INDEX **13**

LIST OF ABBREVIATIONS **15**

INTRODUCTION **21**

1. Tissue-resident macrophages 21
   1.1. Tissue-resident macrophage ontogeny 21
   1.2. Lung macrophages development and function 22
2. Cellular adaptation to hypoxia 25
   2.1. Hypoxia Inducible Factors (HIF) 25
      2.1.1. Structure 26
      2.1.2. Regulation 27
   2.2. HIF-independent adaptation to hypoxia 29
   2.3. Biological processes regulated by hypoxia and HIFs 29
      2.3.1. Macrophage polarization 29
      2.3.2. Myeloid cell function 30
      2.3.3. Self-renewal and differentiation 31
      2.3.4. Lipid metabolism 32

OBJECTIVES **37**

OBJECTIVOS **41**

MATERIALS AND METHODS **45**

RESULTS **55**

1. Postnatal alveolar macrophage (AMs) maturation correlates with decreased hypoxia and glycolysis. 55
   1.1. The expression of gene sets related to hypoxia and glycolysis are gradually downregulated during AM maturation. 55
   1.2. Expression of HIF-target genes is downregulated during AM maturation. 56
2. The absence of VHL alters AM metabolism and phenotype 59
   2.1. Genetic characterization of *Vhl* deletion in AMs. 59
   2.2. Metabolic characterization of VHL-deficient AMs. 60
   2.3. VHL-deficient AMs resemble immature cells. 61
   2.4. VHL-deficient AMs show an altered transcriptional identity. 63
   2.5. VHL-deficient AM phenotype is intrinsic. 66

Index

3. VHL is required to sustain AM physiological functions under steady-state. 70
3.1. Identification of AM functions altered in the absence of VHL under basal conditions. 70
3.2. AM self-renewal requires VHL. 72
3.3. VHL contributes to AM surfactant handling capacity. 75
4. HIF-1 and HIF-2 transcription factors differentially contribute to AM function in the absence of VHL. 79
4.1. Genetic characterization of *Vhl*, *Hif1α* and *Hif2α* deletion in AMs. 79
4.2. HIF-1 and HIF-2 control the metabolic profile of VHL-deficient AMs. 81
4.3. Deletion of both HIF-1 and HIF-2 is required to restore mature phenotype and self-renewal potential in VHL-deficient AMs. 82
4.4. HIF-2 mediates the impairment in surfactant removal by VHL-deficient AM. 87

DISCUSSION 91

1. AMs transcriptionally adapt to increased oxygen concentrations early after birth. 91
2. HIF-1 drives VHL-deficient AM switch towards glycolysis. 92
3. VHL/HIF axis regulates AM terminal maturation. 93
4. HIF regulation by VHL is required for AM self-renewal. 94
5. HIF-2 decreases AM capacity to remove lung surfactant. 96

CONCLUSIONS 101

CONCLUSIONES 105

BIBLIOGRAPHY 109

APPENDIX 119

List of abbreviations

Abbreviation	Full name
Abcg1	ATP-binding cassette sub-family G member 1
Acsl1	Acyl-CoA synthetase long chain family member1
Acsl1	Long-chain-fatty-acid-CoA ligase1
Adrp	Adipose differentiation-related protein
AEC	Alveolar epithelial cell
AM	Alveolar macrophage
Apo	Apolipoprotein
Arg1	Arginase 1
ATP	Adenosin triphosphate
BAL	Bronchoalveolar lavage
BCA	Bicinchoninic acid assay
bHLH-PAS domain	Basic helix-loop-helix-Per-Arnt-Sim domain
BM	Bone Marrow
Brca	Breast cancer protein
BrdU	Bromodeoxyuridine
BRR	Basal respiration rate
C-TAD	C-terminal transactivatioin domain
Car4	Carbonic Anhydrase 4
CBP	CREB binding protein
Cbr2	Carbonyl reductase (NADPH)2
CCCP	carbonyl cyanide m-chlorophenylhydrazone
ccRCC	Clear cell renal cell carcinoma
CD36	Cluster of differentiation 36
CDK	Cyclin-dependent kinase
CEBP	CCAAT/enhancer-binding proteins
Chek	Serine/Threonine kinase Chk1
Cidec	Cell death-inducing DFFA-like effector c
CPT1	Carnitine palmitoyltransferase I
Cx43	Connexin 43
CXCR4	C-X-C chemokine receptor type 4
DOB	Date of birth
ECAR	Extracellular acidification rate
EGFR	Epidermal growth factor receptor

List of abbreviations

Epcam	Epithelial cell adhesion molecule
EPO	Erythropoietin
ER	Endoplasmic reticulum
FA	Fatty acid synthase
Fabp	Fatty acid-binding protein
FAO	Fatty acid oxidation
Fasn	Fatty acid synthase
FBS	Fetal bovine serum
Fcgr1a	Fc fragment of IgG receptor Ia
FDR	False discovery rate
GATA6	GATA-binding protein 6
GLUT	Glucos transporter
GM-CSF	Granulocyte-Macrophage colony-stimulating factor
GSEA	Gene set enrichment analysis
HEPES	4-(2-hydroxyethyl)-1-piperazineethanesulfonic acid
HIF	Hypoxia inducible factor
Hig2	Hypoxia inducible protein 2
HK	Hexokinase
HRE	Hypoxia-response element
HSC	Hematopoietic stem cell
Hsp	Heat shock protein
IFNγ	Interferon gamma
IL	Interleukin
iNOS	indubible nitric oxide synthase
IPAS domain	Inhibitory Pern-Arnt-Sim domain
iTreg	inducible T regulatory cell
LCAD	Long-chain acyl-CoA dehydrogenase
LD	Lipid droplet
LDHA	Lactate dehydrogease A
LPS	Lipopolysacharide
LXR	Liver X receptor
LysM	Lysozyme M
M-CSF	Macrophage colony-stimulating factor
MAPKs	Mitogen-activated protein kinase
MCAD	Medium-chain acyl-CoA dehydrogenase
MCM DNA helicase	Minichromosome DNA helicase

List of abbreviations

MCP-1	Monocyte chemoattractant protein 1
mETC	Mitochondrial electron transport chain
MMP	Matrix metaloproteinase
MPS	Mononuclear phagocyte system
Msi2	Musashi RNA binding protein 2
MSigDB	Molecular signature database
mTOR	Mammalian target of rapamycin
mTORC1	Mammalian target of rapamycin complex 1
N-TAD	N-terminal transactivation domain
NES	Normalized enrichment score
NF-kB	Nuclear factor kappa-light-chain-enhancer of activated B cells
NO	Nitric oxide
NSC	Neural stem cell
Nsmaf	Neutral sphingomyelinase activation associated factor
OCR	Oxygen consumption rate
ODDD	oxygen-dependent degradation domain
OXPHOS	Oxidative phosphorylation
P2ry2	P2Y purinoceptor 2
PAP	Pulmonary alveolar proteinosis
PBS	Phosphate-buffered saline
PDGF	Platelet-derived growth factor
Pdk1	Pyruvate dehydrogease kinase 1
PFA	Paraformaldehyde
Pfk1	Phosphofructokinase 1
PHD	Prolyl hydroxylase domain
PLK	Polo-like kinase
Pltp	Phospholipid transfer protein
PMT	Pulmonary macrophage transplantation
PPAR	Peroxisome proliferator activated receptor
RACK1	Receptor of activated protein C kinase 1
RALDH	Retinaldehyde dehydrogenase
REDD1	Protein regulated in development and DNA damage response 1
RMPI	Roswell Park Memorial Institute medium
ROS	Reactive oxygen species
RXR	Retinoid X receptor
Siglec	Sialic acid binding Ig like lectin

List of abbreviations

SP-D	Surfactant protein D
Spp1	Secreted phosphoprotein 1
Srebf1	Sterol regulatory element-binding transcription factor 1
STAT5	Signal transducer and activator of transcription 5
TGF-α	Transforming growth factor alpha
TGF-β	Transforming growth factor beta
TGFβ2	Transforming growth factor beta 2
TLR	Toll-like receptor
TNF-α	Tumor necrosis factor alpha
TSC1/TSC2	Tuberous sclerosis complex 1/2
VCAM1	Vascular cell adhesion molecule 1
VEGF	Vascular endothelial growth factor
VHL	Von Hippel-Lindau

Introduction

Introduction

1. Tissue-resident macrophages

1.1. Tissue-resident macrophage ontogeny

Macrophages are hematopoietic cells of the myeloid lineage that are specialized in phagocytosis and play a central role in both tissue homeostasis and inflammation (*1*).

For years, it was believed that tissue-resident macrophages are constantly repopulated by monocytes from blood, which arose from progenitors in the adult bone marrow (BM). This dogma, named mononuclear phagocyte system (MPS), was stablished based on studies tracing the differentiation of radiolabeled monocytes in mice with inflammation and thus describes the contribution of monocytes to inflammatory macrophages that accumulate in injured tissues. According to this system, macrophages are fully differentiated cells that have lost proliferative potential and are constantly repopulated (*2*). However, recent studies have suggested that the prevailing monocyte-to macrophage dogma did not apply to all adult macrophage populations. Experiments in parabiotic mice that share blood circulation leading to the mix of circulating precursors revealed that although monocytes were substantially mixed in these mice, Langerhans cells (*3*), microglia (*4, 5*), and alveolar macrophages (*5-7*) do not or hardly mix, whereas macrophage population in the gut, dermis, and heart show some degree of mixing, suggesting some contribution from BM-monocyte-derived cells (*8-11*). In addition, by using a CX3CR1 promoter-driven Cre recombinase expression to fate-map the murine monocyte and macrophage compartment, it was confirmed that most tissue-resident macrophage populations, including microglia, liver Kupfer cells, lung alveolar macrophages and splenic macrophages are established prior to birth and subsequently maintained by self-renewal independently of replenishment by blood monocytes during adulthood (*12*). Altogether, these studies have revealed that the homeostatic contribution of circulating monocytes to macrophage populations is restricted to a few specific tissues, while many tissue-resident macrophages arise form embryonic precursors that take residence in tissues prior to birth and self-maintain locally throughout adulthood.

Regarding their function, tissue-resident macrophages play important homeostatic roles depending on their locations. Microglia, the brain-resident macrophages, prune synapses during development (*13*) (*14*). Peritoneal cavity macrophages regulate the production of gut immunoglobulin (Ig) A by interacting with peritoneal B1 cells (*15*) and lung AMs remove and degrade surfactant produced by lung epithelial cells (*16*).

Several studies have identified the intrinsic factors that determine myeloid cell identity. Transcription factor PU.1 binds throughout the genome to both promoter and enhancer regions (*17*). Other transcription factors such as CCAAT/enhancer-binding proteins (CEBP) also

participate in myeloid cell differentiation and act together with PU.1 (*18*). In addition, the binding motif of MAF transcription factor family is enriched in most tissue-resident macrophage enhancers compared with monocytes and neutrophils (*19*). MAF and MAFB are important for macrophage terminal differentiation, and macrophages lacking these transcription factors are immortalized and proliferate indefinitely in the presence of macrophage colony-stimulating factor (M-CSF) (*20, 21*).

Notably, tissue-resident macrophages share expression of only a few unique transcripts, with most of the transcriptional program being specific to the tissue of residence (*19*). Thus, in addition to intrinsic factors determined by ontogenic cues, environmental signals also contribute to shaping macrophage transcriptional regulation. Therefore, macrophages residing in organs differentially express tissue-specific transcription factors. Transcription factor GATA-binding protein 6 (GATA6) in peritoneal cavity macrophages is induced by retinoic acid, promoting macrophage self-renewal and the production of transforming growth factor beta 2 (TGF**β**2). In turn, TGF**β**2 drives IgA production by peritoneal B-1 cell class. In alveolar macrophages, peroxisome proliferator-activated receptor-gamma (PPARγ) is induced by granulocyte-macrophage colony-stimulating factor (GM-CSF) produced by lung epithelium and is essential for the correct development and maturation of this population (*22*). Finally, senescent erythrocytes containing high levels of haem, are phagocytosed by red pulp macrophages in the spleen, and both M-CSF and haem induced the expression of SPI-C, a transcription factor essential for cell maintenance that also drives the expression of key red pulp macrophage genes, such as vascular adhesion molecule 1 (VCAM1) (*23*). Since most gene promoters are shared between distinct tissue-resident macrophage, open enhancer regions differ among tissue macrophages due to the collaboration of all these tissue-induced specific factors together with PU.1, to bind enhancers and remodel chromatin in a tissue-specific manner (*19, 24*). In conclusion, tissue-specific transcription factors are triggered in macrophages by tissue-specific signals that then contribute to their functional specialization.

1.2. Lung macrophages development and function

Mainly two types of macrophages can be found in the lung in the steady state: AMs, constituting the 90-95% of the cellular content found in the air space of the alveoli, and interstitial macrophages (iMs), a small population located in the parenchymal space, between adjacent alveoli. Regarding development, knowledge about the iM population ontogeny is scarce, while several studies on AMs origin have unveiled many of their developmental cues. Initial lung development occurs in a relatively hypoxic environment beginning in mice on embryonic day 9 (E9) (*25*). Fetal monocytes colonize the developing lung around E16.5 and E18.5 (Figure I1A) and only differentiate into mature AMs after birth (*6*) (Figure I1B).

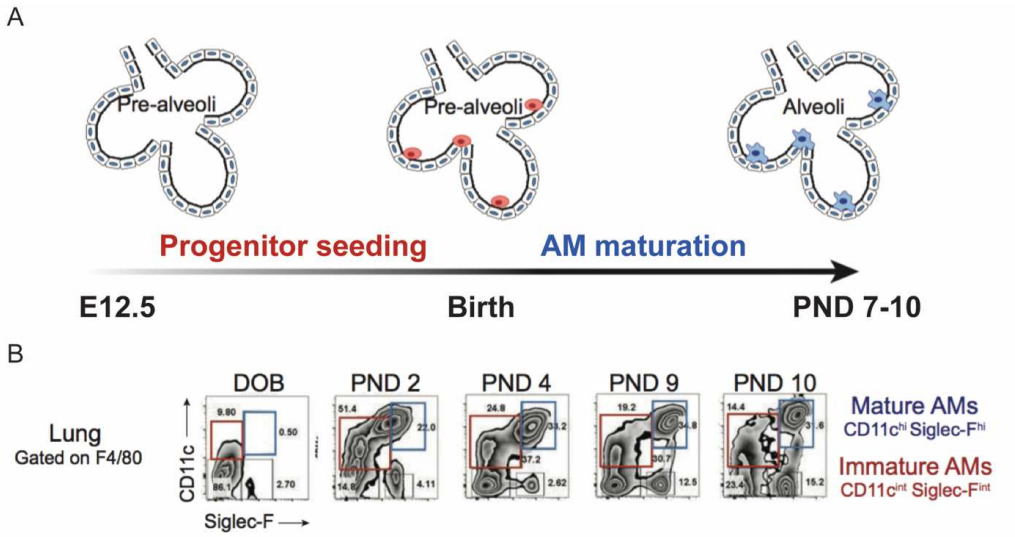

Figure I1. Schematic representation of AM developmental kinetics. (A) During embryogenesis, fetal monocytes generated in the fetal liver around embryonic day (E)12 migrate to and colonize the lung around E16.5. Upon birth, fetal monocyte progenitors differentiate towards mature AMs. (B) Flow cytometry plots showing the differentiation stages towards mature AMs during the first week of life. Upon birth, fetal monocyte progenitors successively increase their expression of the maturation-associated markers CD11c and Siglec-F (depicted) and F4/80 and CD64 (not depicted). Cells represented in plots are gated as alive, $CD45^+$, $F4/80^+$ lung cells. Red squares indicate immature AMs (pre-AMs); blue squares gate $CD11c^{hi}$ $Siglec\text{-}F^{hi}$ fully mature AMs. Fully mature AM population is absent at day of birth (DOB) and it is completely established between PND6 and PND9. PND, postnatal day.

Lung epithelial cell-derived GM-CSF is essential for the early commitment of AM precursors in the postnatal lung (*6, 22*). GM-CSF signaling induces the transcription factors PU.1 (*26*), PPARγ (*22*) and mTOR (*27*), being all these factors required for AM development. Notably, additional factors are required for AM functional maturation independently of GM-CSF, including the transcriptional repressor Bach2 (*28*) and TGF-β (*29*) (Figure I2).

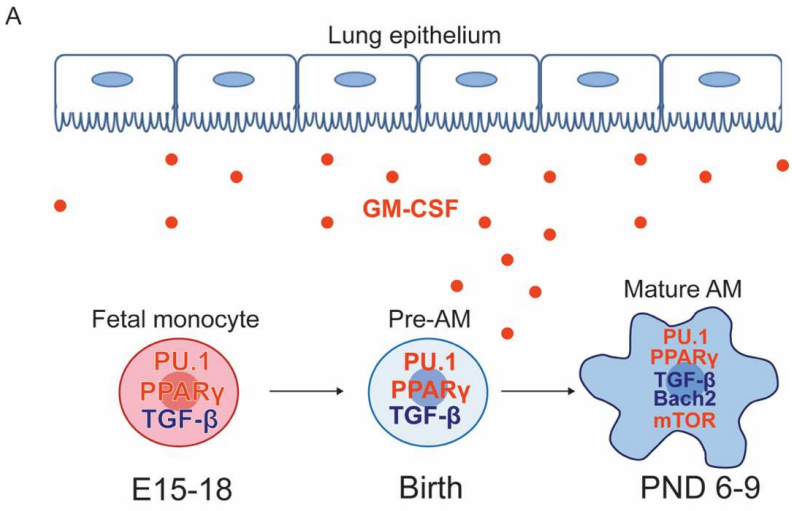

Figure I2. Factors required for AM development and maturation. (A) GM-CSF is required during all stages of AM maturation and for AM maintenance in adulthood. GM-CSF produced by lung epithelium instructs fetal monocyte differentiation shortly before and is induced early after birth. Activation of transcription factors PPARγ and PU.1 downstream GM-CSF and autocrine TGF-β, leads to the first commitment of progenitors into pre-AMs. Pre-AMs differentiate into fully mature AMs during the first week of life. After birth, mTOR signaling is required to maintain the mature AM population constant and together with Bach2 and TGF-β, are essential for the functional maturation of AMs. Red factors: downstream GM-CSF; dark blue factors: GM-CSF-independent factors.

One important feature of mature AMs is their high capacity to self-maintain by local proliferation (*30*), with little contribution to the repopulation of the alveolar niche by blood circulating monocytes in steady-state (*6, 31*). The factors regulating AM self-renewal ability are a focus of current research (*32-34*), being mTOR and Sirtuin 1 recently identified as essential to sustain AM proliferation (*32-34*).

Regarding their function, AMs have fundamental roles in maintaining tissue homeostasis and resolving inflammation. AMs suppress immune responses through the inhibition of DC-mediated activation of T cells and production of TGF-β (*35, 36*). RALDH1 and 2 are also produced by AMs, and are the rate limiting enzymes for the synthesis of the bioactive form of retinoic acid from vitamin A (retinol). Together with TGF-β, retinol induces the generation of $Foxp3^+$ inducible T regulatory (iTreg) cells from naïve $CD4^+$T cells, which was essential to induce tolerance to inhaled innocuous antigens (*37*). AMs are able to prevent pathological lung inflammation via the intercommunication of AMs with alveolar epithelium. Interaction of CD200L ligand expressed by alveolar epithelial cells (AECs) with its receptor CD200R on AMs negatively regulates inflammatory responses mediated by TLR stimulation (*38*). In addition, communication through gap junctions between sessile AMs and AECs mediated by connexin Cx43 hemichannels, was found to inhibit LPS-mediated lung inflammation (*39*).

Little has been explored about which is the combination of tissue-derived signals that lead to the tolerogenic phenotype acquired by mature AMs. In this regard, a recent report has shown that IL-33 is produced by lung epithelial cells upon first breath. IL-33 in turn, leads to IL-13 secretion by type 2 innate lymphoid cells, which contributes to AM polarization to an anti-inflammatory phenotype (*40*).

Another important function of mature AMs is their capacity to degrade surfactant (*22, 41-44*). Surfactant is produced and recycled by lung epithelium and is composed mainly by phospholipids and proteins. Lung surfactant is essential to reduce surface tension at the interface of the alveolus, thus avoiding lung collapse while breathing. Therefore, regulation of surfactant concentration in the lung is crucial for lung homeostasis. In agreement, the lack of functionally mature AMs can lead to pulmonary alveolar proteinosis (PAP), a pathology characterized by the accumulation of surfactant (*45*). In humans, mutations affecting GM-CSF signaling are associated to the development of proteinosis and current treatments consist of repeated bronchoalveolar lavage of patients for life. For this reason, alternative cellular therapies are under current research (*46, 47*). Proteinosis is reproduced in mice lacking GM-CSF ($Csf2^{-/-}$ mice) and GM-CSF receptor ($Csf2r^{-/-}$ mice) (*41, 42*). Accordingly, the absence of downstream transcription factors PU.1 (*26*), PPARγ (*22, 43, 44*) and mTOR (*27*) in mouse AMs, also leads to proteinosis. All the above mouse models of proteinosis harbor a minority of foamy immature AMs that accumulates lipids intracellularly, arguing that correct lipid metabolism is essential for AM maturation. In agreement, *Bach2*-deficient mice also develop severe proteinosis without apparently affecting AM development (*28*). More recently, it has been reported that disrupting TGF-β autocrine sensing by AMs leads to defects in PPAR*γ* activation and the formation of foam-like cells present in BAL in a GM-CSF-independent manner (*29*).

2. Cellular adaptation to hypoxia

2.1. Hypoxia Inducible Factors (HIF)

Physiological tissue oxygen tensions are significantly lower than ambient oxygen tensions (*48*). Oxygen gradients play an important role in mammalian physiology: low oxygen or hypoxia provides the required extracellular stimulus for proper embryogenesis (*49*) and maintains the pluripotency of several types of stem cells (*50*). In contrast, high altitude or localized ischemia caused by the disruption of blood flow into a given area can lead to pathological hypoxia. In addition, most solid tumors contain hypoxic regions because of the severe structural abnormality of tumor micro-vessels (*51*). In order to adapt to such varied contexts, the best-documented response to low oxygen levels is the induction of hypoxia-inducible factors (HIFs). HIFs are heterodimers of a constitutively expressed β subunit (HIFβ or ARNT) and an oxygen-sensitive subunit (1α, 2α or 3α) (Figure I3), thus conforming HIF-1, HIF-2 (also known as endothelial PAS

domain protein 1, EPAS-1) and HIF-3, respectively. Once stabilized, they induce the expression of several genes that mediate the cellular and systemic adaptation to reduced oxygen availability.

2.1.1. Structure

HIF factors belong to the basic helix-loop-helix-Per-ARNT-Sim (bHLH-PAS) protein family. The bHLH motif is required for DNA binding while PAS motif enables heterodimer formation between HIF-α and HIF-β subunits. Two transactivation domains, N-terminal (N-TAD) and C-terminal (C-TAD), are located in the C-terminal half of the HIF-1α and HIF-2α subunits. HIF-α subunits also contain an oxygen-dependent degradation domain (ODDD) that mediates oxygen-regulated stability (*52*) (Figure I3A). N-TAD overlaps with the ODDD, and thus, its transcriptional activity is coupled with HIF stability. In contrast, regulation of C-TAD activity is connected with the hydroxylation of a conserved asparagine residue, which impairs the association of C-TAD and coactivators CBP/p300.

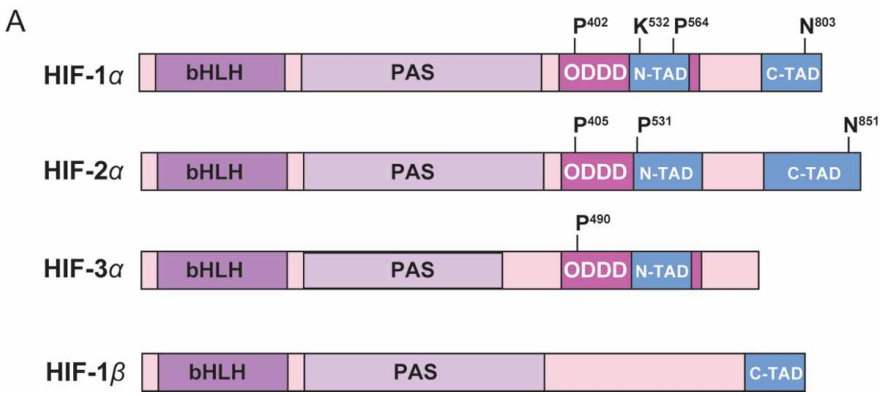

Figure I3. Domain structure of HIF-α subunits and HIF-1β. (A) HIF-α contains an ODDD that mediates oxygen-regulated stability through the hydroxylation of two proline (P) residues and the acetylation of a lysine (K). The proline residues are conserved in HIF-1α, HIF-2α and HIF-3α. HIF-1α and HIF-2α bear two transactivation domains (C-TAD and N-TAD), whereas HIF-1β has only one TAD.

Regarding their expression, HIF-1α and HIF-1β mRNA are ubiquitously expressed, while HIF-2α mRNA expression seems to be more restricted, and has been found highly expressed in vascular tissues such as lung, heart, placenta and kidney (*53, 54*). HIF-3α is very similar to HIF-1α and HIF-2α in the bHLH and PAS domains but lacks the C-TAD domain. This α subunit has multiple splice variants, being the most studied the inhibitory PAS domain protein (IPAS), which acts as a dominant negative inhibitor of HIF-1α (*55*).

2.1.2. Regulation

Under normoxic conditions, the α subunits are hydroxylated by three specific prolyl hydroxylase paralogues (PHDs 1-3) at two conserved proline residues located in the ODD domain. This reaction requires oxygen, 2-oxoglutarate, ascorbate and iron as a cofactor. HIF-α hydroxylation facilitates binding of von Hippel-Lindau protein (VHL), which forms the substrate recognition module of an E3 ubiquitin ligase complex comprising elongin C, elongin B, cullin-2 and ring-box 1. The VHL/E3 ubiquitin ligase complex recognizes hydroxylated HIF-α subunits and directs their polyubiquitylation, which targets them for proteasomal degradation (Figure I4A). When oxygen concentration drops, PHD activity is inhibited and VHL binding abrogated. Thus, HIF-α subunits are stabilized and enter the nucleus, where they heterodimerize with HIFβ and coactivators. The protein complex then binds to a conserved DNA sequence known as the hypoxia responsive element (HRE), and transactivate a variety of hypoxia-responsive genes involved in angiogenesis, erythropoiesis, autophagy and energy metabolism (Figure I4B) (*48*). Another layer of HIF regulation is exerted by the factor inhibiting HIF 1 (FIH1), an iron- and 2-oxoglutarate-dependent dioxygenase that in the presence of oxygen hydroxylates HIF-1α and HIF-2α CTADs at a conserved asparaginyl residue, preventing the recruitment of the coactivators p300 and CBP (*56, 57*).

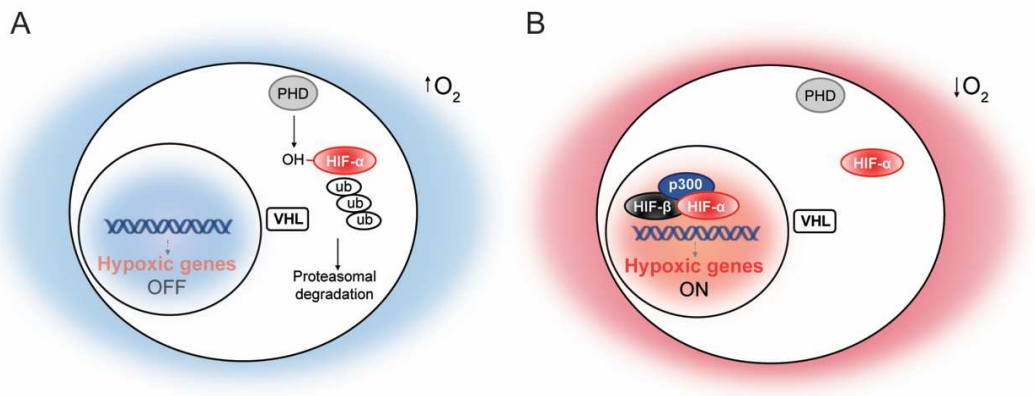

Figure I4. Cellular regulation of HIF activity. (A) In normoxia, PHD enzymes become active upon oxygen binding and hydroxylate HIF-α. This hydroxylation allows their recognition by VHL protein, which leads to their ubiquitination and proteasomal degradation. (B) Under hypoxic conditions, PHD enzymes are inactive due to the lack of oxygen and HIF-α is not degraded. In turn, it translocates into the nucleus, where it binds to HIF-β and coactivators such as p300. The protein complex induces the expression of genes implicated in cellular adaptation to low concentrations of oxygen.

VHL is a tumor suppressor protein, and its mutation leads to the so-called von Hippel-Lindau syndrome, a hereditary, autosomal-dominant disease associated with retinal

angiomatosis, cerebellar spinal haemangioblastomas and various tumor types, including clear-cell renal cell carcinoma (ccRCC) and pancreatic neuroendocrine tumors, among others. Besides HIF transcription factors, VHL has other potential ubiquitination substrates, such as atypical protein kinase C (*58*) and large subunit of RNA polymerase II (*59*). However, the best-characterized VHL functions are those dependent on HIF. HIF proteins regulate angiogenesis and glucose uptake via VEGF and PDGF production, and glucose import and metabolism, through regulation of GLUT1, GLUT3, HK2 and LDHA levels. HIF factors also regulate chemotaxis and cell survival through the modulation of CXCR4 and TGF-α and EGFR expression, respectively. HIF also regulates the expression of E-cadherin and matrix metalloproteinases (MMPs), implicated in the assembly of the extracellular matrix. Finally, HIF can also regulate p53 and NF-kB activity, and adipose differentiation (*60*).

Notably, there are other oxygen-dependent modulators of HIF-α subunits besides VHL. Hypoxia-associated factor (HAF) causes HIF-1α ubiquitylation and degradation, but promotes HIF-2α transactivation under prolonged hypoxia (*61*). The heat-shock protein 70/carboxyl terminus of Hsp70-interacting protein (Hsp70/CHIP) complex degrades HIF-1α but not HIF-2α under prolonged hypoxia or under high glucose conditions (*62*). Moreover, there are also several oxygen-independent HIF regulatory pathways, such as activated protein kinase C (RACK1), which competes with heat shock protein (Hsp)90 for binding to HIF-1α and thus promotes its degradation (*63*) and human double minute 2 (Hdm2), which induces HIF-1α proteasomal degradation through p53-HIF-1α interaction (*64*). In an immune context, HIF stabilization can be promoted by inflammatory stimuli independently of oxygen concentration. The proinflammatory cytokines TNF-α and IL-1β promote HIF-1α stabilization and accumulation in an NF-κB-dependent manner and bacterial products, such as LPS, can also stabilize HIF-1α under normoxia through multiple pathways, including NF-κB, ROS, PHDs and MAPKs (*65*).

Finally, another level of regulation of HIF stabilization relies on their expression kinetics; despite their similar protein structures, HIF-1 and HIF-2 have non-redundant roles and distinct target genes and mechanisms of regulation. In some cell lines, HIF-1 is more active during short periods (2-24h) of intense hypoxia or anoxia (<5% O2), and continues to be active even after 48-72h of hypoxia (*66*). In contrast, during chronic hypoxic exposure, HIF-2 plays the major role in driving the hypoxic response (*61*). This differential HIF activity suggests that HIF-1 and HIF-2 play divergent but complementary roles in tissues under physiological and pathophysiological hypoxia.

2.2. HIF-independent adaptation to hypoxia

Hypoxic responses can also be HIF-independent. Hypoxia suppresses mTOR activity independently of HIF signaling, via the mTOR inhibitor REDD1 and the TSC1/TSC2 complex (*67*). Other hypoxia-responsive pathways include endoplasmic reticulum (ER) stress and NF-κB pathways (*68*).

2.3. Biological processes regulated by hypoxia and HIFs

Virtually in every cell type, the immediate response to low oxygen concentrations consists on suppressing ATP consumption by arresting protein translation and ion channel activity, two major ATP sinks under normoxia. Consecutively, hypoxia-responsive gene expression increases dramatically, including genes involved in glucose transport, glycolysis, erythropoiesis, angiogenesis, vasodilation, and respiratory rate (*69*). These changes in gene expression profile, function to minimize the effects caused by low oxygen at cellular, tissue and systemic levels.

2.3.1. Macrophage polarization

The transcription factor HIF-1 promotes the switch to glycolysis, ensuring that cells exposed to hypoxia can continue to produce ATP. In this context of anaerobic glycolysis, pyruvate does not feed TCA cycle to boost subsequent oxidative phosphorylation (OXPHOS) but is instead metabolized to lactate. HIF-1 facilitates this metabolic switch by inducing the expression of genes codifying for glucose transporter GLUT1 (*Slc2a1*) (*70*) to increase glucose uptake, and genes involved in the glycolytic pathway, such as phosphofructokinase 1 (*Pfk1*) and lactate dehydrogenase A (*Ldha*) (*71-73*). In addition, HIF-1 induces the expression of pyruvate dehydrogenase kinase 1 (*Pdk1*) (*74, 75*). PDK1 inhibits pyruvate dehydrogenase, the enzyme that catalyzes the formation of acetyl-CoA from pyruvate, thus restraining mitochondrial respiration and the associated oxygen consumption.

Metabolic reprogramming can determine macrophage response to microbial stimuli. LPS-treated macrophages acquire a pro-inflammatory or “M1” phenotype characterized by a robust metabolic shift towards glycolysis, pentose-phosphate activity and basal oxidative phosphorylation. In contrast, immunomodulatory or “M2” macrophages show moderate glycolysis but higher oxidative activity. Regarding the function of HIF in macrophage polarization, HIF-2 induction of arginase 1 (*Arg1*) in macrophages contributes to IL-4-induced M2 polarization (*76*), suggesting that HIF-2 might outcompete HIF-1, limiting the glycolytic shift associated to M1 polarization and promoting thus, differentiation towards M2. Notably, HIF-1 can also drive immunosuppressive functions by myeloid cells, through the induction of inducible (i)NO synthase (*Nos2*) expression (*77*). Moreover, macrophages lacking HIF-2 fail to mount an inflammatory response upon LPS challenge (*78*), which suggests that different functions of the HIF isoforms on macrophage polarization are not necessarily exclusive and can overlap depending on the

physiological context. However, it is still unclear whether metabolic adaptation is the cause or consequence of the myeloid cellular differentiation program, both in steady state and under inflammatory conditions.

2.3.2. Myeloid cell function

Several genetically-modified mice have been employed to study the role of HIF in myeloid cells. Tie-2-Cre *Hif-1α*$^{fl/fl}$ mice, which lack *Hif1α* in endothelial cells and hematopoietic precursors, have been used to demonstrate the role of HIF-1 in GM-CSF-BM-derived DC maturation and dependent activation of the adaptive immune response (*79*). Lysozyme M–driven Cre was used to target *Hif1α* in myeloid lineage cells (LysM-Cre *Hif1α*$^{fl/fl}$). In combination with Tie-2-Cre *Hif-1α*$^{fl/fl}$ and Tie-2-Cre *Hif-2α*$^{fl/f}$ mice, these mouse models have helped to dissect the roles of HIF-1 and HIF-2, promoting and preventing eosinophil chemotaxis, respectively (*80*). Furthermore, the essential role of HIF-1 in the myeloid compartment for the development of airway hyperresponsiveness in an OVA model of asthma was demonstrated in LysM-Cre *Hif1α*$^{fl/fl}$ mice (*80*).

While monocyte and neutrophil development and differentiation are not affected by specific deletion of *Hif1α* in the myeloid lineage in steady state, macrophages lacking HIF-1 showed impaired aggregation, invasion and motility (*81*). *In vivo*, mice with *Hif1α* myeloid-specific deletion showed impaired inflammatory responses in rheumatoid arthritis synovial tissue and several models of skin inflammation, correlating with a lower glycolytic rate and ATP production, and indicating that HIF-1 contributes to inflammation (*81*). HIF-2 is also relevant for the pro-inflammatory functions of immune cells. Mice lacking HIF-2 in the myeloid compartment fail to mount an inflammatory response upon LPS challenge, due to an impaired TNF-α, IFNg, IL-12 and IL-1B production. In contrast, HIF-2 does not regulate either nitric oxide (NO) production or alter the expression of activation markers by macrophages (*78*).

Analysis of the bactericidal capacities of phagocytes in LysM-Cre *Hif1α*$^{fl/fl}$ mice have unveiled a major role for HIF-1 in the killing of Gram-positive and Gram-negative bacteria (*77, 81*). In an Influenza virus infection model, LysM-Cre *Hif1α*$^{fl/wt}$ mice showed an increased survival that correlated with a significant decrease in neutrophil recruitment into the lung (*82*). Finally, during *Leishmania* infection, mice with a targeted depletion of HIF-1 in CD11c^{+} cells had a significantly lower splenic parasite burden, suggesting that HIF-1 can act as an immune evasive mechanism adopted by the parasites to establish persistent infections (*83*).

In contrast, to evaluate the effects of HIF stabilization, PHD3-deficient mice have been used. In these mice, the activity of HIF positively correlated with an improved neutrophil survival under hypoxia or inflammatory conditions(*84, 85*). LysM-Cre *Vhl*$^{fl/fl}$ mice were used to

demonstrate that HIF stabilization increased the maturation, phagocytic and bactericidal capacity of BM-derived macrophages (*77*). Finally, *in vivo*, LysM-Cre *Vhl*$^{fl/fl}$ mice showed a hyperinflammatory response in a phorbol ester-induced ear inflammation model (*81*), supporting the role of HIF driving inflammatory processes.

2.3.3. Self-renewal and differentiation

One property shared by tissue-resident macrophages and stem cells is their capacity to self-renew. The relevance of this process in tissue-resident macrophages is that it allows the maintainance of their population constant, minimizing the contribution of monocytes that could potentially add functional variations to the resident population (*86*). In the case of stem cells, the rate of self-renewal versus multi-potent differentiation defines their potential to replenish ageing mature cells and perpetuate themselves. Interestingly, hematopoietic stem cells (HSC) and adult tissue stem cells generally reside in specialized microenvironments, where specific local conditions might influence their quiescence, characterized by the preservation of their self-renewal potential. In this regard, experimental evidence indicates that hypoxia contributes to the maintenance of an stem cell undifferentiated state, rather than their cell-fate commitment (*87*). In fact, several studies show that HSCs exhibit hypoxic status, express high levels of HIF-1 (*88*) and rely on anaerobic glycolysis rather than mitochondrial OXPHOS to support their energy demands (*89*). These observations suggest that they need to limit mitochondrial respiration to remain in a quiescent state (*90, 91*). In agreement, HIF-1 depletion in HSCs leads to their exhaustion, correlating with a decreased glycolysis and increased mitochondrial potential (*90*). On its side, HIF-2 is implicated in protecting HSCs from endoplasmic reticulum (ER) stress-induced apoptosis (*92*). Similarly, in adult stem cells, ROS derived from mitochondrial activity in normoxia primes them for differentiation (*93, 94*). Thus, hypoxia seems to preserve the pluripotent and undifferentiated state of stem cells. However, the effect of low oxygen concentration on stem cell proliferative potential is more controversial. Hypoxia can mediate low cell-cycle activity in HSCs, increasing the proportion of long-term HSCs *in vitro* (*95*). In addition, HIF-1 depletion can rescue defects in HSC quiescence (*96*). In contrast, hypoxia enhances proliferation of human neural stem cells (*97*) and HIF-target genes VEGF and EPO stimulates neurogenesis and production of neural progenitors in forebrain, respectively (*98*).

Interestingly, a recent report has shown that the gene network controlling self-renewal is shared by proliferating resident macrophages and embryonic stem cells, demonstrating that the differential regulation of this network in each cell type relies on its association with specific enhancers (*32*). Whether the metabolic status of tissue-resident macrophages imprinted by their niche can regulate the activity of those enhancers and thus contribute to the maintenance of their proliferative potential remains unknown.

2.3.4. Lipid metabolism

Several reports link hypoxia with the formation of foam cells, being described HIF-1 as the main driver in the process. Human macrophages became triglyceride-loaded foam cells under hypoxia *in vitro* (*99, 100*). Hypoxia, through HIF-1 stabilization, has been linked with an increased lipid transport through the induction of expression of lipid transporters such as CD36 (*101*). Several studies have proved evidence of a HIF-mediated accumulation of lipids in cancer cells. For example, hypoxia promoted increased fatty acid (FA) synthesis by inducing Sterol Regulatory element-binding transcription factor 1 (*Srebf1*) and FA synthase (*Fasn*) expression in a HIF-1-dependent manner (*102*). HIF-1 was shown to directly regulate phosphatidate phosphatase isoform 1 (Lipin1), essential for triglyceride biosynthesis, and hypoxia-inducible protein 2 (Hig2), which promotes lipid droplet accumulation on membranes (*103, 104*). In a model of glioblastoma tumor treated with anti-angiogenic therapy, tumors that had grown through early growth arrest, showed an increased expression of HIF-1 target genes. Interestingly, in this setting, adaptation to hypoxia induces the accumulation of intracellular lipids droplets, which was essential for protection against ROS toxicity in a context of hypoxia-reoxygenation. This lipid accumulation relied on HIF-1-dependent induction of adipophilin (*Adrp*) and Fabp3 and Fabp7, which are involved in the formation of lipid droplet (LD) membranes and the uptake of FA, respectively (*105*).

Hypoxia has also been reported to diminish FAO in cultured cardiac myocytes through inhibition of PPARα/RXR gene regulatory pathway in a HIF-1-independent fashion (*106*). In a cardiac hypertrophy model, HIF-1-dependent induction of PPARγ led to increased glycolytic rate, FA uptake and glycerolipid biosynthesis. These changes then resulted in a glucose-to-lipid conversion that caused cardiac steatosis, apoptosis and cardiac dysfunction (*105*).

A direct link between HIF stabilization and lipid beta-oxidation inhibition has been shown in ccRCC, the most common form of renal cancer, in which the canonical molecular alteration is the inactivation of VHL. Notably, in these cells, carnitine palmytoyltransferase (*Cpt1a*), the rate-limiting enzyme controlling FA entry into the mitochondria, was repressed by HIF-1 and HIF-2 transcription factors. The decrease in CPT1a activity reduced FA catabolism and promoted lipid accumulation in ccRCC (*107*). In another report, *Cpt1a* and the oxidative enzyme acyl-CoA synthase long-chain family member 1 (*Acsl1*), were suppressed by specific activation of HIF-2 in conditional liver-specific VHL-deficient mice. This translated into an impaired FAO and hepatic steatosis (*108*). Finally, in a recent report, HIF-1 suppressed the medium-chain (MCAD) and long-chain (LCAD) acyl-CoA dehydrogenases and FAO, contributing to hepatocellular carcinoma progression (*109*).

Overall, the role of HIF in lipid metabolism seems to be cell-dependent, driving lipid accumulation in most of the cases reported, and being associated to different prognosis depending on the context.

In summary, most of the research about HIF focuses on its role in the mechanistic adaptation to hypoxia mainly by tumor and stem cells. More recently, HIF has become relevant in immune cell function, particularly in macrophages, where HIF stands out as a regulator of their antimicrobial activity and tissue-repair potential, both intrinsically associated with macrophage polarization status. Compared to monocyte-derived macrophages or macrophage cell lines, tissue-resident macrophages and particularly lung alveolar macrophages, differentiate from embryonic precursors and occupy a relatively closed niche where they exert tolerogenic functions under steady-state. Therefore, since they are long-lived cells, a better understanding of their molecular requirements for adaptation to their niche could improve our knowledge about the etiology of certain lung pathologies. This in turn could help in the design of therapies based on specific targeting to enhance their homeostatic properties.

Objectives

Objectives

The general aim of this work was to evaluate the regulation of lung-resident alveolar macrophage (AM) physiology in steady state by von Hippel-Lindau (VHL) and hypoxia inducible factors (HIF)-1 and HIF-2 as sensors of oxygen. For this purpose, the specific aims of this work were:

1. Explore *in silico* whether adaptation from hypoxia to normoxia is linked to AM terminal differentiation.
2. Evaluate the effect of hypoxia inducible factor (HIF) stabilization through von-Hippel Lindau (*Vhl*) gene deletion in adult AMs.
3. Analyze the relative contribution of HIF-1 and HIF-2 in changes observed in adult VHL-deficient AMs.

Objectivos

Objectivos

El objetivo general de esta tesis doctoral fue evaluar el papel de la proteína von Hippel-Lindau (VHL) y los factores inducibles por hipoxia (HIF)-1 y HIF-2 en las funciones fisiológicas de los macrófagos alveolares (MAs) de pulmón.

Los objetivos específicos fueron:

1. Explorar *in silico* si la adaptación de hipoxia a normoxia ocurre durante la última fase de maduración de los MAs tras el nacimiento.
2. Estudiar el efecto de la estabilización de las proteínas HIF mediante la deleción de *Vhl*, en MAs adultos.
3. Analizar la contribución relativa de HIF-1 y HIF-2 en los cambios observados en MAs adultos deficientes en VHL.

Materials and Methods

Materials and Methods

1. Mouse strains

C57BL/6J-Crl mice (Charles River), *Csf2rb*$^{-/-}$ mice (*42*), *Vhl*$^{fl/fl}$ mice (*110, 111*) mated with CD11c-Cre BAC transgenic mice (*112*) were used. B6/SJL (Ptprca Pepcb/BoyJ) mice expressing the CD45.1 allele and DsRed (Actb-DsRed.T3) mice expressing the red fluorescent protein DsRed.MST, were both from The Jackson Laboratory (Bar Harbor, ME, USA). Mice were bred at CNIC under specific pathogen-free conditions. Except where indicated, we used 8- to 12-week-old age-matched animals (males or females) for all experiments. The local ethics committee approved all animal studies. All animal procedures were reviewed and approved by Animal Ethics Committee at the CNIC, Madrid Autonomous University Ethics Committee, and the Community of Madrid authority. All animal procedures were compliant with the EU Directive 2010/63/EU and Recommendation 2007/526/EC regarding the protection of animals used for experimental and other scientific purposes, enforced by the Spanish law under Real Decreto 1201/2005. Mice were allocated randomly in the different experimental procedures.

2. Lung cell suspension preparation

Adult lungs were collected in RPMI, cut into small pieces, and enzyme digested at 37ºC with Liberase TM (Sigma-Aldrich) for 30 min. Cells were passed through a 70µm cell strainer (Falcon) and washed with flow cytometry buffer. After red blood cell lysis, cells were centrifuged and resuspended in 1ml of cold flow cytometry buffer. Cells were counted with CASYton cell counter (Roche Innovatis) and stained for flow cytometry analysis.

3. Antibodies and Flow cytometry

Stainings were performed at 4ºC with the appropriate antibody (Ab) cocktail in cold flow cytometry buffer. Samples were processed with a Spectral Analyzer flow cytometer (SP6800, SONY), and data were analyzed with FlowJo software (Tree Star). CD16/CD32 (TONBO bioscience, San Diego, CA) was used to reduce non-specific binding. The following Abs were used for the analysis of *AM surface expression profile*: anti-CD11c-Brilliant Violet 510 (HL3, BD Biosciences), anti-Siglec-F-PE, anti-Siglec-F-PerCP-Cy5.5, anti-Siglec-F-BV421 or anti-Siglec-F-Alexa Fluor 647 (All of them: clone E50-2440, BD Biosciences), anti-CD64-APC (X54-5/7.1, BD Biosciences), anti-CD11b-PE-Cy7 (M1/70, BD Biosciences), anti-CD115-biotin (AFS98, eBiosciences), Streptavidin-APC (eBiosciences). During the analysis, we realized that control *Vhl*$^{fl/fl}$ and CD11cΔ*Vhl* AMs had a distinct intrinsic autofluorescence (AUF), thus, we used Spectral analyzer software to normalize GMOF for each fluorochrome based on genotype-specific AUF. The following Abs were used for *lung staining for FACs and for AM/pre-AM sorting*: anti-CD45-

PerCP-Cy5.5 (30-F11, eBiosciences) or anti-CD45-BV570 (30-F11, Biolegend), anti-CD45.1-APC (A20, eBiosciences), anti-F4/80 biotin (BM8, Life Technologies), anti-CD11c, anti-Siglec-F, anti-CD11b, anti-I-A/I-E-FITC (2G9, BD Biosciences) or anti-I-A/I-E-APC (M5/114.15.2, BD Biosciences), anti-Ly6G-APC or anti-Ly6G-PE (1A8, BD Pharmingen), and anti-Ly6C-FITC (AL-21, BD Biosciences). The following Abs were used for *blood staining*: anti-CD45.1-APC, anti-Ly6G-PE, anti-Ly6C-FITC and anti-CD11b-PerCP-Cy5.5 (M1/70, eBiosciences). Hoechst 33258 (Invitrogen) was used at 0.1μM as a counterstain to exclude dead cells. Lung AM population was defined as: $CD45^{+}$, $F4/80^{+}$, $CD11c^{+}$, Siglec-F^{+}, $CD11b^{-/mid}$, I-A/I-E^{lo}. Blood and lung monocytes were defined as: $CD45^{+}$, $CD11b^{hi}$, $Ly6G^{-}$, $Ly6C^{hi}$. For *intracellular Ki67 staining*, same AM number were stained for surface markers, washed twice and mixed with unstained thymocytes, used as a cell carrier. Just after, cells were fixed and permeabilized using the FoxP3 staining buffer set (eBiosciences), and then stained with anti-Ki67-eFluor 660 (SolA15, eBiosciences) or isotype control Rat IgG2aκ (eBR2a, eBiosciences). For *intracellular BrdU staining*, AMs were stained and mixed with carrier cells as explained above, and then fixed and permeabilized using the BrdU staining set (BD Pharmingen). Then, cells were treated with DNAse and stained with anti-BrdU Ab (BD Pharmingen).

4. RNA isolation and quantitative-PCR

Cell lysis was performed with buffer RLT (Qiagen), containing 10μ/ml β-mercaptoethanol and RNA was isolated with RNeasy Plus Mini Kit (Qiagen). RNA concentration was measured with nanodrop and integrity was determined with an Agilent 2100 Bioanalyzer (Caliper Life Science). Samples with RNA integrity values > 8 were further processed. cDNA was prepared using the High Capacity cDNA reverse transcription kit (Applied Biosystems, Foster City, CA). Quantitative PCR was performed in a 7900-FAST-384 instrument (Applied Biosystems) by using the GoTaq qPCR master mix from Promega (Madison, WI). Primers used in this work (synthetized by Sigma) were as follows:

β-actin Fw: 5′-GGCTGTATTCCCCTCCATCG-3′, *β-actin* Rv: 5′-CCAGTTGGTAACAATGCCATGT-3′, *Vhl* Fw: 5′-TGTGCCATCCCTCAATGTCG-3′, *Vhl* Rv: 5′-CTTCCGCACACTGGGTAGT-3′, *Slc2a1*Fw: 5′-GGGCATGTGCTTCCAGTATGT-3′, *Slc2a1* Rv: 5′-ACGAGGAGCACCGTGAAGAT-3′, *Ldha* Fw: 5′-TGTCTCCAGCAAAGACTACTGT-3′, *Ldha* Rv: 5′-GACTGTACTTGACAATGTTGGGA-3′, *Arg1* Fw: 5′-CTCCAAGCCAAAGTCCTTAGAG-3′ , *Arg1* Rv: 5′-AGGAGCTGTCATTAGGGACATC-3′, *Itgax* Fw: 5′-AGTGCTAGGGGACGTGAATG-3′, *Itgax* Rv: 5′-TCTGGGATGCTGAAATCCTC-3′ , *Siglec5* Fw: 5′-TTACCTGGCACTGGTGTTACTG-3′, *Siglec5* Rv: 5′-ATCTGCAGAGATGCTCCACTC-3′, *Fcgr1* Fw: 5′-GACAGTGGCGAATACAGGTGT-3′, *Fcgr1* Rv: 5′-ATGGCGACCTCCGAATCTGA-3′, *Itgam* Fw: 5′-ATGGACGCTGATGGCAATACC-3′, *Itgam* Rv: 5′-TCCCCATTCACGTCTCCCA-3′,

Ccnb1 Fw: 5′-AAGGTGCCTGTGTGTGAACC-3′, *Ccnb1* Rv: 5′-GTCAGCCCCATCATCTGCG-3′, *Ccnb2* Fw: 5′-GCCAAGAGCCATGTGACTATC-3′, *Ccnb2* Rv: 5′-CAGAGCTGGTACTTTGGTGTTC-3′, *Cdk1* Fw: 5′-AGAAGGTACTTACGGTGTGGT-3′, *Cdk1* Rv: 5′-GAGAGATTTCCCGAATTGCAGT-3′, *Cd25c* Fw: 5′-AGCGTAGCACATCTGCACATA-3′, *Cd25c* Rv: 5′-AGGAACCGTAGTAATGGGACTG-3′, *Plk3* Fw: 5′-GCACATCCATCGGTCATCCAG-3′, *Plk3* Rv: 5′-GCCACAGTCAAACCTTCTTCAA-3′, *Brca1* Fw: 5′-AGGAGGCGTCGATCATCCA-3′, *Brca1* Rv: 5′-ACAGATTTCTTTCGAGGTTGGG-3′ , *Chek1* Fw: 5′-TTCCACCAACTCATGGCAGG-3′, *Chek1* Rv: 5′-GCGTTCACGATTATTATGCCGAA-3′, *Chek2* Fw: 5′-GATCATTAGCAAGCGGAGGTT-3′, *Chek2* Rv: 5′-CACCACCCGGTCAAATAGTTC-3′, *Tp53* Fw: 5′-CTCTCCCCCGCAAAAGAAAAA-3′, *Tp53* Rv: 5′-CGGAACATCTCGAAGCGTTTA-3′, *Cdkn1a* Fw: 5′-CCTGGTGATGTCCGACCTG-3′, *Cdkn1a* Rv: 5′-CCATGAGCGCATCGCAATC-3′, *Nr1h3* Fw: 5′-CTCAATGCCTGATGTTTCTCCT-3′, *Nr1h3* Rv: 5′-TCCAACCCTATCCCTAAAGCAA-3′, *Nr1h2* Fw: 5′-CGTGGTCATCTTAGAGCCAGA-3′; *Nr1h2* Rv: 5′-GCTGAGCACGTTGTAGTGGAA-3′, *Abcg1* Fw: 5′-CTTTCCTACTCTGTACCCGAGG-3′, *Abcg1* Rv: 5′-CGGGGCATTCCATTGATAAGG-3′, *Apoe* Fw: 5′-CTGACAGGATGCCTAGCCG-3′, *Apoe* Rv: 5′-CGCAGGTAATCCCAGAAGC-3′, *Pltp* Fw: 5′-CGCAAAGGGCCACTTTTACTA-3′, *Pltp* Rv: 5′-GCCCCCATCATATAAGAACCAG-3′. *Pparg* Fw: 5′-TCGCTGATGCACTGCCTATG-3′, *Pparg* Rv: 5′-GAGAGGTCCACAGAGCTGATT-3′, *Fabp4* Fw: 5′-AAGGTGAAGAGCATCATAACCCT-3′, *Fabp4* Rv: 5′-TCACGCCTTTCATAACACATTCC-3′, *Cd36* Fw: 5′-GAACCACTGCTTTCAAAAACT-3′, *Cd36* Rv: 5′-TGCTGTTCTTTGCCACGTCA-3′,mRNA levels are shown as relative expression to β-actin ($\Delta\Delta$Ct) as indicated in figure legends.

5. Alveolar macrophage isolation

Mice were sacrificed with a lethal dose of pentobarbital (Dolethal, Vetoquinol). In order to obtain an enriched AM population for cell culture, ten bronchoalveolar lavages (BALs) per mouse were performed with a blunt fill needle (18G x 1 ½; 1.2mmx40mm, BD Safety products), with 1ml of phosphate-buffered saline (PBS), 2.5mM EDTA, 2% fetal bovine serum (FBS, HyClone) (flow cytometry buffer) at 37ºC. Samples were kept on ice until further processing. Red blood cell lysis was performed at room temperature (RT) for 3 min (RBC Lysis Buffer, Sigma-Aldrich). Cells were counted with a Neubauer chamber, and then cultured in RPMI 1640 (Gibco) supplemented with 10% FBS, plus 100 U/ml penicillin and 2 mM L-glutamine (complete RPMI) at 37ºC and 5% CO_2.

- For *BrdU in vitro Assay*, $2x10^5$ BAL AMs from pools of mice were plated in triplicates (RPMI, M-CSF and rGM-CSF) in non-tissue cultured treated 24well-plates (Falcon) in 1.5 ml per well of complete RPMI. 2-3h after plating, rM-CSF and rGM-CSF (both from Peprotech) were added to stimulate cell proliferation at a final concentration of 1 ng/ml and 10 pg/ml, respectively.

After 10-12h in the presence of cytokines, first pulse of BrdU (BD Pharmingen) was added to the cultures at 10µM. Since cells are not synchronized, a second pulse of BrdU was added to the cultures 24h later, in order to detect all proliferating AMs. 24h after the second pulse, cells were washed once with PBS to remove remaining FBS and incubated with accutase (StemCell Technologies) at 37ºC. After 15-20 min, cells were carefully detached by pipetting. In order to avoid losing semi-adherent cells, RPMI supernatant and PBS from washes were saved and mixed for each well. After centrifugation, cells were counted and the same cell number per condition and genotype was stained for surface markers and BrdU.

- For *Cell morphology analysis or lipid content visualization*, $2x10^5$ AMs from individual mice were cultured on crystals previously sterilized with a cycle of UV radiation, placed in 24well-plates in complete RPMI at 37ºC and 5% CO_2. After 5 days, supernatant was carefully removed and cells were fixed for 10 min with paraformaldehyde (PFA) 4% (Thermo Fisher) at RT. Then, cells were washed twice with PBS and crystals stained with Hematoxylin and Eosin or with 0.5% Oil Red O (Sigma-Aldrich) in propylene glycol for 10 min at 60ºC; cells were counterstained with hematoxylin. Red lipid droplets were visualized by microscopy.

6. Cell image acquisition & analysis of size and circularity

Cells were examined with a Leica DM 2500 light microscope and images captured with a Leica DFC 420 digital camera. At least 3 images of different fields of a single mouse were acquired and further analyzed. Image processing and quantification of AM size and circularity were developed as a macro in Fiji (ImageJ 1.50e x64). A first preprocessing step converts the 10X color image into grayscale, applies a gaussian blurring (sigma=3), and normalizes it in order to reduce noise and standardize the intensity values. An initial segmentation of objects is done using a marker-controlled watershed algorithm (*113*) trying to maximize the differential detection of cells closely situated or clustered, without over-segmenting elongated cells as multiple objects. “Marker” and “mask” images used to that end were created by automatic thresholding using Minimum and Otsu implementations respectively, followed by morphological operations in order to condense the segmented objects and discard noisy elements (hole filling, closing, area opening, and removal of objects partially detected in the boundaries). The stricter first threshold allows a proper definition of seed locations (“marker”) and the more permissive Otsu method achieves robust and accurate segmentation of complete macrophages (“mask”). Objects segmented in “mask” image and split by the explained watershed strategy are later filtered to discard mistakes (dirtiness and shadows typical of the image modality), by removing those ones where the ratio between mean intensity inside the object and its 10-pixel outer-ring is lower than 120% and with dimensions very far from the typical values. Circularity (4π*area/perimeter^2) and size are measured for each final detected cell and mean values are reported for each individual

image. Statistical analysis was performed comparing average of the mean values obtained from groups of at least 5 mice per genotype and/or condition.

7. Parabiosis

Parabiosis was performed as previously described (*114*). Sex- and age-matched CD11c-Cre^{+} *Vhl*$^{fl/fl}$ and CD11c-Cre^{-} *Vhl*$^{fl/fl}$ littermates were joined with B6/SJL, expressing the CD45.1 congenic marker to facilitate cell tracking in blood and lung after one month of parabiosis.

8. BM chimeras

B6/SJL mice expressing the CD45.1 congenic marker were lethally irradiated (12 Gy) and were reconstituted intravenously with 5x10^{6} cells of a 1:1 mixture of CD45.2^{+} wild-type DsRed^{+} BM cells and CD45.2^{+} CD11cΔ*Vhl* BM cells, or CD45.2^{+} wild-type DsRed^{+} BM cells and CD45.2^{+} control *Vhl*$^{fl/fl}$ BM cells. Mice were analyzed 47 days after reconstitution and blood was harvested one day before sacrifize.

9. Metabolic measurements

Real-time oxygen-consumption rate (OCR) and extracellular acidification rate (ECAR) in AMs were determined with an XF-96 Extracellular Flux Analyzer (Seahorse Bioscience). The assay was performed in DMEM supplemented with 100 µg/ml streptomycin, phenol red and 25mM glucose + 2mM L-glutamine + 1mM Na-pyruvate or 5mM L-carnitine + 50 µM palmitoyl-CoA. The pH was adjusted to 7.4 with KOH. Three consecutive measurements were performed under basal conditions and after the sequential addition of the following mitochondrial electron transport chain (mETC) inhibitors: 1µM oligomycin. 1µM carbonyl cyanide m-chlorophenyl (CCCP) and 1µM rotenone + 1µM antimycin A (Sigma-Aldrich). Basal respiration rate (BRR) was defined as OCR in the absence of any inhibitor. Basal ECAR (B. ECAR) was measured in the absence of drugs. AMs newly obtained from BAL were pooled from 5 to 10 mice per genotype. After red blood cell lysis, AMs were counted, washed once with Seahorse media, and 2.5x10^{5} AMs were plated in 180µl of seahorse media per well in 3 to 10 wells (replicates) previously coated with Cell-Tak (Corning). After spin down, plates were incubated at 37ºC without CO_2 for 30 min before Cell Mito Stress Test was run.

10. BrdU proliferation *in vivo*

Four groups of mice (2 groups of each genotype) were daily injected with 1mg BrdU (Sigma-Aldrich) for 2 weeks. One day and 21 days after the last injection, two groups (one of each genotype) were sacrificed and BAL AMs were analyzed for BrdU incorporation (*31*). The ratio of frequencies of BrdU^{+} AMs at day 21 and day 1 was calculated as a measurement of BrdU dilution during 21 days.

11. Immunoblot

AMs were obtained from BAL performed with RMPI-2.5 mM EDTA (FBS-free) at 37ºC. AMs were pooled from at least 10 mice per genotype and 10^6 cells per condition were resuspended in 1ml of RMPI in a 15-ml falcon tube for starving at 37ºC in a water bath. After 35 minutes, rGM-CSF was added at a final concentration of 10 pg/ml or 1 ng/ml. Cells were stimulated for 30 min at 37ºC and then centrifuged for lysis. Cell lysates were prepared in RIPA buffer containing protease and phosphatase inhibitors (Roche). Samples were run on Mini-PROTEAN TGX PRECAST Gels and transferred onto a nitrocellulose membrane (both from Bio-Rad Laboratories, Hercules, CA) for blotting with the following antibodies: β-ACTIN (C4) from Santa Cruz (Dallas, TX); pY694-STAT5 (Abcam; ab32364); STAT5a+STAT5b (Abcam; ab200341). Alexa Fluor-680 (Life Technologies) or Qdot-800 (Rockland, Limerick, PA) conjugated secondary antibodies were used and gels were visualized in an Odyssey instrument (LI-COR, Lincoln, NE). Band intensity was quantified with Fiji (ImageJ 1.50e x64).

12. Pulmonary macrophage transplantation (PMT)

Csf2rb$^{-/-}$ mice were pulmonary transplanted with $5x10^4$ AMs newly obtained from BAL pools of control *Vhl*$^{fl/fl}$ and CD11cΔ*Vhl* mice. Before transplantation, receptor mice were anesthetized with Ketamine (Imalgene, Merial) and Xylacine (Rompun, Bayer). When fully unconscious, a small incision was done to partially expose trachea. Then, animals were carefully intubated orotracheally with an I.V. catheter (22 GA, 0.9x25 mm; BD Insyte). Cells were inoculated with a pipette in 30µl of PBS. Next, mice were extubated and the incision sutured. Mice were finally injected with anesthesia reversor (Medeson, Urano) and kept in a warm plaque until full recovery. AMs viability was higher than 90% after the last transplantation. Six weeks after transplantation, we performed BAL of transferred mice with 1ml of PBS. In order to get rid of debris, BAL was centrifuged at 1700rpm for 5 min at RT, and BAL supernatant was used to measure total protein content in BAL and surfactant protein D (SP-D) concentration. Cell engraftment was compared by flow cytometry of total lung cells.

13. BCA protein measurement

Total protein concentration was determined using Pierce BCA Protein Assay Kit (Thermo Scientific) according to the manufacturer's instruction. Albumin (Thermo scientific) was used as standard.

14. ELISA surfactant protein D

SP-D DUO ELISA kit and capture/detection antibodies were from R&D Systems. It was used according to manufacturer's instructions. Detection antibody was biotinylated and labeled

with streptavidin-conjugated horseradish peroxidase (HRP) and visualized by incubation with 5,5′-tetramethylbenzidine solution (TMB, KPL). Reaction was stopped with TMB-stop solution (KPL). Recombinant SP-D served as standard and was included in the kit. Optical density was determined using a microplate reader (Benchmark Plus, Bio-Rad) set to 450 nm subtracting absorbance at 570 nm (wavelength correction).

15. Bioinformatic Analysis

GSE60249 array data (*22*)

Array data (CEL files) were downloaded from GEO and imported into the R software environment with functions provided by packages GEOquery and oligo. RMA (affy package) was used for data processing, normalization and calculation of log2 transformed expression values. The corresponding array annotation database (mogene11sttranscriptcluster.db) was used to map expression values with their associated Ensembl gene IDs, by selecting the associated transcript clusters with the higher median value across all samples.

Gene Set Enrichment Analysis tool from the Molecular Signature Database MSigDB (http://software.broadinstitute.org/gsea/msigdb/collections.jsp), was used to identify enriched gene sets, using the Hallmark gene sets. Enriched gene sets, having up-regulated and down-regulated genes, were identified using weighted enrichment statistic and a log2 ratio metric for ranking genes. Significance was defined by FDR q value < 0.25, obtained after one thousand phenotype permutations.

Heatmaps were generated with Heatmapper (*115*), using no clustering method and Euclidean as distance measurement method.

RNA Seq

BAL AMs were pooled from 5-7 mice per genotype and further purified by positive selection with anti-CD11c-microbeads (Miltenyi Biotec), following manufacturer's instructions. A total of 3 pools per genotype were used for RNA Seq.

Differential expression analysis.

Sequencing reads were pre-processed by means of a pipeline that used FastQC (www.bioinformatics.babraham.ac.uk/projects/fastqc) to assess read quality, and Cutadapt v1.6 (http://journal.embnet.org/index.php/embnetjournal/article/view/200) to trim sequencing reads, eliminate Illumina adaptor remains, and to discard reads that were shorter than 30 base pairs. The resulting reads were mapped against the mouse transcriptome (GRCm38 assembly, Ensembl release 76) and quantified using RSEM v1.2.3 (*116*). Raw expression counts were then processed with an analysis pipeline that used the Bioconductor package EdgeR (*117*) for

normalization (using TMM method) and differential expression testing. Only genes expressed at a minimal level of 1 count per million, in at least 3 samples, were considered for differential expression analysis. Changes in gene expression were considered significant if associated to a Benjamini and Hochberg adjusted p-value < 0.05.

Functional analysis.

Collections of differentially expressed genes were analyzed with Ingenuity Pathway Analysis (IPA) (https://www.qiagenbioinformatics.com/products/ingenuity-pathway-analysis) to determine significant associations to canonical pathways, biological functions and upstream transcriptional regulators; significance was defined by a Benjamini and Hochberg adjusted p-value < 0.05. GOrilla and ReViGO were used to identify and summarize Gene Ontology terms enriched in the collections of differentially expressed genes; significance was defined by FDR q value < 0.05. Venn diagram was generated by term lists comparison with Venny (http://bioinfogp.cnb.csic.es/tools/venny/index.html) to identify and visualize specific and shared elements. Circular plots representing the association between genes and enriched functional categories were generated with GOplot. GSEA was used to identify enriched gene sets, from the Hallmark collection of MSigDB, having up-regulated and down-regulated genes, using a weighted enrichment statistic and a log2 ratio metric for ranking genes. Significance was defined by FDR q value < 0.25, obtained after one thousand phenotype permutations.

16. Statistical analysis

Statistical comparisons were made with Prism v7 (GraphPad Software, La Jolla, CA). Statistical tests are detailed in figure legends. p-values: ns, not significant; *p < 0.05; **p < 0.01; ***p < 0.001.

Results

Results

1. Postnatal alveolar macrophage (AMs) maturation correlates with decreased hypoxia and glycolysis.

1.1. The expression of gene sets related to hypoxia and glycolysis are gradually downregulated during AM maturation.

In order to explore whether detection of increasing oxygen concentration after birth could be linked to AM maturation, we analyzed a publicly available microarray containing the transcriptional profile of AMs from pups at postnatal days 2 and 11 and from 8-12-week-old adult mice (*22*). Gene set enrichment analysis (GSEA) was performed on the gene expression profiles using the hallmark collection of the Molecular Signatures Database (MSigDB). Results showed significant enrichment of both hypoxia and glycolysis gene sets in immature AMs from 2-day-old pups compared with mature AMs from adults (Figure R1A-B).

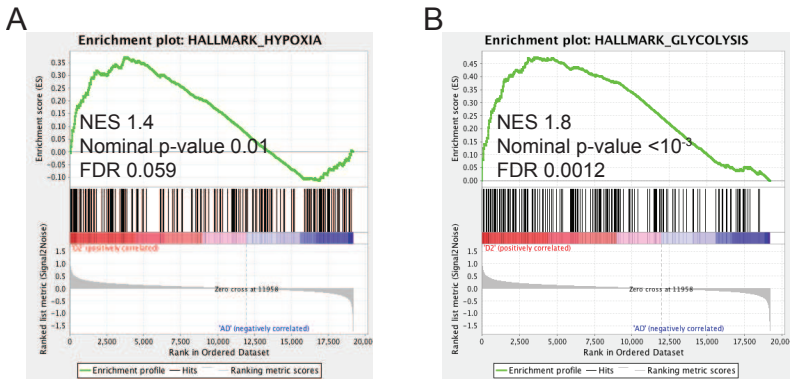

Figure R1. Enrichment of hypoxia and glycolysis gene sets in pre-AMs, compared to mature AMs. Enrichment plots of "hypoxia" (A) and "glycolysis" (B) from GSEA of postnatal day 2 ("D2") compared with adult ("AD") AMs using the hallmark gene set collection from the Molecular Signature Database (MSigDB). Normalized enrichment score (NES) accounts for the degree to which a gene set is overrepresented at top or bottom of a ranked list of genes. Nominal p-value estimates the statistical significance of the enrichment score for a single gene set. False discovery rate (FDR) is the estimated probability that a gene set with a given NES represents a false positive finding.

In addition, mapping the expression of the core genes from these two enriched gene sets revealed a gradual downregulation throughout the several stages of AM maturation analyzed (Figure R2A-B). Together, these *in silico* analysis show that the expression of genes involved in adaptation to hypoxia and glycolysis is downregulated during AM maturation after birth.

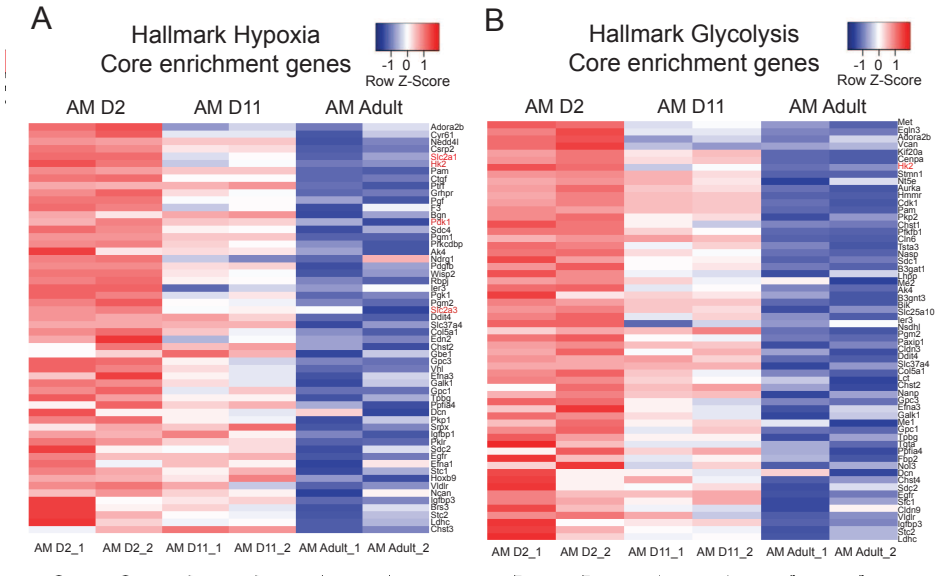

Figure R2. Downregulation of expression of core genes from hypoxia and glycolysis gene sets during postnatal maturation. mRNA expression (Log_2 of intensity) of genes from the core of hallmark gene sets "hypoxia" (A) and "glycolysis" (B) in lung AMs from postnatal day 2 ("D2"), "D11" and adult mice ("Adult"). Each sample group is composed by two samples (duplicates). Red squares correspond to over-expressed genes and blue squares correspond to under-expressed genes. Genes depicted in red are well-known HIF-target genes.

1.2. Expression of HIF-target genes is downregulated during AM maturation.

Among the core genes comprised in hypoxia and glycolysis gene sets, we identified well-known HIF targets such as *Slc2a1* (GLUT-1), *Hk2* (Hexokinase 2), *Pdk1* (Pyruvate dehydrogenase 1) and *Slc2a3* (GLUT-3) (*73*) (Figure R2 and Table 1. Red genes).

Table 1. Canonical HIF target genes

Gene	Description	HIF
Slc2a1	Solute carrier/Glucose transporter 1	1,2
Hk2	Hexokinase 2	1
Pdk1	Pyruvate dehydrogenase kinase 1	1
Slc2a3	Solute carrier/Glucose transporter 3	1
Hk1	Hexokinase 1	1
Ldha	Lactate dehydrogenase a	1
Pkm	Pyruvate kinase, muscle	1
Pgk1	Phosphoglycerate kinase 1	1
Pfkl	Phosphofructokinase, Liver	1
Nos2	Inducible NO Synthase	1
Arg1	Arginase 1	2
Vegfa	Vascular endothelial growth factor A	1,2

Table 1. Canonical HIF target genes. Genes depicted in red are found among core genes of Hypoxia and Glycolysis hallmark gene sets. Genes colored in black correspond to other canonical HIF target genes.

Mapping the expression of other classical HIF-target genes (Table 1. Black genes) revealed in most cases their downregulation during AM maturation (Fig. R3A). Consequently, we found that the mean expression of all HIF-target genes analyzed (Table 1), was significantly higher in immature AMs (Day 2) than in mature AMs from adult mice, whereas no significant changes were found between postnatal day 11 and adulthood (Figure R3B).

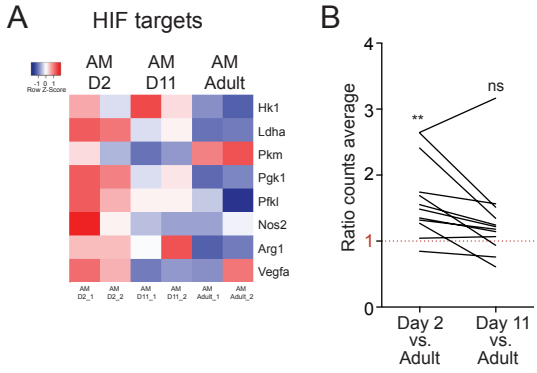

Figure R3. Significant downregulation of expression of most of HIF-target genes during early AM maturation. (A) mRNA expression (Log_2 of intensity) of HIF-target genes from table 1 (marked in black), not included in the hallmark gene sets "hypoxia" and "glycolysis" during AM maturation. Color intensity defined as in Figure R2. (B) Mean expression of HIF-target genes from table 1 in D2 and D11. Expression values for each gene are shown as the ratio of mean expression on D2 or D11 to the mean expression in adult AMs. ns, not significant; **, p-value< 0.01 (Column Statistics analysis, hypothetical value=1).

These results indicate that some HIF-target genes are part of the core enrichment genes of hypoxia and glycolysis and that their expression is significantly downregulated in AMs from adult mice compared to pre-AMs and occurs specifically during the time period comprising AM maturation after birth. In agreement with these results, we sorted AMs from adult mice and fetal monocytes at date of birth (DOB) (Figure R4A) (*6*) and confirmed that the expression of selected HIF-target genes was significantly downregulated in AM, compared to fetal monocytes (Figure R4B).

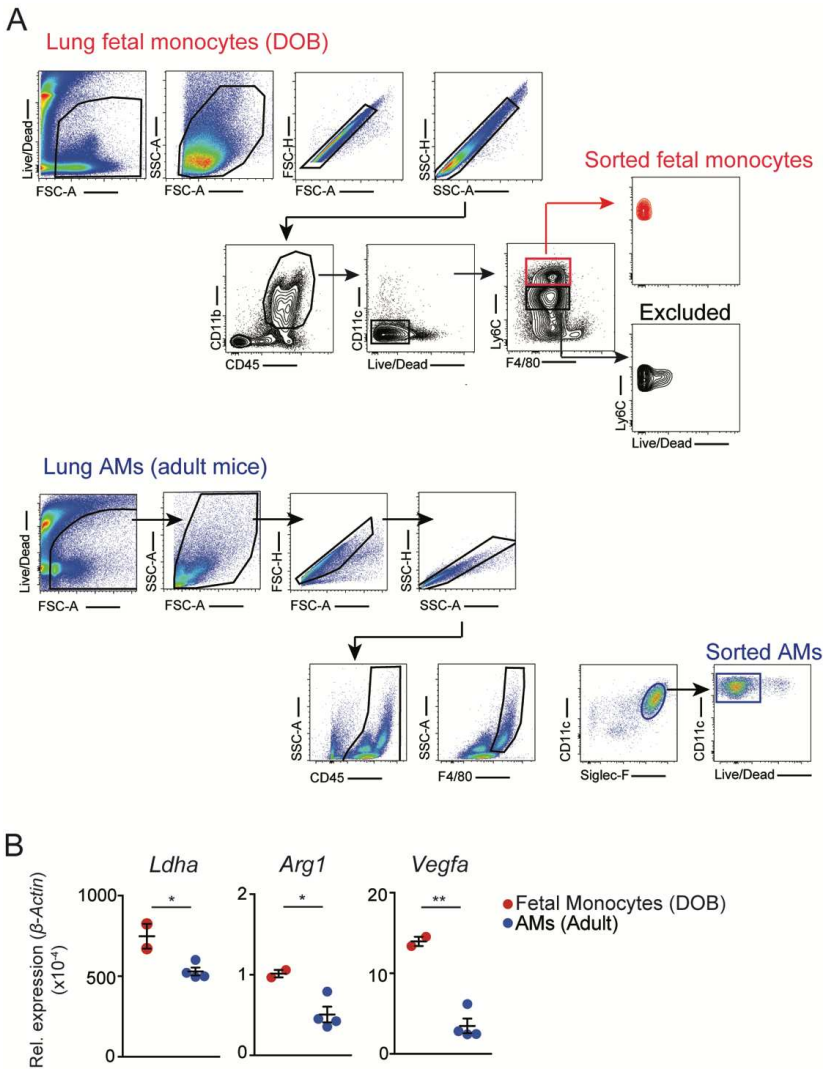

Figure R4. Expression of selected HIF-target genes is upregulated in fetal monocytes compared to mature AMs. Gating strategy used to sort fetal monocytes and mature AMs. (A, upper panel) Lungs from three DOB pups were pooled and CD45^{+} CD11b^{+} CD11c^{-} F4/80^{lo} Ly6C^{hi} fetal monocytes were sorted for RNA extraction. Ly6C^{mid} population was excluded based on viability. Two pools of cells were sorted. (A, lower panel) Lungs from four individual mice were stained and CD45^{+} F4/80^{+} CD11c^{hi}SiglecF^{hi} AMs were sorted. (B) Quantitative PCR for the expression of *Ldha*, *Arg1* and *Vegfa*. Data correspond to two pools of three pups at DOB and four individual adult mice, represented as individual dots and corresponding to one representative experiment of two performed. *, p-value< 0.05; **, p-value< 0.01 (unpaired Student *t*-test).

2. The absence of VHL alters AM metabolism and phenotype

2.1. Genetic characterization of *Vhl* deletion in AMs.

To dissect the effects of prevention of HIF degradation in response to high postnatal oxygen pressure on AMs, we generated CD11c-Cre *Vhl*$^{fl/fl}$ mice, since the CD11c-Cre driver targets AMs specifically after birth (*6*). In order to get rid of debris and a few other cell types found in the lung alveoli, we performed bronchoalveolar lavage (BAL) and sorted CD11c^{+} AMs by magnetic columns (Figure R5A). CD11c-Cre^{+} *Vhl*$^{fl/fl}$ (CD11cΔ*Vhl*) mice showed significantly decreased *Vhl* mRNA levels relative to AMs from CD11c-Cre^{-} *Vhl*$^{fl/fl}$ littermates (control *Vhl*$^{fl/fl}$) (Figure R5B). Notably, VHL depletion in AMs resulted in increased expression of HIF-1 targets such as *Ldha* (Lactate dehydrogenase) (*73*), HIF-2 targets such as *Arg1* (Arginase 1) (*76*), and common HIF-1 and HIF-2 targets such as *Slc2a1* (*70*) (Figure R5C).

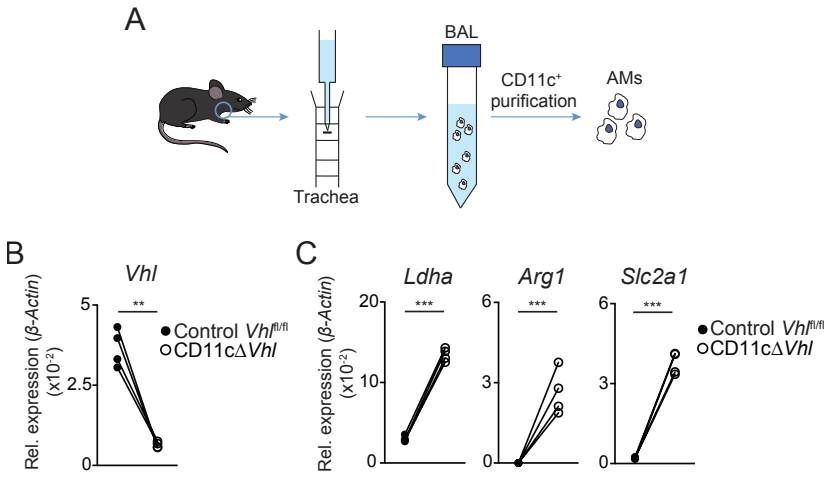

Figure R5. Characterization of *Vhl* deletion in BAL AMs from CD11c-cre *Vhl*$^{fl/fl}$ mice. (A) BAL was performed by introducing a cannula into the mouse trachea. Then, 1ml of PBS1x was instilled and immediately recovered. BAL was kept in a 15ml-falcon tube and on ice. Positive selection of AMs was done by incubating BAL cells with CD11c^{+} microbeads and then sorting with a magnet. Quantitative PCR for the expression of *Vhl* (B), *Ldha*, *Arg1* and *Slc2a1* (C) in purified BAL AMs from the indicated mouse genotypes. Data correspond to four pools of mice (n=4-5) represented as individual dots and corresponding to four independent experiments: **, p<0.01; ***, p<0.001 (ratio paired Student *t*-test).

To deeply explore the transcriptional changes due to Vhl deletion in AMs, we conducted an RNA sequencing analysis to compare the transcriptome of BAL AMs isolated from CD11cΔ*Vhl* and control *Vhl*$^{fl/fl}$ mice. GSEA showed very significant enrichment of hypoxia and glycolysis gene sets from the hallmark collection in the absence of VHL, reflected by the extremely low nominal p-value and false discovery rate (FDR) (Figure R6A-B), resembling the comparison of day 2 postnatal versus adult AMs (Figure R1). These results indicate that, at a transcriptional level, the absence of VHL affects the ability of AMs to detect oxygen and its associated metabolic profile.

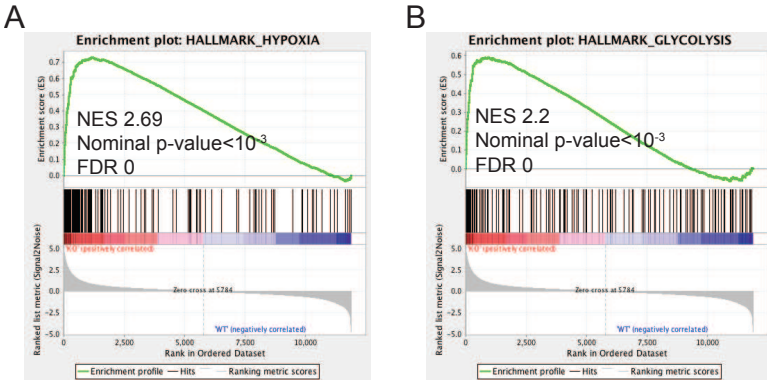

Figure R6. Enrichment of hypoxia and glycolysis gene sets in VHL-deficient AMs. Enrichment plots from GSEA of CD11cΔ*Vhl* (KO), compared with control $Vhl^{fl/fl}$ (WT) AMs using the hallmark gene set collection from the Molecular Signature Database MSigDB for "hypoxia" (A) and "glycolysis" (B) gene sets.

2.2. Metabolic characterization of VHL-deficient AMs.

In order to address whether enrichment in glycolysis gene set in *Vhl*-deficient AMs translates into functional metabolic alterations, we measured real-time metabolic profile of VHL-deficient AMs from BAL in the presence of glucose, pyruvate and glutamine. The absence of VHL in AMs significantly decreased their basal respiratory rate (BRR) (Figure R7A-B) and increased their basal extracellular acidification rate (ECAR) (Figure R7C-D), which is usually linked to increased glycolysis. This increased medium acidification capacity was also evidenced after culturing BAL AMs for ten days in complete RPMI without HEPES (Figure R7E). These results indicate that depletion of VHL in AMs alters their metabolic profile towards partial desensitization to oxygen and to increased glycolytic capacity.

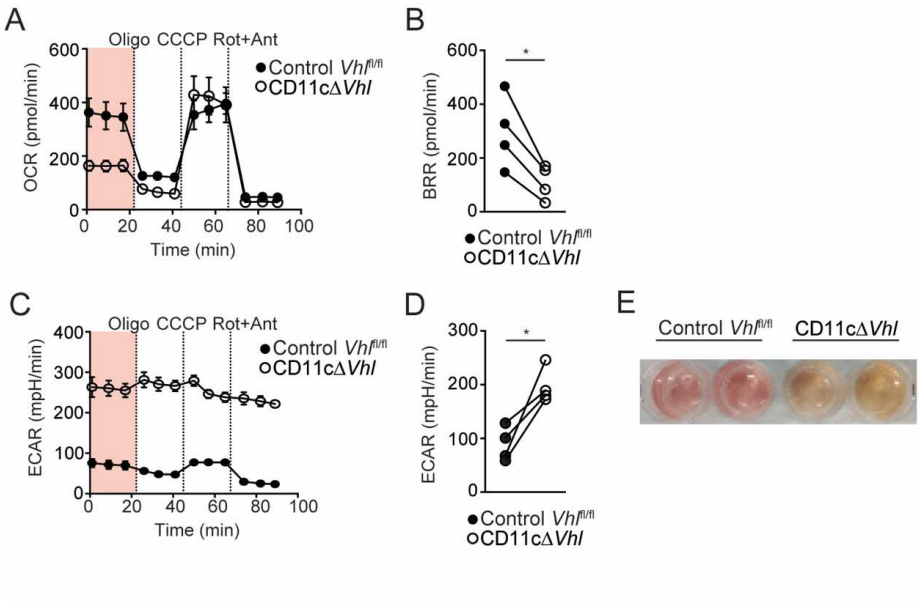

Figure R7. VHL-deficient AMs show an altered metabolic profile. (A) Oxygen consumption rate (OCR) in the presence of glucose, glutamine and pyruvate by BAL AMs from the indicated genotypes sequentially treated with oligomycin (Oligo), carbonyl cyanide m-chlorophenylhydrazone (CCCP) and rotenone + antimycin A (Rot + Ant). Data are means ± s.d. using AMs pooled from 6-7 mice per genotype in a representative experiment of four performed. (B) Basal respiratory rate (BRR) in AMs measured as in A. (C) Extracellular acidification rate (ECAR) measured in the same assay as A. (D) Basal extracellular acidification rate (ECAR) in AMs from the indicated genotypes. (B,D) Paired independent experiments (AMs pooled from 6-7 mice per experiment): *, $p<0.05$ (ratio paired Student t test). (E) Pictures depicting the *de visu* acidification of the media after ten days in culture with complete RPMI without HEPES. Picture from one representative experiment out of two performed.

Together with transcriptional changes previously depicted (Figure R6), these functional results validate the CD11c-Cre *Vhl*$^{fl/fl}$ mice as an adequate model to study the effects of stabilizing HIF and desensitize AMs to oxygen sensing in their maturation and function after birth.

2.3. VHL-deficient AMs resemble immature cells.

Defects in AM terminal differentiation can lead to the development of AM-like cells with a distorted phenotype (*22*). We first realized that VHL-deficient AMs from BAL were smaller and more granular by flow cytometry, based on forward and side scatter, respectively (Figure R8A-B). In addition, VHL-deficient AMs were unable to acquire the fusiform morphology of control *Vhl*$^{fl/fl}$ AMs after *ex vivo* culture for five days (Figure R8C-D), and instead, maintained a rounded shape similar to precursor cells or monocytes (*6*).

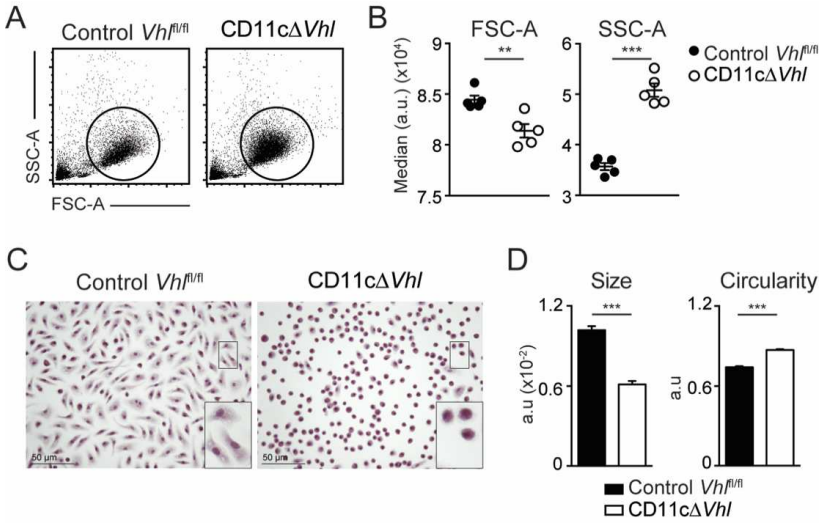

Figure R8. VHL-deficient AMs show an altered morphology. (A) Representative plots showing the size (FSC-A) and complexity (SSC-A) of the AM population in BAL from the indicated mouse genotypes. (B) Graphs representing the median FSC-A and SSC-A of the AM population gated in A. Morphological parameters of BAL AMs after 5-day culture in complete medium. (C) Representative images of Hematoxylin & Eosin staining of BAL AMs from the indicated genotypes, bars 50µm; (D, left) mean AM size ± s.e.m. (D, right) mean AM circularity ± s.e.m. (B) one representative experiment showing mean± s.e.m. of 5 biological replicates. ***, p<0.001; **, p<0.01 (unpaired Student *t*-test). (D) one representative experiment showing mean± s.e.m. of 4-5 biological replicates with analysis of at least 3 images containing >100 cells per replicate. ***, p<0.001 (unpaired Student *t*-test).

Since altered maturation can affect AM phenotype (*22*), we measured the expression of canonical surface markers on BAL AMs *ex vivo*. VHL-deficient AMs expressed slightly lower mRNA for *Itgax* (CD11c) and decreased mRNA and protein for *Siglec5* (Siglec-F) and *Fcgr1a* (CD64), whereas *Itgam* (CD11b) was increased (Figure R9). This phenotype has been previously linked to an immature AM state (*6, 22*), suggesting that VHL-deficient AMs are partially arrested and do not reach the full maturation state.

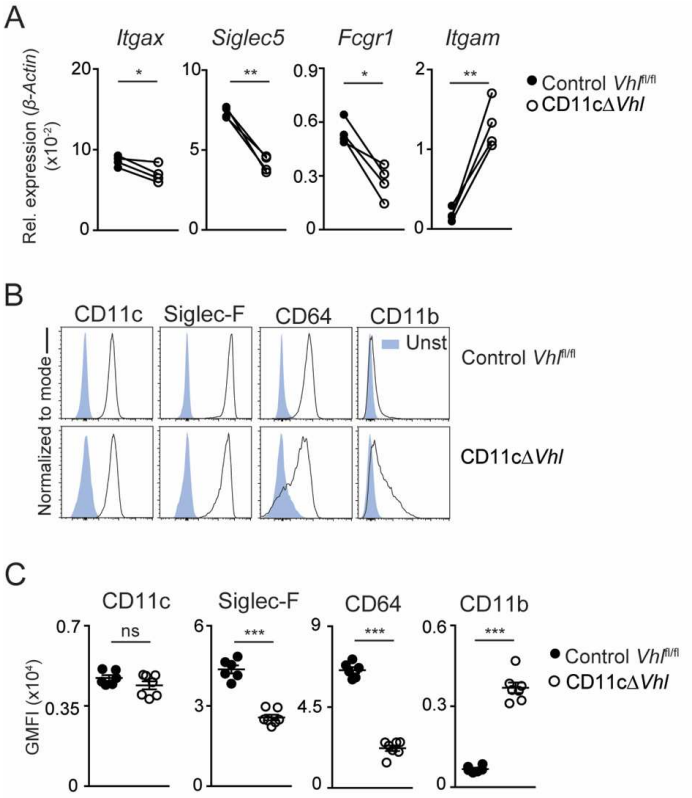

Figure R9. VHL-deficient AMs show an immature-like phenotype. (A) Quantitative PCR for the expression of *Itgax*, *Siglec5*, *Fcgr1*, and *Itgam* in sorted BAL AMs from mice of the indicated genotypes. Individual dots correspond to four independent experiments, with AMs from 4-5 pooled mice per experiment: *, p<0.05; **, p<0.01 (ratio paired Student *t*-test). (B) Representative flow cytometry histograms for CD11c, Siglec-F, CD64, and CD11b (black line) compared with unstained samples (tinted blue) in BAL AMs from the indicated genotypes. (C) Normalized geometric mean fluorescence intensity (GMFI) for the selected markers in AMs from the indicated genotypes. Data shown as mean ± s.e.m. from one representative experiment of three performed. Each dot represents the normalized GMFI of an individual mouse (n=6-7 per genotype): ns, not significant; ***, p<0.001 (unpaired Student *t*-test).

2.4. VHL-deficient AMs show an altered transcriptional identity.

To further evaluate whether deletion of VHL modified the lung AM-specific transcriptional signature, we compared the transcriptome of CD11cΔ*Vhl* and control *Vhl*$^{fl/fl}$ AMs, and directed our analysis on specific AM signature genes comprised in “module 296” (*118*). We found that while the expression of most of them was even increased in CD11cΔ*Vhl* AMs, compared to WT AMs, some were downregulated, such as *Spp1*, implicated in the regulation of IL-10 production by human (*119*), *P2ry2*, that induce increased production of MCP-1 in rat alveolar and peritoneal macrophages (*120*) or the carbonyl reductase *Cbr2* (Figure R10, upper gene set). In contrast, several transcription factors associated with this module were upregulated in CD11cΔ*Vhl* AMs compared to WT AMs (Figure R10, upper gene set, black square). Next, we focused our analysis on the 21 transcription factors whose expression is described to be selectively upregulated in lung

AMs, and we found that the expression of 9 was downregulated in VHL-deficient AMs (Figure R10, lower gene set).

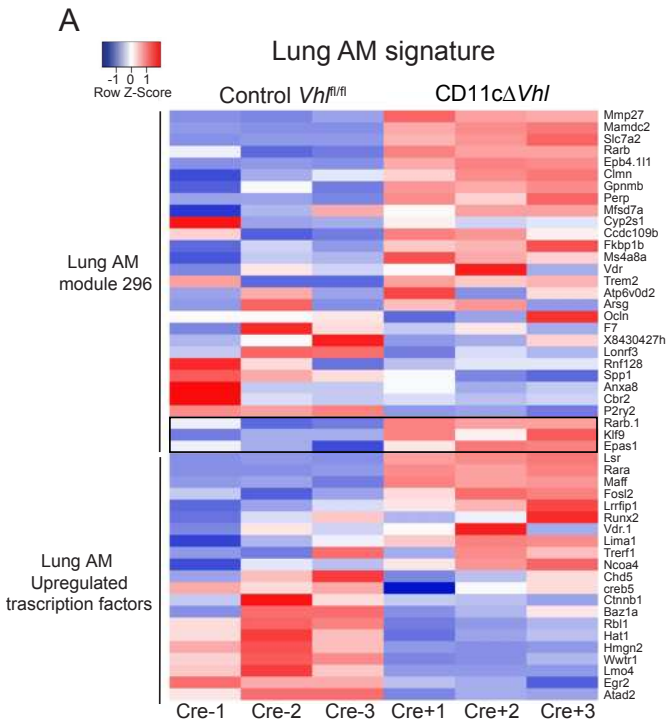

Figure R10. Lung AM signature is altered in VHL-deficient AMs. (A) mRNA expression (Log_2 of intensity) of genes from lung AM associated fine module 296 (upper panel) and lung AM upregulated transcription factors (lower panel). Expression depicted for control *Vhl*$^{fl/fl}$ and CD11cΔ*Vhl* AMs. Each sample group is composed by three replicates.

We then analyzed the expression of those genes upregulated in lung AM lineage ("signature-up" genes) and some of them were downregulated, including *Siglec5*, previously confirmed by quantitative PCR (Figure R9A). In addition, we found *Car4*, related with AM identity (*29*) and *Epcam*, implicated in cell adhesion (Figure R11A).

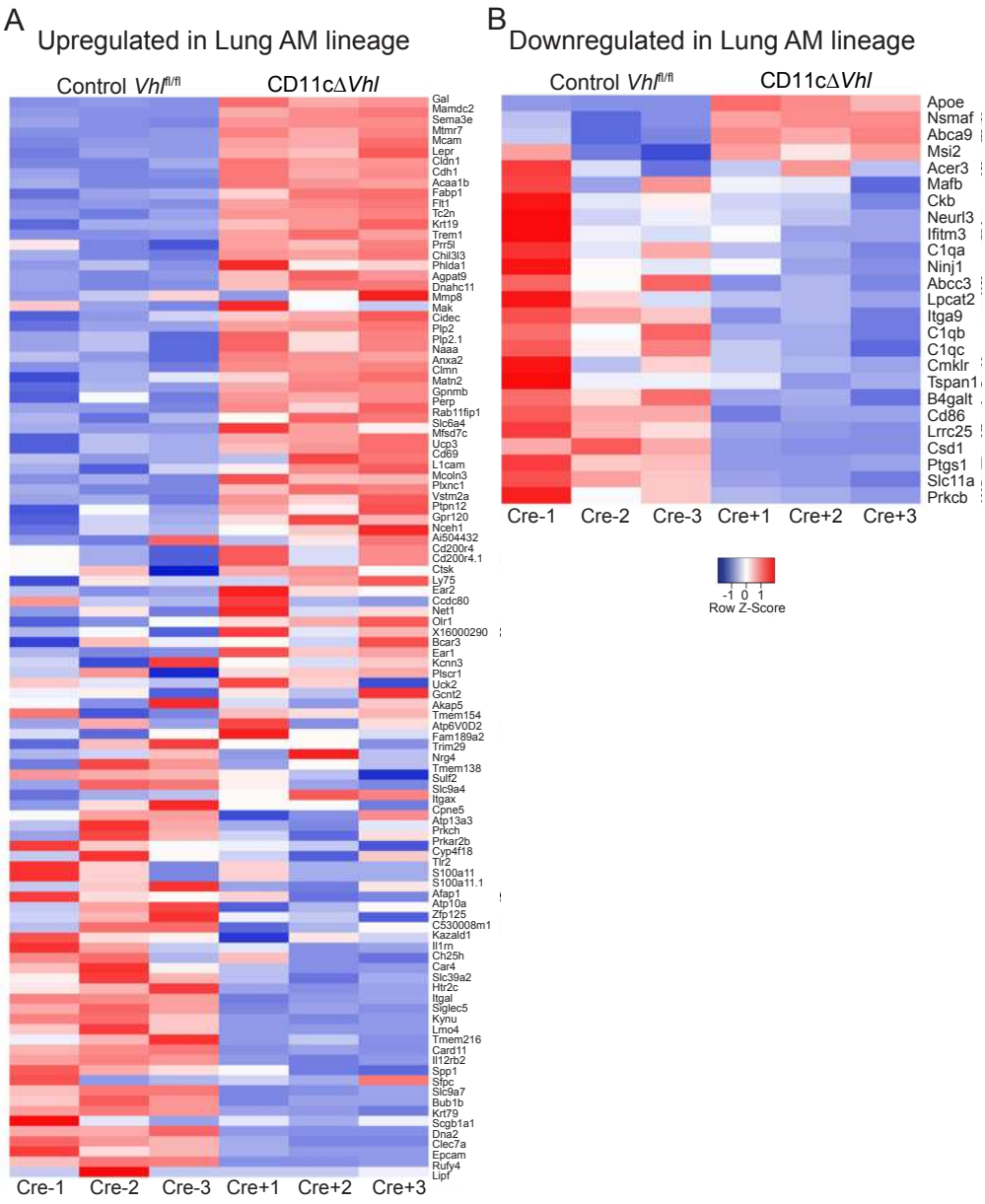

Figure R11. Expression of upregulated genes in lung AM lineage. (A) mRNA expression (Log2 of intensity) of genes from the "signaling-up" gene set in control Vhlfl/fl and CD11cΔVhl AMs. (B) mRNA expression (Log2 of intensity) of genes from the "signaling-down" gene set in control Vhlfl/fl and CD11cΔVhl AMs. Each sample group is composed by three replicates.

Finally, we compared the expression of genes downregulated specifically in lung AMs ("signature-down" genes). We found four of them upregulated: *Apoe* and *Abca9*, implicated in lipid import and metabolism, *Msi2*, a cell cycle regulator and *Nsmaf*, required for TNF-induced cellular responses (Figure R11B). Together, these results indicate that the absence of VHL also affects AM transcriptional identity.

2.5. VHL-deficient AM phenotype is intrinsic.

Access to the alveolar niche is restricted in steady-state conditions, however, blood monocytes can get into the lung alveoli and differentiate into AMs under specific conditions (*12*) (*31*). Thus, the immature like-phenotype of VHL-deficient AMs could be either intrinsic or caused by increased infiltration of monocytes in CD11cΔ*Vhl* mice. To investigate this, we performed surgical parabiosis of CD45.1$^+$ WT mice with either CD45.2$^+$ control *Vhl*$^{fl/fl}$ or CD11cΔ*Vhl* mice (Figure R12A). After 30 days, analysis of peripheral blood in CD45.2$^+$ parabionts revealed equivalent frequencies of CD45.1$^+$ neutrophils and Ly6C^{hi} monocytes in both genotypes (Figure R12B-C). Lung CD45.1$^+$ Ly6C^{hi} monocytes and BAL AMs frequencies were also similar (Figure R12D-E). These results suggest that the immature-like phenotype of VHL-deficient AMs is intrinsic and not a consequence of differential lung infiltration by monocytes.

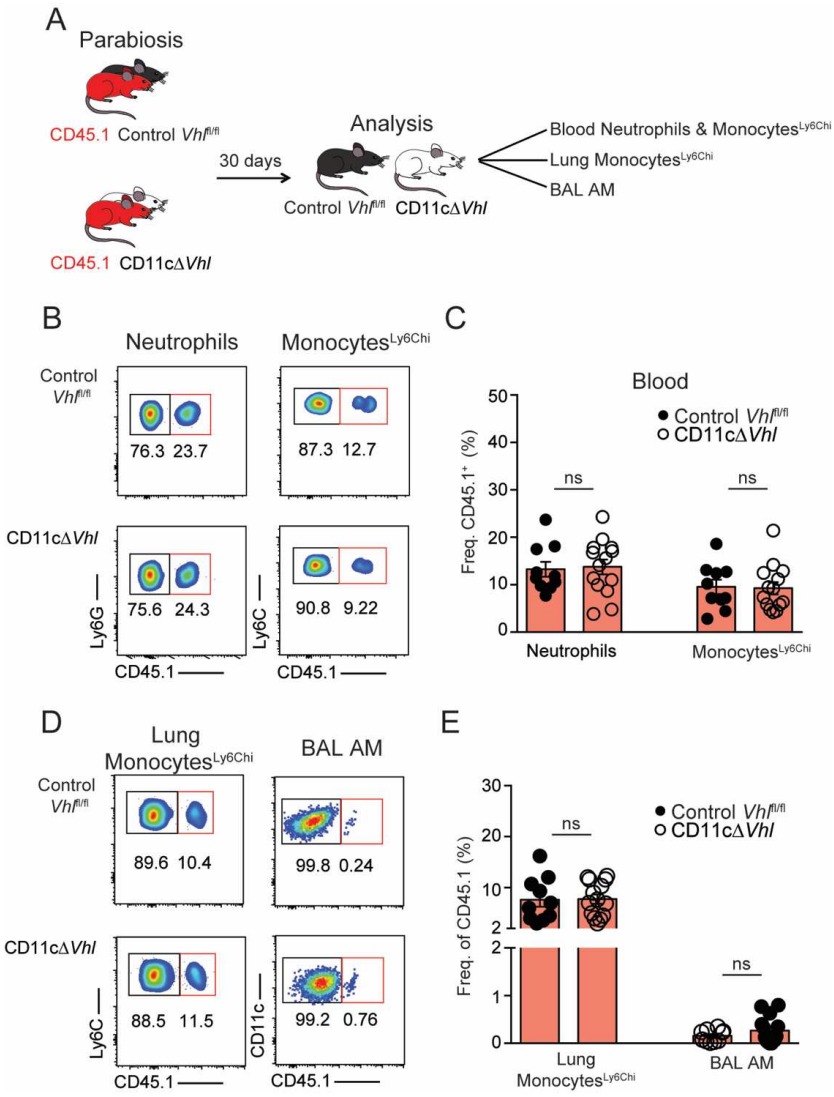

Figure R12. Vhl-deficient AM phenotype is intrinsic. CD45.2 control *Vhl*$^{fl/fl}$ and CD11cΔ*Vhl* mice were surgically joined to CD45.1 mice in parabiosis. Thirty days after surgery, CD45.2 parabionts were analyzed. (A) Scheme of the procedure. (B, C) Representative flow cytometry plots (B) and frequencies of CD45.1$^+$ cells (C) in neutrophils (gated on CD11b$^+$Ly6G$^+$) and Ly6C^{hi} monocytes (gated on CD11b$^+$Ly6C^{hi}) from peripheral blood. (D, E) Representative flow cytometry plots (D) and frequencies of CD45.1$^+$ cells (E) in lung Ly6C^{hi} monocytes (gated on CD45$^+$ Siglec-F$^-$ CD11b$^+$ Ly6C^{hi}) and BAL AMs (gated on Siglec-F$^+$ CD11c$^+$). (C, E) Frequencies shown as mean ± s.e.m. of a pool of three independent experiments performed, where each dot represents an individual mouse (n=10-14 per genotype): ns, not significant (unpaired Student *t*-test).

We next asked whether VHL could also affect the replenishment of AMs after irradiation-induced cytoablation. We generated chimeras by intravenous adoptive transfer of a mixture of bone marrow (BM) cells from CD45.2$^+$ DsRed mice (WT, DsRed$^+$) and CD45.2$^+$ CD11cΔ*Vhl* mice (DsRed$^-$) (or CD45.2$^+$ control *Vhl*$^{fl/fl}$) at a ratio 1:1 into lethally irradiated CD45.1$^+$ WT mice (Figure R13). After 47 days, the frequency of the AM population was analyzed. Most BAL and lung AMs

(after BAL) were of donor origin (CD45.2^{+}) in both types of chimeras at this time point (Figure R13A-B) (*31*). As a control, similar frequencies of lung eosinophils of the different genotypes were found (Figure R13C), suggesting that the potential of progenitors to differentiate into CD11c^{-} cells was not affected. The frequency of CD11cΔ*Vhl* AMs in the BAL of the recipient mice was significantly lower than that of *Vhl*$^{fl/fl}$ AMs, (Figure R13D), and the same result was observed for lung AMs (after BAL) (Figure R13E), consistent with an homogeneous reconstitution. Moreover, BAL CD11cΔ*Vhl* AMs showed an immature-like phenotype compared to WT (DsRed^{+}) AM counterparts (Figure R13F-G) and a significantly decreased expression of Ki67 (Figure R13H-I), suggesting a diminished self-renewal capacity.

In conclusion, VHL-deficient AMs capacity to reconstitute the alveolar niche is decreased in a context of competition with WT AMs. Moreover, our results suggest that the absence of VHL prevents AM terminal phenotypic maturation and restrain AM self-renewal capacity. These findings recapitulate the features found in tissue-resident VHL-deficient AMs derived from embryonic precursors and further support the intrinsic nature of their phenotype.

Results

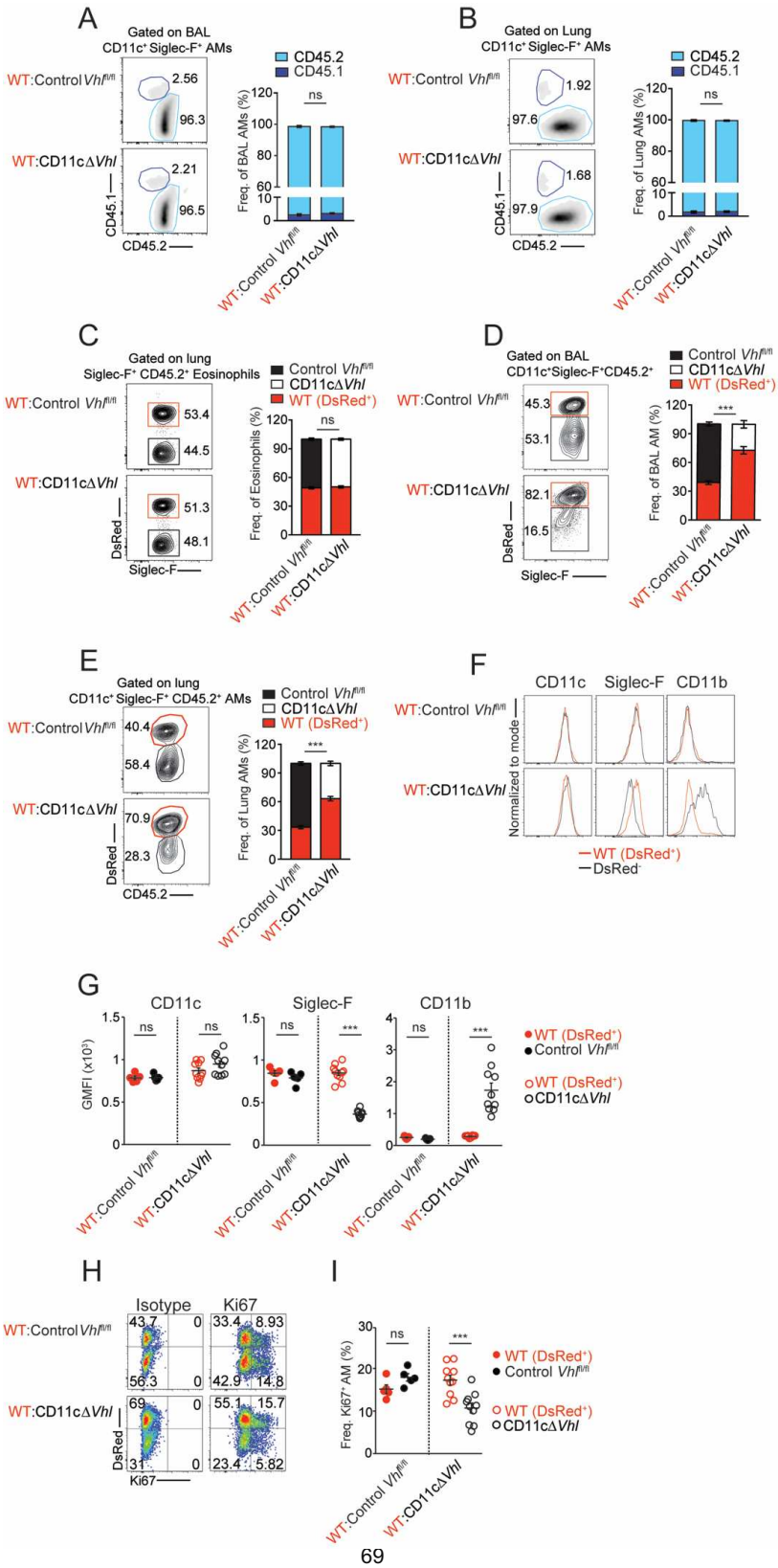
A
Gated on BAL
CD11c+ Siglec-F+ AMs
WT:Control Vhlfl/fl
WT:CD11cΔVhl
2.56
96.3
2.21
96.5
CD45.1
CD45.2
CD45.2
CD45.1
Freq. of BAL AMs (%)
ns
WT:Control Vhlfl/fl
WT:CD11cΔVhl
B
Gated on Lung
CD11c+ Siglec-F+ AMs
1.92
97.6
1.68
97.9
Freq. of Lung AMs (%)
C
Gated on lung
Siglec-F+ CD45.2+ Eosinophils
Control Vhlfl/fl
CD11cΔVhl
WT (DsRed+)
53.4
44.5
51.3
48.1
DsRed
Siglec-F
Freq. of Eosinophils (%)
D
Gated on BAL
CD11c+Siglec-F+CD45.2+
45.3
53.1
82.1
16.5
Freq. of BAL AM (%)
***
E
Gated on lung
CD11c+ Siglec-F+ CD45.2+ AMs
40.4
58.4
70.9
28.3
Freq. of Lung AMs (%)
F
CD11c
Siglec-F
CD11b
Normalized to mode
WT (DsRed+)
DsRed-
G
CD11c
Siglec-F
CD11b
GMFI (x10³)
WT (DsRed+)
Control Vhlfl/fl
WT (DsRed+)
CD11cΔVhl
H
Isotype
Ki67
43.7
0
56.3
0
33.4
8.93
42.9
14.8
69
0
31
0
55.1
15.7
23.4
5.82
I
Freq. Ki67+ AM (%)

Figure R13. Cell intrinsic requirement of VHL for AM terminal maturation and self-renewal. (A-B) Representative flow cytometry plots and frequencies of host CD45.1$^+$ cells and donor CD45.2$^+$ cells in BAL AMs (A) and lung AMs (after BAL) (B) from BM chimeras. (C-E) Representative flow cytometry plots and frequencies of WT(DsRed$^+$) and DsRed$^-$(Control *Vhl*$^{fl/fl}$ or CD11cΔ*Vhl*) cells (normalized to blood Ly6Chi monocyte frequency in each mouse and genotype) in CD45.2$^+$ lung eosinophils (C), BAL AMs (D) and lung AMs (after BAL) (E) from BM chimeras. (A-E) Frequencies shown as mean ± s.e.m. of one experiment of three independent experiments performed (n=5-10 per genotype). ns, not significant; ***p-value<0.001 (ratio paired Student *t*-test). (F) Representative flow cytometry histograms for CD11c, Siglec-F and CD11b (red line for WT DsRed+ AMs or black line for Control Vhlfl/fl or CD11cΔVhl AMs) in BAL AMs from the indicated BM chimera. (G) Normalized GMFI for the selected markers in AMs from the indicated genotypes and chimera. (H-I) Staining of Ki67 in ex vivo BAL AMs of the indicated genotypes from BM chimeras. Representative flow cytometry plots showing the positive staining for Ki67 compared with isotype control of WT(DsRed+) and DsRed-(Control Vhlfl/fl or CD11cΔVhl) AMs in each chimera (H) and frequencies of Ki67+ BAL AMs (I). (G,I) Data shown as mean ± s.e.m. from one representative experiment of two performed (n=5-10 per genotype). Each dot represents the normalized GMFI of an individual mouse (G) and the frequency of Ki67+ BAL AMs (I) (n=5-10 per genotype). ns, not significant; ***p-value<0.001 (ratio paired Student *t*-test).

3. VHL is required to sustain AM physiological functions under steady-state.

3.1. Identification of AM functions altered in the absence of VHL under basal conditions.

RNAseq identified 2531 differentially expressed genes in CD11cΔ*Vhl* AMs relative to control *Vhl*$^{fl/fl}$ and control CD11cCre$^+$ AMs (Figure R14A). Clustering of these genes with Ingenuity Pathway Analysis software revealed several pathways altered by the absence of VHL in AMs (Figure R14B).

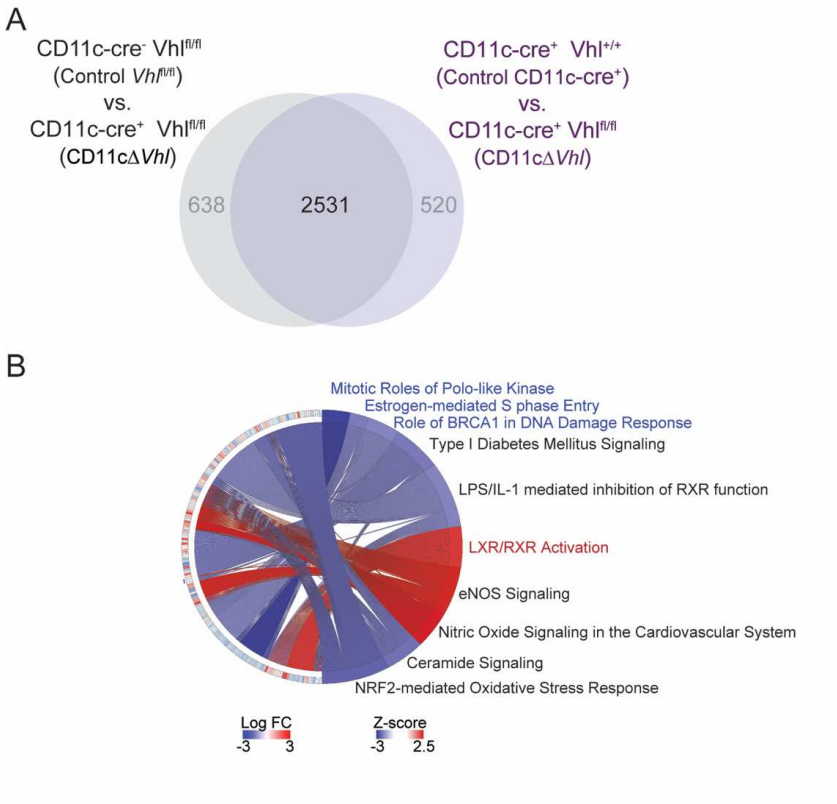

Figure R14. Several functional pathways are altered in VHL-deficient AMs. (A) Venn diagram showing genes differentially expressed in CD11cΔ*Vhl* AMs versus control *Vhl*$^{fl/fl}$ AMs or control CD11c-cre^{+}. (B) Circular plot representing Ingenuity Pathway Analysis of differentially expressed genes from pathways with Z-score > |2| and p-value (-log (B-H p-value)) >2.5 in VHL-deficient AMs (CD11cΔ*Vhl*) versus control *Vhl*$^{fl/fl}$ AMs from BAL.

We validated the expression of selected genes in pathways related to relevant features of AM physiology, such as cell cycle and LXR/RXR activation, implicated in intracellular lipid sensing (Figure R15A and R15B). The absence of VHL in AMs resulted in reduced expression of genes implicated in cell cycle progression, such as those encoding cyclin B1 (*Ccnb1*), cyclin B2 (*Ccnb2)*, CDK1 (*Cdk1*), CD25c (*Cd25c*) and PLK3 (*Plk3*) (Figure R15A, upper panel) and cell cycle control, including BRCA1 (*Brca1*), CHEK1 (*Chek1*), and CHEK2 (*Chek2*), but showing similar expression of the cell cycle master regulators p53 (*Tp53*) and p21 (*Cdkn1a*) (Figure R15A, lower panel). Among those genes clustered in the "LXR/RXR activation" pathway, we confirmed upregulated transcript expression of LXRα (*Nr1h3*) and LXRβ (*Nr1h2*). Accordingly, we confirmed increased expression of genes involved in cholesterol efflux, such as the transporters ABCG1 (*Abcg1*) and apolipoprotein E (*ApoE*) and the lipoprotein-remodeling enzyme PLTP (*Pltp*) (Figure R15B). These results suggest that crucial distinctive features of AMs, such as proliferation and lipid handling, are affected by the absence of VHL.

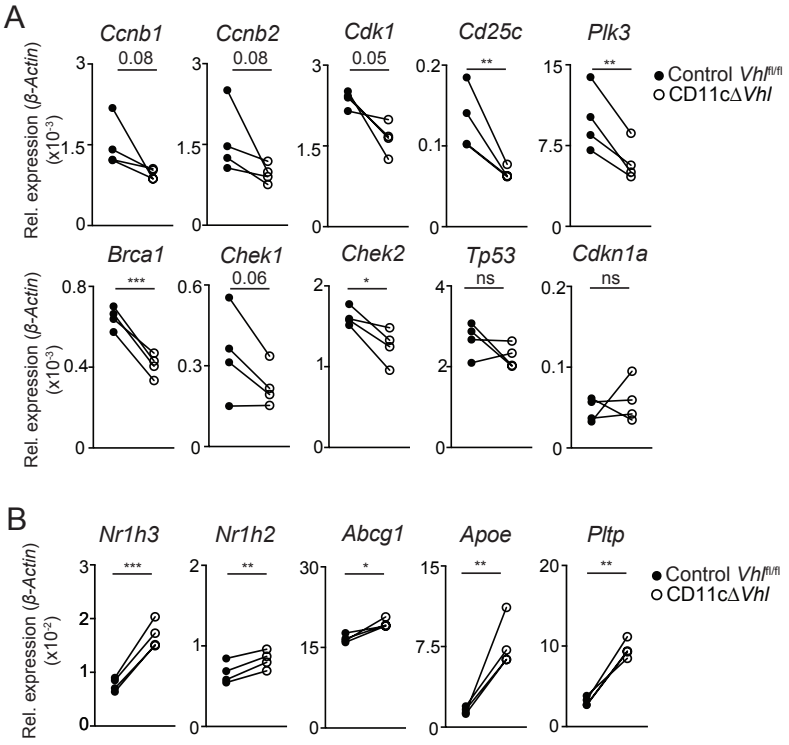

Figure R15. VHL-deficient AMs have an altered gene expression profile. Quantitative PCR of selected differentially expressed genes related to cell cycle (A) and lipid sensing (B), ns, not significant; *, p-value<0.05; **, p-value<0.01; ***, p-value<0.001 (ratio paired Student *t*-test).

3.2. AM self-renewal requires VHL.

Both hypoxia and HIF are able to regulate cell cycle. In cancer cells, HIF leads to cell cycle arrest by counteracting Myc (*121*) and by interacting with MCM DNA helicases (*122*). Thus, to investigate the potential role of VHL in AM self-renewal, we analyzed BAL AMs *ex vivo*. These experiments revealed significantly reduced Ki67 staining in VHL-deficient AMs than in control *Vhl*$^{fl/fl}$ AMs (Figure R16).

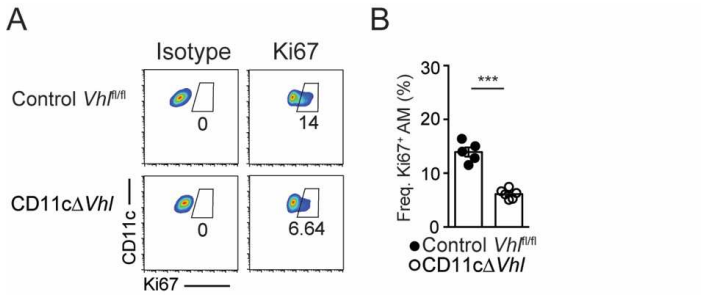

Figure R16. VHL-deficient AMs express less Ki67. Staining of Ki67 in *ex vivo* BAL AMs isolated from the indicated genotypes. Representative flow cytometry plots showing the positive staining for Ki67 compared with isotype control (A) and frequencies of Ki67$^+$ BAL AMs (B). Data are shown as means ± s.e.m. of one experiment of three performed (n=4-5 mice per genotype). ***, p<0.001 (unpaired Student *t*-test).

We next tracked self-renewal *in vivo* by injecting BrdU intraperitoneally every day for three consecutive weeks (Figure R17A). One day after the last pulse, VHL-deficient AMs from BAL showed lower BrdU incorporation than control *Vhl*$^{fl/fl}$ AMs (Figure R17B). In contrast, 21d after the last pulse, BrdU labeling was similar in both genotypes (Figure R17B), which translated into a lower fold dilution of the incorporated BrdU in the absence of VHL (Figure R17C). Despite the reduced turnover in VHL-deficient AMs, AM numbers were similar in both genotypes (Figure R17D), suggesting an improved survival or longer lifespan of Vhl-deficient AMs.

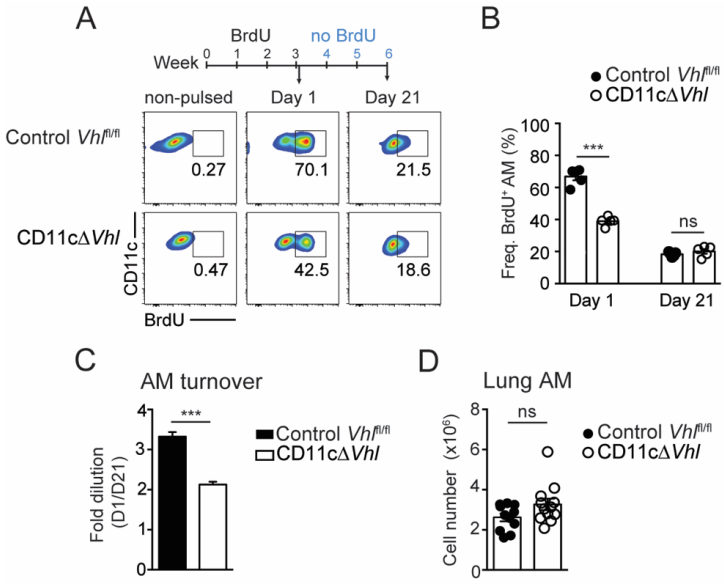

Figure R17. VHL-deficient AMs proliferate less *in vivo*. (A) Mice were pulsed with BrdU for three weeks (1mg i.p. daily), and BrdU incorporation into BAL AMs was assessed 1 and 21 days after the last pulse. Representative flow cytometry plots. (B) Frequencies of BrdU$^+$ AMs. (C) AM turnover calculated as the ratio of the frequency of BrdU$^+$ AMs at day 1 versus day 21. (D) Total lung AM number. Data are shown as individual data points and means ± s.e.m. of one experiment of three performed (n=4-5 mice per genotype) (C) or a pool of two experiments of four performed (n=11-12 per group) (E). ***, p<0.001; ns: not significant (unpaired Student *t*-test).

Results

To investigate whether the absence of VHL affected AM self-renewal capacity in response to specific tissue-derived cytokines that contribute to AM proliferation, we measured BrdU incorporation in BAL AMs cultured *in vitro* in the absence or presence of M-CSF and GM-CSF (*31, 123*) (Figure R18A). Unstimulated AMs retained very low proliferative capacity, and GM-CSF was more potent than M-CSF at inducing AM proliferation, coinciding with a recent report (*33*). VHL-deficient AMs proliferated significantly less than control *Vhl*$^{fl/fl}$ AMs in the absence or presence of these cytokines (Figure R18B). Notably, mature macrophages from tissues different than the lung are inefficient at giving rise to mature AMs when transplanted into mice lacking AMs in the alveoli, and defects in GM-CSF early signaling seem to contribute to this disability (*124*). Thus, we decided to check whether GM-CSF early signaling was affected in the absence of VHL. For this purpose, we stimulated control *Vhl*$^{fl/fl}$ or CD11cΔ*Vhl* AMs with GM-CSF *ex vivo* and measured STAT5 phosphorylation at Y694 residue by immunoblot (Figure R18C). The amount of pY694 compared to total STAT5 was not changed in CD11cΔ*Vhl* AMs compared to control *Vhl*$^{fl/fl}$ AMs both in basal or following GM-CSF treatment (Figure R18D). Taken together, these results show that the absence of VHL leads to a partial self-renewal impairment in steady-state that is not compensated by growth factor treatment.

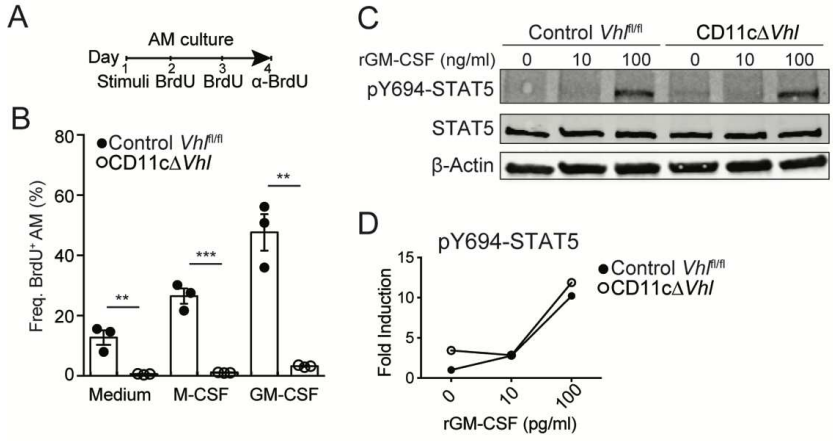

Figure R18. The absence of VHL decreases AM self-renewal potential independently of the stimuli. (A) *In vitro* BrdU assay of AM pools from the indicated genotypes left unstimulated in complete RPMI (medium) or stimulated with rM-CSF (1 ng/ml) or rGM-CSF (10 pg/ml) for 4 days, as indicated. (B) Frequency of BrdU^{+} AM after 4 days. Data shown as means ± s.e.m. of one independent experiment of three performed. Each dot represents a replicate of BAL AMs pooled from 5-6 mice per condition. **, p<0.01; ***, p<0.001; (unpaired Student *t*-test). (C) Immunoblot depicting band intensity corresponding to pY694-STAT5, total STAT5 and β-Actin in lysates of AMs stimulated for 30 min with different doses of rGM-CSF *ex vivo*. (D) Fold induction of STAT5 phosphorylation. Band intensities of pY694-STAT5 were normalized to total STAT5. Fold induction was calculated as a ratio of normalized pY694-STAT5 for each condition, into control *Vhl*$^{fl/fl}$ AMs unstimulated.

In order to find any evidence that the impaired self-renewal capacity of VHL-deficient AMs was affected by an oxygen-dependent mechanism regulated by VHL, we measured BrdU

incorporation in AMs exposed at 21% or 1% of O_2 and stimulated as in Figure 18B (Figure R19A). We observed that AM proliferation was impaired compared with AM cultured at normoxia, both under basal conditions and after GM-CSF or M-CSF stimulation (Figure R19B).

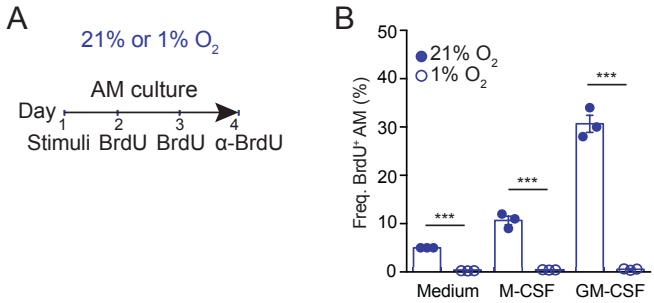

Figure R19. Hypoxia impairs AM self-renewal *ex vivo*. (A) *In vitro* BrdU assay of WT AM left unstimulated in complete RPMI (medium) or stimulated with rM-CSF (1 ng/ml) or rGM-CSF (10 pg/ml) for 4 days in normoxia or at 1% of O_2. (B) Frequency of $BrdU^+$ AM after 4 days. Data shown as means ± s.e.m. of one independent experiment of three performed. Each dot represents a replicate of BAL AMs pooled from 5-6 mice per condition. ***, p<0.001; (unpaired Student *t*-test)

Taken together, our results indicate that VHL is required to sustain the full self-renewal potential of AMs *in vivo*. Hypoxia mimics the inhibition in self-renewal *ex vivo* found in VHL-deficient AMs, suggesting that HIF interferes with AM proliferative capacity.

3.3. VHL contributes to AM surfactant handling capacity.

Mice deficient for *Csf2* (GM-CSF) or *Csf2r* or with *Pparγ* deleted in AMs show impaired AM maturation, resulting in low numbers of lung immature AMs that accumulate lipids intracellularly (*22, 41, 42*). Interestingly, LXR pathway, implicated in intracellular lipid sensing, was predicted to be more active in VHL-deficient AMs, (Figure R14B) and indeed, the expression of LXR-target genes implicated in lipid efflux was significantly increased in VHL-deficient AMs (Figure R15B).

Since we had realized that CD11cΔ*Vhl* AMs were more granular than control $Vhl^{fl/fl}$ (Figure R8A and R8B), we stained AMs with oil red in order to assess whether this was due to an accumulation of lipids (Figure R20A). Although we did not observe the formation of foam cells in the absence of VHL, we observed more oil red positive cells in cytospins of VHL-deficient AM than in control $Vhl^{fl/fl}$ AM samples (Figure R20A).

We then compared the expression of genes whose expression has been found to be up- or down-regulated by intracellular lipid accumulation in PPARγ-deficient AMs, that are impaired in surfactant removal and become foamy, leading to lung proteinosis (*118*). Interestingly, we found the same pattern of expression of these genes in CD11cΔ*Vhl* AMs and PPARγ-deficient AMs, compared to control $Vhl^{fl/fl}$ AMs, supporting that the absence of VHL leads to an increased lipid accumulation in AMs (Figure 20B).

Next, we quantified the lipid β-oxidation capacity of AMs by measuring the oxygen consumption rate of BAL AMs in the presence of palmitoyl-CoA as exclusive carbon source (Figure 20C-D). The basal respiration rate was significantly lower in AMs lacking VHL, indicating a reduced lipid oxidation capacity (Figure R20D), whereas the basal extracellular acidification rate was unaltered, confirming that cells were deprived of glucose and the oxygen consumption was only due to fatty acid oxidation (FAO) (Figure 20E).

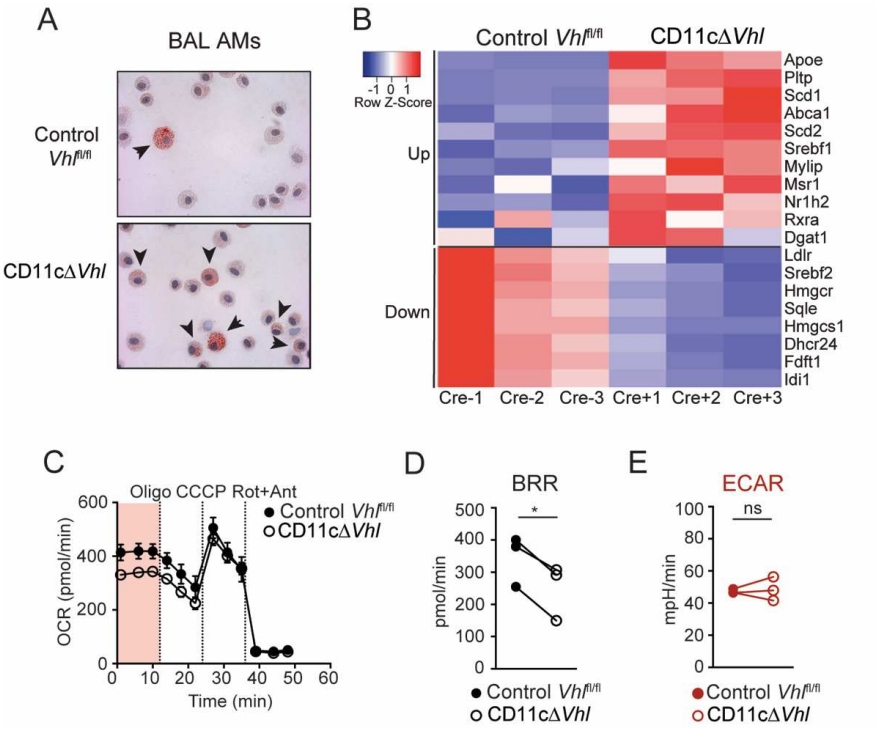

Figure R20. The absence of VHL decreases AM self-renewal potential independently of the stimuli. (A) Oil red staining of BAL AMs from the indicated genotypes, bars 50μm. Representative images of one experiment of three performed. (B) mRNA expression (Log_2 of intensity) of genes regulated by intracellular lipid accumulation in control *Vhl*$^{fl/fl}$ and CD11cΔ*Vhl* AMs. "up" and "down" refers to genes whose expression is upregulated or downregulated upon intracellular accumulation of lipids, respectively. Each sample group is composed by three replicates. (C) Oxygen consumption rate (OCR) in the presence of palmitoyl Co-A by BAL AMs from the indicated genotypes treated as in Figure R7. Data are means ± s.d. using AMs pooled from 6-7 mice per genotype in a representative experiment of three performed. (D) Analysis of basal respiratory rate (BRR) in AMs measured as in A. (E) Basal extracellular acidification rate (ECAR) in BAL AMs from the indicated genotypes. (D,E) Paired independent experiments (AMs pooled from 6-7 mice per experiment): *, p<0.05. ns, not significant (ratio paired Student *t*-test).

We then compared the expression of genes implicated in different pathways related to lipid metabolism. We observed that the expression of all genes implicated in lipid import was upregulated in CD11cΔ*Vhl* AMs compared to control CD11cΔ*Vhl* AMs (Figure R21A). Among them, *Fabp4* and *Cd36* are well-known targets of PPARγ (*125*), suggesting that this transcription factor was more active in the absence of VHL. Indeed, we confirmed the increased expression of *Pparγ* and its target genes in CD11cΔ*Vhl* AM by qPCR (Figure R21B), correlating with published data indicating HIF-1 targets PPARγ and induces its expression (*125*).

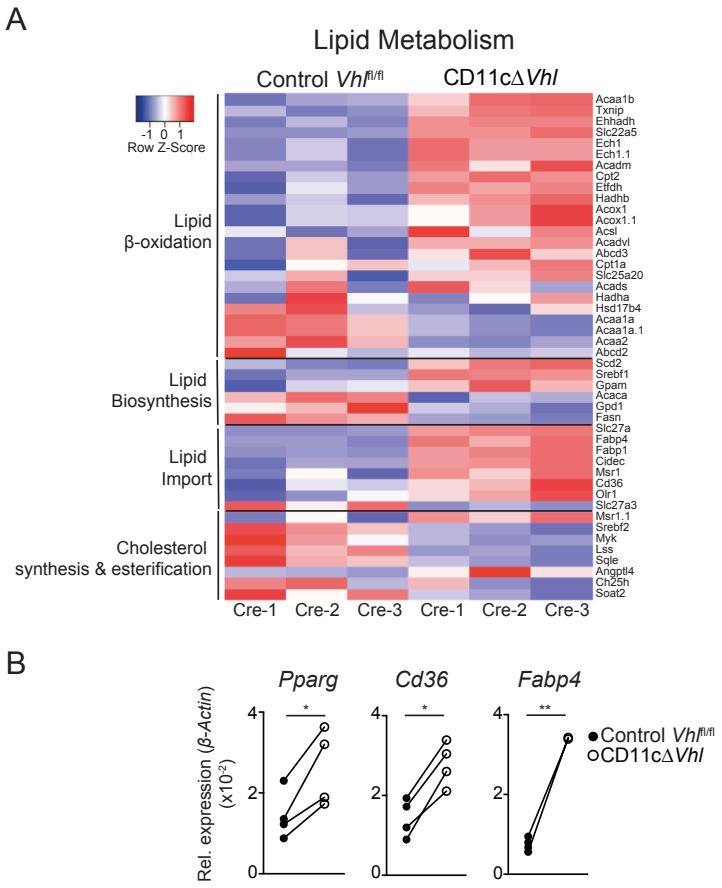

Figure R21. Expression of genes related to lipid metabolism in VHL-deficient AMs. (A) mRNA expression (Log_2 of intensity) of genes implicated in different pathways related to lipid metabolism in control *Vhl*$^{fl/fl}$ and CD11cΔ*Vhl* AMs. Each sample group is composed by three replicates ratio paired Student *t*-test. (B) Quantitative PCR of *Pparg*, *Cd36* and *Fabp4*. *p-value<0.05; **p-value<0.01; (ratio paired Student *t*-test).

Strikingly, 3-month-old CD11cΔ*Vhl* mice did not show increased accumulation of total protein in bronchoalveolar lavage (BAL) supernatants (not shown), in contrast with other models of impaired AM function. However, we cannot rule out that older CD11c-Cre+ *Vhl*$^{fl/fl}$ mice develop some degree of proteinosis. To determine whether the decreased ability to oxidize lipids of VHL-deficient AMs affected their potential to degrade surfactant *in vivo*, we transplanted a limited amount of AMs from BAL of CD11cΔ*Vhl* or control *Vhl*$^{fl/fl}$ mice into *Csf2rb*$^{-/-}$ mice, which lack mature AMs and spontaneously develop lung proteinosis (Figure R22) (*42*). As a marker of disease severity, we measured total protein and surfactant protein D concentrations in BAL supernatants at 1.5 months after pulmonary macrophage transplantation (Figure R22A), a time point at which transferred WT AMs had removed surfactant nearly to the levels found in healthy mice (Figure R22C-D) (*46, 47*). Consistent with our earlier results (Figure R17D), AM engraftment in the lung was similar in both genotypes (Figure R22B). Transplanted AMs from CD11cΔ*Vhl* mice

were less efficient than control *Vhl*$^{fl/fl}$ AMs at reversing surfactant accumulation in *Csf2rb*$^{-/-}$ recipient mice BAL (Figure R22C and R22D).

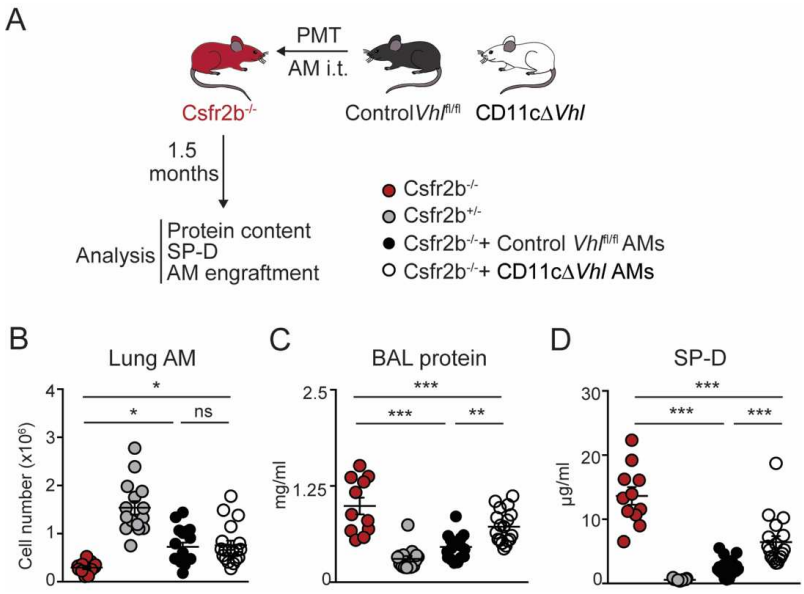

Figure R22. VHL contributes to the surfactant removal capacity of AMs. (A-D) 5x10^4 AMs from control *Vhl*$^{fl/fl}$ or CD11cΔ*Vhl* AMs were transferred intratracheally (i.t.) to *Csfr2b*$^{-/-}$ mice. After 1.5 months, AMs from total lung were counted (B) and BAL concentrations of total protein (C) and SP-D (D) were measured. Data are shown as individual data points and means ± s.e.m. of a pool of three independent experiments. Control mice (*Csfr2b*$^{-/-}$ and *Csfr2b*$^{+/-}$) are from four independent experiments (n=10-18 per group): ns, not significant; *, p-value<0.05; **, p-value<0.01; ***, p-value<0.001 (one-way ANOVA, Bonferroni post-hoc test).

Csf2rb$^{-/-}$ mice lack mature AMs and have in turn, few immature and foamy cells in the AM compartment. We observed that while maintaining high levels of CD11c, these cells expressed less Siglec-F than mature AMs found in healthy *Csf2rb*$^{+/-}$ heterozygous mice (Figure R23, see *Csf2rb*$^{-/-}$ and *Csf2rb*$^{+/-}$). After pulmonary macrophage transplantation (PMT), mice transferred with control *Vhl*$^{fl/fl}$ AMs showed a Siglec-F^{hi} and a Siglec-F^{lo} population, the last one likely corresponding to the resident immature cell population (Figure R23, *Csf2rb*$^{-/-}$ + control *Vhl*$^{fl/fl}$). In contrast, mice transferred with CD11cΔ*Vhl* AMs had an homogeneous Siglec-F^{lo} AM population, correlating with the immature-like phenotype of transferred cells, that likely accumulated intracellular surfactant (Figure R23, see *Csf2rb*$^{-/-}$ + CD11cΔ*Vhl* AMs).

These results suggest that VHL contributes to mitochondrial oxidation of lipids by AMs and to their capacity to clear pulmonary surfactant *in vivo*.

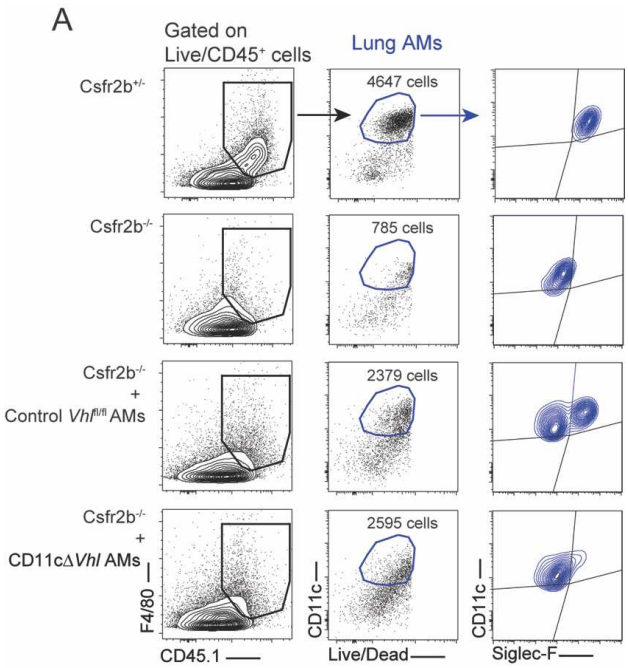

Figure R23. AM phenotype after PMT. (A) Representative plots depicting strategy of gating and lung AM phenotype in *Csf2rb*$^{-/-}$, control heterozygous *Csf2r*$^{+/-}$ and *Csf2rb*$^{-/-}$ mice after PMT. First, live CD45^{+} cells were gated, then F4/80^{+} cells were selected excluding DCs and lymphoid cells. The CD11c^{+} compartment, corresponding to AMs in healthy mice was analysed for Siglec-F expression level.

4. HIF-1 and HIF-2 transcription factors differentially contribute to AM function in the absence of VHL.

In order to address whether the phenotypic and functional changes observed in CD11cΔ*Vhl* AMs were dependent on HIF, and to dissect the differential contribution of HIF-1 and HIF-2, we generated CD11c-Cre^{+} *Vhl*$^{fl/fl}$*Hif1α*$^{fl/fl}$ (CD11cΔ*Vhl*Δ*Hif1α*), CD11c-Cre^{+} *Vhl*$^{fl/fl}$ *Hif2α*$^{fl/fl}$ (CD11cΔ*Vhl*Δ*Hif2α*) and CD11c-Cre^{+} *Vhl*$^{fl/fl}$*Hif1α*$^{fl/fl}$*Hif2α*$^{fl/fl}$ (CD11cΔ*Vhl*Δ*Hif1α*Δ*Hif2α*) mice.

4.1. Genetic characterization of *Vhl*, *Hif1α* and *Hif2α* deletion in AMs.

First, we measured the transcriptional expression of *Vhl*, *Hif1α*, *Hif2α* and their specific target genes in AMs from CD11cΔ*Vhl*Δ*Hif1α*, CD11cΔ*Vhl*Δ*Hif2α* and CD11cΔ*Vhl*Δ*Hif1α*Δ*Hif2α* mice and their control littermates (Figure R24). We confirmed that *Vhl* and *Hif1α* expression was blunted in CD11cΔ*Vhl*Δ*Hif1α* and CD11cΔ*Vhl*Δ*Hif1α*Δ*Hif2α*, compared to control AMs. *Hif1α* expression was also downregulated in CD11cΔ*Vhl*Δ*Hif2α* AMs, compared to control AMs, suggesting transcriptional control of *Hif1α* by *Hif2α*. In contrast, *Hif2α* expression was specifically reduced in CD11cΔ*Vhl*Δ*Hif2α* and CD11cΔ*Vhl*Δ*Hif1α*Δ*Hif2α* AMs (Figure R24A).

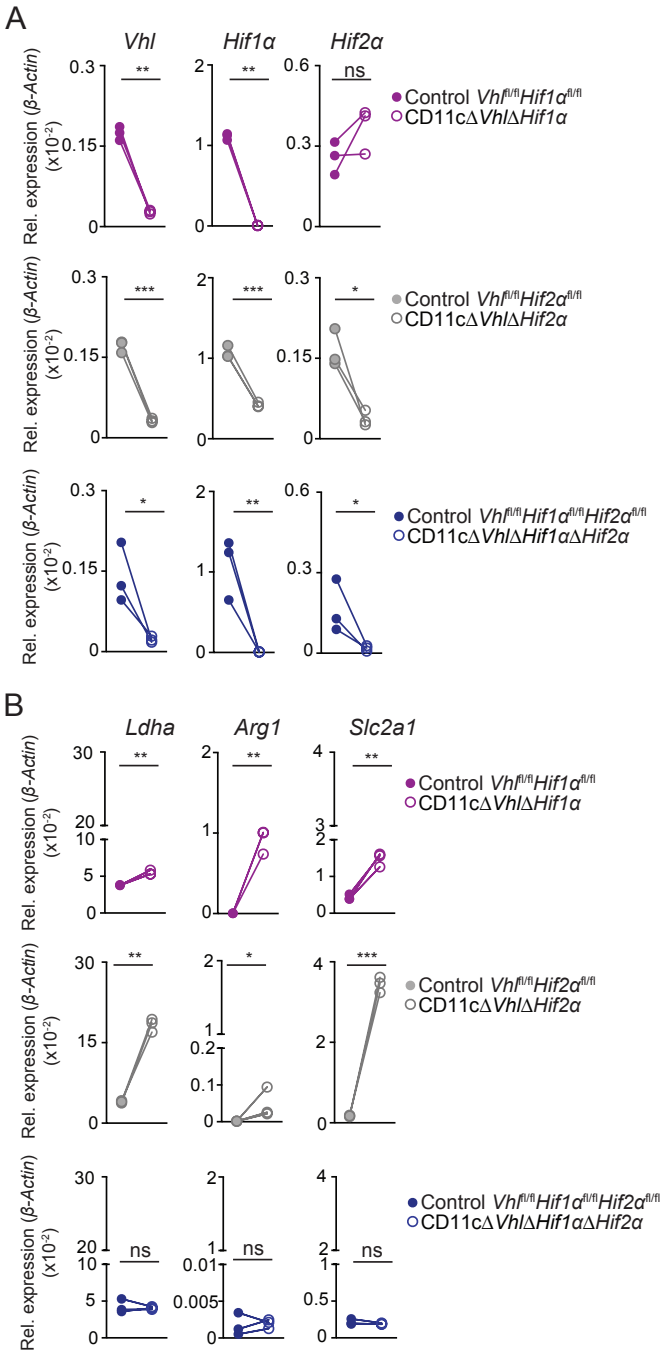

Figure R24. Genetic characterization of *Vhl*, *Hif-1α* and *Hif-2α* deletion in AMs. Quantitative PCR for the expression of *Vhl*, *Hif-1α* and *Hif-2α* (A) and *Ldha*, *Arg1* and *Slc2a1* (B) in sorted BAL AMs from mice of the indicated genotypes. Individual dots correspond to three independent experiments, with AMs from 4-5 pooled mice per experiment: ns, not significant; *, p-value<0.05; **, p-value<0.01; ***, p-value<0.001 (ratio paired Student *t*-test).

Next, we measured the expression of HIF-target genes (Figure R24B). We found that the expression of *Ldha* was slightly but significantly increased in CD11cΔ*Vhl*Δ*Hif1α* and on a larger scale in CD11cΔ*Vhl*Δ*Hif2α* AMs, suggesting that despite expressing less *Hif1α* than control counterparts, HIF-1 is more active in CD11cΔ*Vhl*Δ*Hif2α* AMs than in control *Vhl*$^{fl/fl}$*Hif2α*$^{fl/fl}$ AMs. We observed that *Arg1* expression was significantly induced in CD11cΔ*Vhl*ΔHif1α and also slightly in CD11cΔ*Vhl*Δ*Hif2α* AMs, despite having a lower expression of *Hif2α* compared to control *Vhl*$^{fl/fl}$*Hif2α*$^{fl/fl}$ AMs. Finally, we compared the expression of *Slc2a1*, and we found that it was significantly increased in both CD11cΔ*Vhl*Δ*Hif1α* and CD11cΔ*Vhl*Δ*Hif2α* AMs. Notably, no difference in expression was detected in any of these target genes in CD11cΔ*Vhl*Δ*Hif1α* Δ*Hif2α* AMs compared with control *Vhl*$^{fl/fl}$*Hif1α*$^{fl/fl}$*Hif2α*$^{fl/fl}$ AMs, indicating that their expression changes upon *Vhl* deletion relied entirely on either HIF-1 and/or HIF-2.

4.2. HIF-1 and HIF-2 control the metabolic profile of VHL-deficient AMs.

Consecutively, we analyzed the metabolic profile of the different genotypes in order to evaluate whether the differential expression of glycolytic genes translated into functional changes in their metabolism (Figure R25).

Relative to the metabolic profile observed in CD11cΔ*Vhl* AMs compared to their control counterparts (Figure R7), the additional deletion of *Hif1α* in CD11cΔ*Vhl*Δ*Hif1α* AMs only restored AM BRR (Figure R25A-B) and basal ECAR (Figure R25C-D) partially, correlating with the slight but significant increased levels of *Ldha* and *Slc2a1* still observed in CD11cΔ*Vhl*Δ*Hif1α* AMs (Figure R24B, upper panel). In contrast, the additional deletion of *Hif2α* did not restore BRR (Figure R25E-F) and ECAR (Figure R25G-H) in CD11cΔ*Vhl*Δ*Hif2α* AMs, thus resembling CD11cΔ*Vhl* AMs.

Taken together, these results suggest that although HIF-2 is able to induce certain degree of metabolic switch towards glycolysis, HIF-1 is more potent at desensitizing AMs to oxygen and at increasing their glycolytic capacity in the absence of VHL.

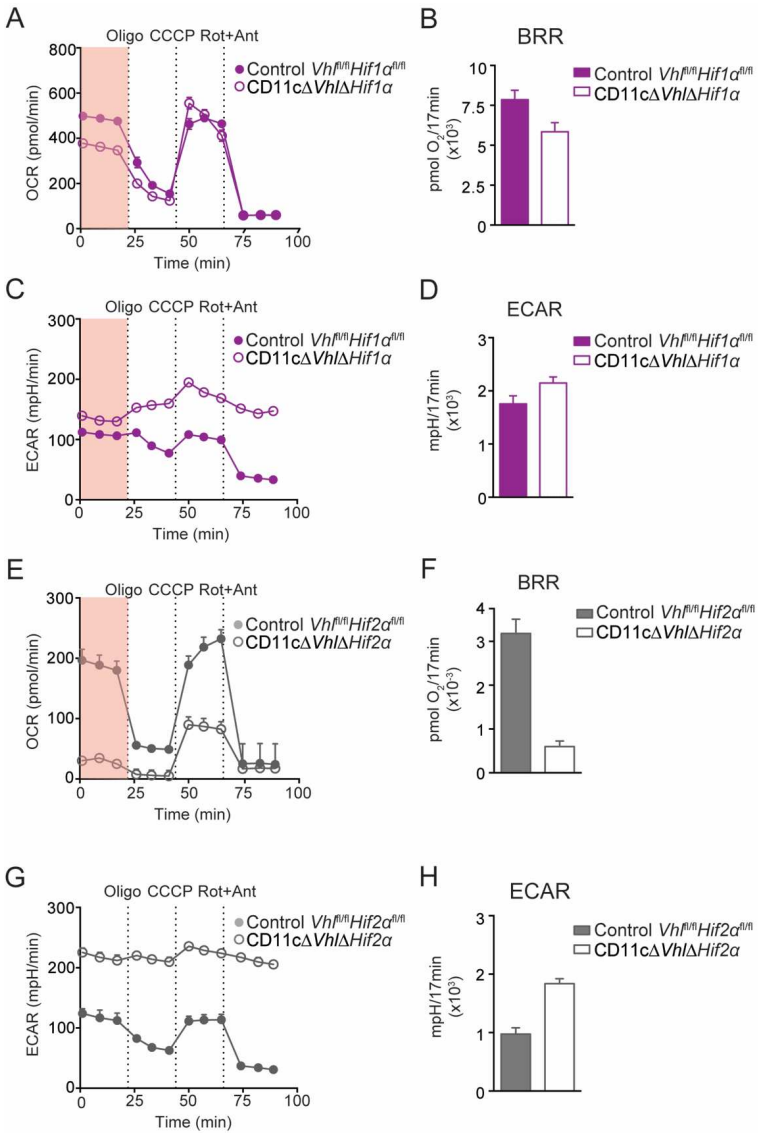

Figure R25. Metabolic characterization of CD11cΔ*Vhl*Δ*Hif1α* and CD11cΔ*Vhl*Δ*Hif2α* AMs. (A,E) Oxygen consumption rate (OCR) in the presence of glucose, glutamine and pyruvate by BAL AMs from the indicated genotypes sequentially treated as in R7. Data are means ± s.d. using AMs pooled from 6-7 mice per genotype in a representative experiment of two performed. (B,F) Basal respiratory rate (BRR) in AMs measured as in A. (C,G) Extracellular acidification rate (ECAR) measured in the same assay as A. (D,H) Basal extracellular acidification rate (ECAR) in AMs from the indicated genotypes. (B,D,F,H) Mean ± s.d of 5-10 replicates of AMs pooled from 6-7 mice per experiment. Representative experiment of two performed.

4.3. Deletion of both HIF-1 and HIF-2 is required to restore mature phenotype and self-renewal potential in VHL-deficient AMs.

VHL has other target genes besides HIF transcription factors (*58, 59*). To address whether any of the phenotypic and functional changes that we observed in CD11cΔ*Vhl*Δ AMs depend on

HIF transcription factors, we measured the expression of classical AM markers at the mRNA (Figure R26) and protein level (Figure R27) in AMs of the different genotypes. We observed that deletion of *Hif1α* and *Hif2α* only restored WT levels of *Itgam* and *Siglec5* expression, respectively. In contrast, deletion of both *Hif1α* and *Hif2α* completely restored the mature AM phenotype (Figure R26A). Interestingly, the comparison of the magnitude of change in expression of all markers in the different AM genotypes unveiled that those markers whose expression was significantly changed upon deletion of *Hif1α* or *Hif2α*, were in fact partially restored when compared with CD11cΔ*Vhl*Δ AMs (Figure R26B).

Then, we assessed by flow cytometry whether changes in mRNA expression correlated with the protein level for each marker. We found that compared to control $Vhl^{fl/fl}Hif1\alpha^{fl/fl}$ AMs, CD11cΔ*Vhl*Δ*Hif1α* AMs expressed increased levels of CD11b, and decreased levels of CD11c, Siglec-F and CD64, highly resembling CD11cΔ*Vhl* AMs. In contrast, CD11cΔ*Vhl*Δ*Hif2α* AMs expressed increased CD11b and decreased CD64 compared to control $Vhl^{fl/fl}Hif2\alpha^{fl/fl}$ AMs, correlating with mRNA expression. Finally, the expression level of all surface markers also correlated with mRNA expression in CD11cΔ*Vhl*Δ*Hif1α*Δ*Hif2α* AMs, showing slight but significant increased levels of CD11c and CD64. However, given the minimal magnitude of these changes, statistical significance does not seem to reflect real changes in the expression of these markers (Figure R27A). Correlating with mRNA expression results, the surface marker expression fold change allowed us to compare the magnitude of change with that observed in CD11cΔ*Vhl*Δ AMs, revealing that only deletion of both *Hif1α* and *Hif2α* fully restored mature AM phenotype (Figure R27B).

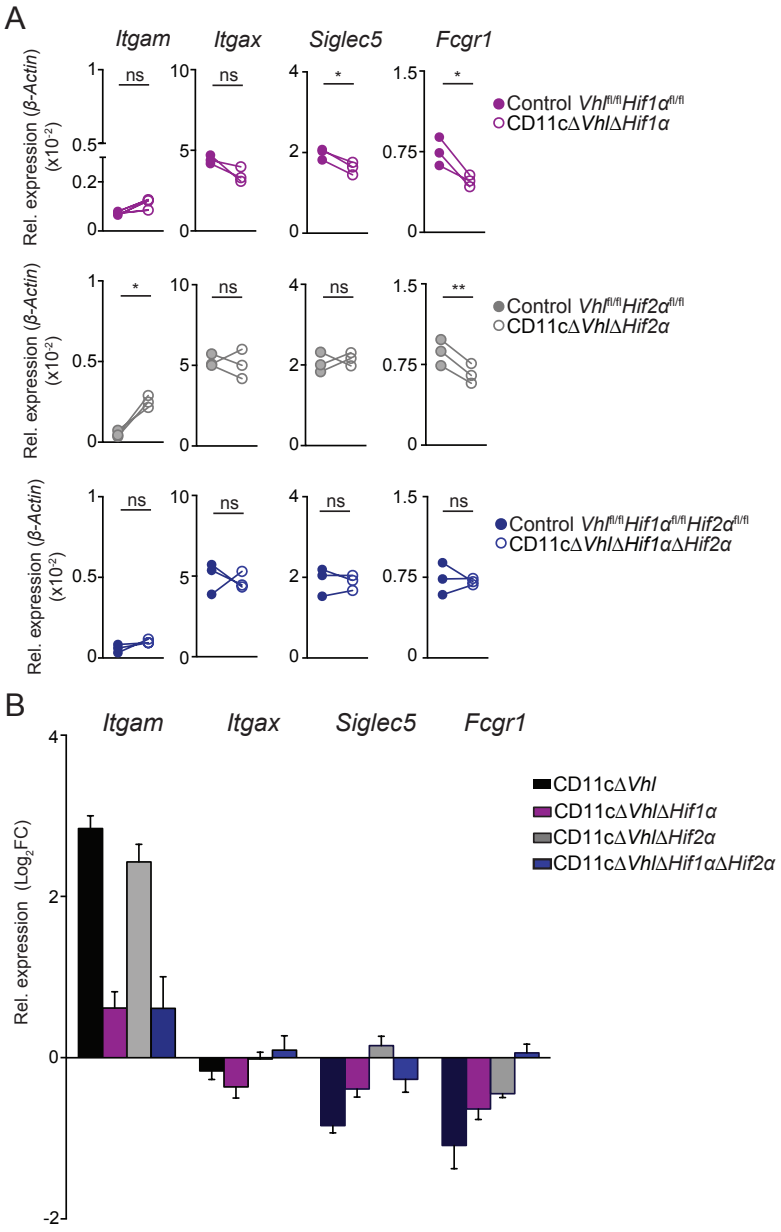

Figure R26. Deletion of both *Hif1α* and *Hif2α* fully restores mRNA levels of surface markers associated with mature AMs. (A) Quantitative PCR for the expression of *Itgam, Itgax*, *Siglec5* and *Fcgr1* in sorted BAL AMs from mice of the indicated genotypes. Individual dots correspond to three independent experiments, with AMs from 4-5 pooled mice per experiment: ns, not significant; *, p-value<0.05; **, p-value<0.01 (ratio paired Student *t*-test). (B) Normalized mRNA expression for the selected markers in AMs from the indicated genotypes. Data expressed as Log_2FC; Fold change (FC) refers to the ratio of expression of each marker for each genotype into its control counterpart. Data shown as mean ± s.e.m. from one representative experiment of three performed.

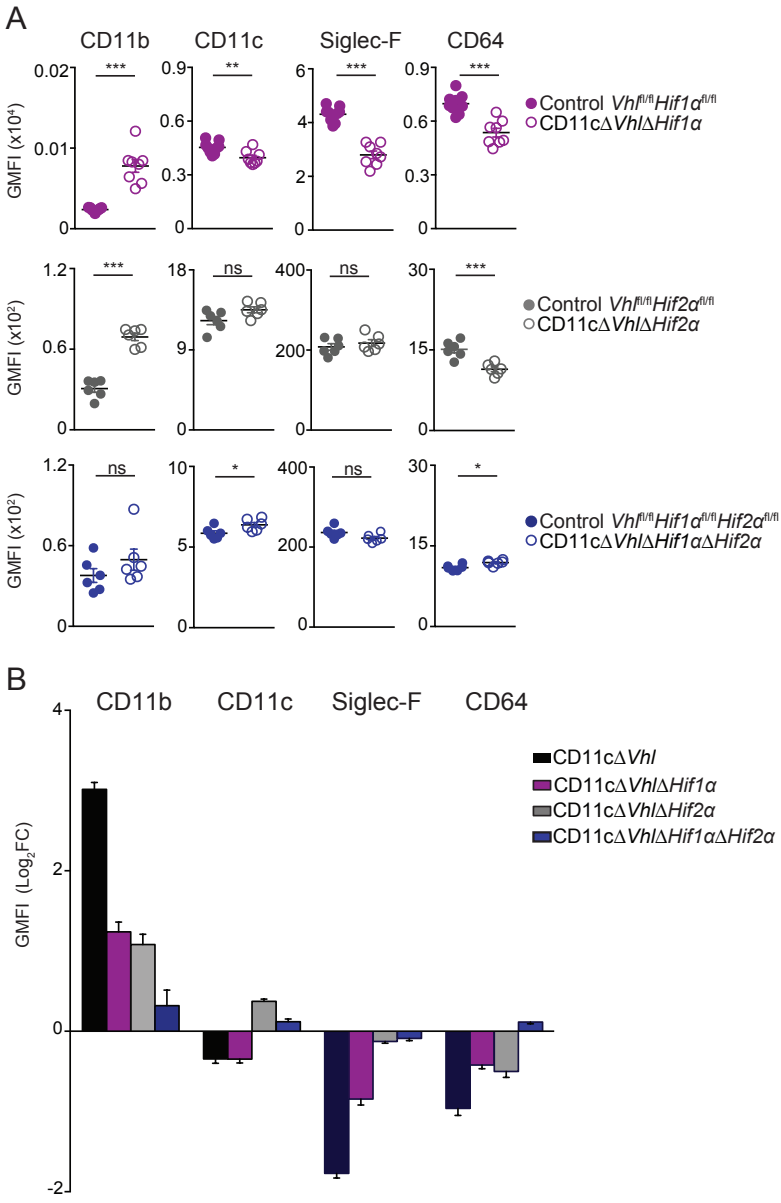

Figure R27. Deletion of both *Hif1α* and *Hif2α* fully restores mature AM surface marker expression. (A) Normalized geometric mean fluorescence intensity (GMFI) for the selected markers in AMs from the indicated genotypes. Data shown as mean ± s.e.m. from one representative experiment of three performed. Each dot represents the normalized GMFI of an individual mouse (n=6-7 per genotype): ns, not significant; *, p-value<0.05; **, p-value<0.01; ***, p-value<0.001 (unpaired Student *t*-test). (B) Normalized expression for the selected markers in AMs from the indicated genotypes. Data expressed as Log_2FC GMFI; Fold change (FC) refers to the ratio of expression of each marker for each genotype into its control counterpart. Data shown as mean ± s.e.m. from one representative experiment of three performed.

In renal carcinoma cells, it has been demonstrated that HIF-2 induces proliferation while HIF-1 acts rather as a cell cycle repressor, both acting at different levels on c-Myc (*105*). In

addition, VHL can directly interact with p53, being potentially able to arrest cell cycle (*126*) and also affects microtubules stability, which could affect mitosis (*127, 128*). Thus, in order to evaluate whether the decreased self-renewal potential of CD11cΔ*Vhl* AMs was dependent on HIF, we stained nuclear Ki67 in BAL AMs of each genotype (Figure R28). We found that the frequency of Ki67$^+$ CD11cΔ*Vhl*Δ*Hif1α* and CD11cΔ*Vhl*Δ*Hif2α* AMs was significantly lower than their control counterparts (Figure R28A-D). However, deletion of both *Hif1α* and *Hif2α* restored WT levels of Ki67 expression in CD11cΔ*Vhl Hif1α*Δ*Hif2α* AMs (Figure R28E-F).

Taken together, these results show that in the absence of VHL, both immature-like phenotype and impaired self-renewal ability depend on HIF-1 and HIF-2, and deletion of both transcription factors is required to restore these features.

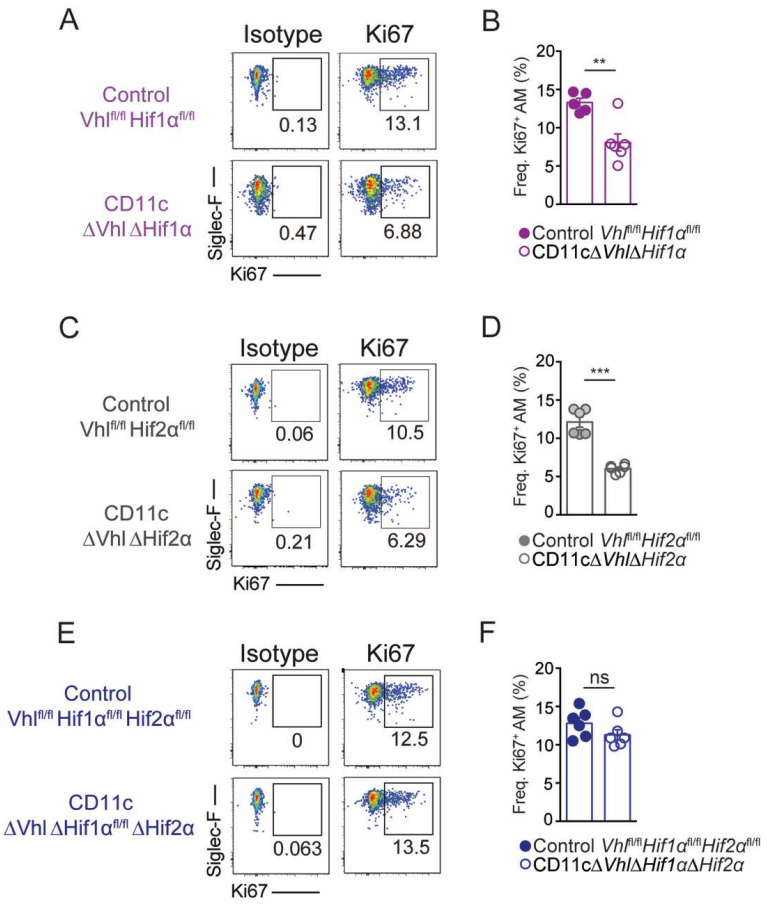

Figure R28. Deletion of both *Hif1α* and *Hif2α* fully restores Ki67 expression in VHL-deficient AM. Staining of Ki67 in *ex vivo* BAL AMs isolated from the indicated genotypes. Representative flow cytometry plots showing the positive staining for Ki67 compared with isotype control (A, C, E) and frequencies of Ki67$^+$ BAL AMs (B, D, F). Data are shown as means ± s.e.m. of one experiment of three performed (n=6 mice per genotype). ns, not significant; **, p-value<0.01; ***, p-value<0.001 (unpaired Student *t*-test).

4.4. HIF-2 mediates the impairment in surfactant removal by VHL-deficient AM.

Several reports have linked HIF-1 and hypoxia to the formation of foam cells (*100*) by enhancing lipid uptake in macrophages (*101*). In addition, HIF-1 can also promote lipid synthesis (*105*) and decrease the overall cellular fatty acid oxidation rate (*109*). In contrast, fewer reports link HIF-2 to lipid accumulation, being described as a regulator of lipid metabolism in hepatic cells (*108*) and renal carcinoma cells (*107*).

To elucidate whether the decreased surfactant handling ability of VHL-deficient AMs relied on HIF activity, we performed PMT of CD11cΔ*Vhl*Δ*Hif1α* or CD11cΔ*Vhl*Δ*Hif2α* BAL AMs into *Csfr2b*$^{-/-}$ mice and compared their efficiency at removing surfactant as previously performed (Figure R22). After 1.5 months, we observed that CD11cΔ*Vhl*Δ*Hif1α* and CD11cΔ*Vhl*Δ*Hif2α* AM lung engraftment was equivalent to that observed in their control counterparts (Figure R29A-B). However, the absence of *Hif1α* was not enough to restore homeostasis, since transplanted CD11cΔ*Vhl*Δ*Hif1α* AMs were less efficient than control *Vhl*$^{fl/f}$*Hif1α*$^{fl/fl}$ AMs at reversing surfactant accumulation in BAL of *Csf2rb*$^{-/-}$ recipient mice (Figure R29A). In contrast, transplanted CD11cΔ*Vhl*Δ*Hif2α* AMs were as efficient as control *Vhl*$^{fl/fl}$*Hif2α*$^{fl/fl}$ AMs at surfactant clearance, as evidenced by the similar levels of BAL total protein and SP-D found in lungs of *Csf2rb*$^{-/-}$ recipient mice transplanted with both genotypes (Figure R29B).

These results suggest that the impairment in surfactant elimination upon inoculation of VHL-deficient AMs *in vivo*, is specifically driven by HIF-2.

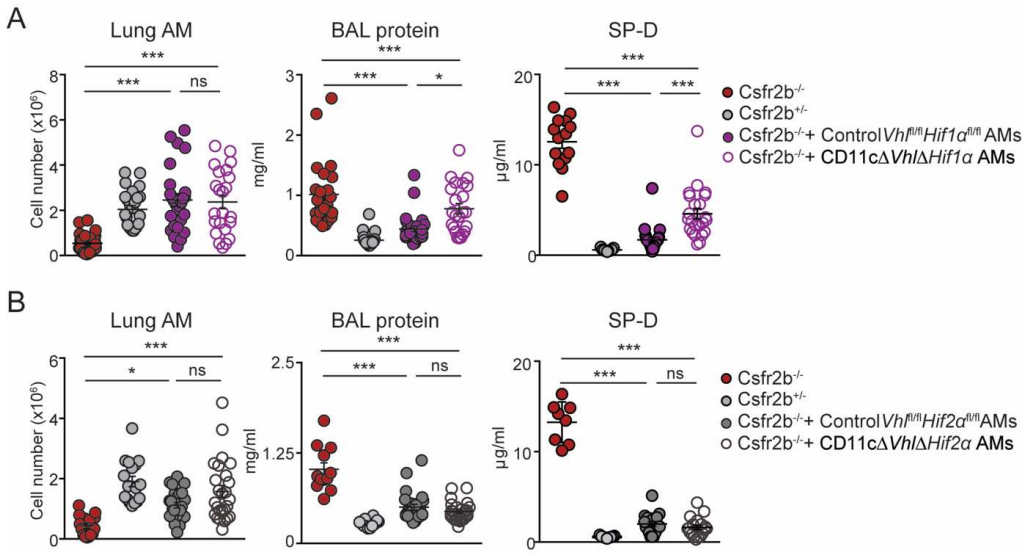

Figure R29. CD11cΔ*Vhl*Δ*Hif1α* and CD11cΔ*Vhl*Δ*Hif2α* AM engraftment after PMT. 5x10^4 BAL CD11cΔ*Vhl*Δ*Hif1α* (A) and CD11cΔ*Vhl*Δ*Hif2α* AMs (B) and their control counterparts were transferred intratracheally (i.t.) to *Csfr2b*$^{-/-}$ mice. After 1.5 months, measurements were made of AM numbers in total lung and of the BAL concentrations of total

protein and SP-D (A,B). Data are shown as individual data points and means ± s.e.m. of a three pooled independent experiments. Control mice (*Csfr2b*$^{-/-}$ and *Csfr2b*$^{+/-}$) are from four independent experiments (n=10-18 per group): ns, not significant; *, p-value<0.05; ***, p-value<0.001 (one-way ANOVA, Bonferroni post-hoc test).

Discussion

Discussion

This thesis aimed to investigate the potential relevance of the adaptation to oxygen fluctuations for lung AM maturation and function after birth. We found *in silico* evidences indicating that negative regulation of HIF occurs during post-birth AM terminal differentiation, suggesting a role of HIF in the maintenance of an immature or pre-AM status. We found that in the absence of VHL, HIF-1 and HIF-2 differentially regulated AM phenotypic maturation and both HIF isoforms had a similar potential to restrain AM self-renewal. Finally, HIF-2 contributed to the decreased ability of VHL-deficient AMs to remove surfactant excess in the lung alveoli (Figure D1).

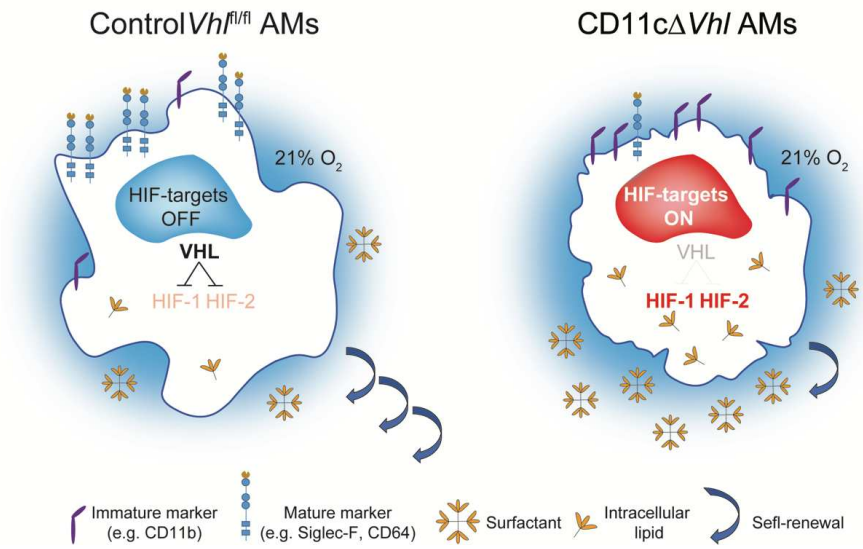

Figure D1. Working model for the regulation of AM maturation and function by HIF. In the lung alveoli, HIF is regulated post-transcriptionally by VHL in mature AM. Preventing VHL-mediated HIF regulation in AMs in an oxygen-enriched environment, increases the expression of HIF-target genes, prevents their terminal phenotypic maturation and decreases their capacity to proliferate and to remove lung surfactant excess.

1. AMs transcriptionally adapt to increased oxygen concentrations early after birth.

AMs differentiate from embryonic precursors seeded in lung before birth. This process is driven by the cytokines GM-CSF and TGF-β (*6, 29*) and leads to pre-AMs. However, pre-AMs reach full maturation only when the alveoli are exposed to air after birth. This late stage of maturation lasts for the first week of life and depends on additional factors such as mTOR. Thus, we reasoned that pre-AMs must likely adapt to their new oxygen-enriched niche as part of their differentiation program. Indeed, GSEA analysis of public available data (*22*) revealed that the expression of genes related to glycolysis and adaptation to hypoxia was gradually downregulated during AM differentiation, suggesting a decreased requirement of these functions within

maturation and thus, an adaptation to increased oxygen concentrations. In addition, these *in silico* results suggested that the negative regulation of HIF transcription factors in AMs shortly after birth can be relevant for their maturation. These results correlate with a recently published work showing that VHL/HIF-1 axis is required for the late stage of ILC2 differentiation at peripheral tissues. In this work, the dysregulation of VHL/HIF-1/glycolysis pathway was associated to epigenetic changes that finally translated into a decreased expression of ST2, restraining IL-33 sensing and thus leading to severe defects in the number and function of ILC2s in lung and intestine (*129*). In contrast, it was proposed that VHL is not required for the first stage of ILC2 differentiation in BM, correlating with the lack of an IL-33 source in this niche. In this regard, it would be interesting to evaluate whether VHL is also redundant for the first phase of AM maturation in the embryo. Interestingly, another recent report showed that upon first breath, mechanical pressure in the lung of newborns stimulated the production of IL-33 by lung epithelial cells, which finally drove AM polarization into M2 (*40*). However, the potential contribution of oxygen sensing coupled to lung inflation was not addressed. Taken together, *in silico* data and previous works suggest that HIF regulation might become relevant when progenitors reach an oxygen-enriched environment. Moreover, these observations also suggest that particularly in the lung, first breath could promote the coordinated adaptation of different cell types (epithelium, ILC2s, AMs) to increased oxygen concentrations.

2. HIF-1 drives VHL-deficient AM switch towards glycolysis.

In order to evaluate whether HIF regulation is relevant for AM terminal differentiation, we used the conditional CD11c-Cre *Vhl*$^{fl/fl}$ mouse model, since CD11c starts to be expressed by AMs shortly after birth (*6*).

We confirmed that VHL-deficient AMs showed an increased extracellular acidification rate (ECAR) and decreased basal respiration rate (BRR), compared to WT AMs. In addition, *Vhl* deletion in AMs resulted in the significant upregulation of HIF-target genes *Ldha* and *Slc2a1*, involved in glycolysis and in agreement with a previous work (*81*). Moreover, HIF-2-specific target *Arg1* was also upregulated in VHL-deficient AMs, indicating that both HIF-1 and HIF-2 were active in the absence of VHL. These results correlated with the significant enrichment of genes associated to both hypoxia and glycolysis hallmarks in AM lacking VHL. Notably, the degree of enrichment of these genes in VHL-deficient AMs largely overcame that observed in pre-AM, suggesting that *Vhl* deletion intensify the effects of HIF stabilization induced by environmental cues.

We then analyzed the contribution of each HIF transcription factor in the glycolytic metabolic profile shown by VHL-deficient AMs. We observed that CD11cΔ*Vhl*Δ*Hif1*α AMs still showed a significant increased expression of *Ldha* and *Slc2a1* compared to control WT AMs,

suggesting a compensatory effect mediated by HIF-2, given that both bind to similar hypoxia responsive elements (HRE) in DNA (*48*). The same effect was observed for *Arg1* in CD11cΔ*Vhl*Δ*Hif2α* AMs. In contrast, deletion of both *Hif1α* and *Hif2α* in VHL-deficient AMs totally restored WT expression levels of the genes analyzed, indicating that the observed changes were totally mediated by HIF. Correlating with the expression of *Ldha* and *Slc2a1*, CD11cΔ*Vhl*Δ*Hif1α* AMs showed a partial decreased OCR and increased ECAR compared to WT counterparts. However, the differences observed were not so dramatic as in CD11cΔ*Vhl*Δ*Hif2α* AMs, which highly resembled CD11cΔ*Vhl* AMs. These results are in agreement with previous works indicating that HIF-1, rather than HIF-2, is the main driver of the metabolic switch towards glycolysis under hypoxia, upon infection or in VHL-deficient mouse models (*130*).

3. VHL/HIF axis regulates AM terminal maturation.

The first evidence obtained during the initial characterization of the VHL-deficient AMs suggesting a defect in maturation was that BAL AMs lacking VHL were significantly smaller than control WT AMs, and upon *in vitro* culture, they remained rounded rather than fusiform, resembling precursor cells or monocytes (*6*). Since certain mutations in VHL can affect its ability to associate with microtubules and protect them from depolarization, we cannot discard that this can be the cause of AM morphological alterations (*127*). However, when we analyzed the expression of markers associated with AM maturation status, compared to control WT cells, VHL-deficient AMs showed a specific reduction in the expression of mature-associated markers (CD11c, Siglec-F and CD64) and an increased expression of CD11b, highly expressed by precursors (*6*). Notably, this pattern of expression has been observed in arrested PPARγ-deficient pre-AMs (*22*). This contrasts with reports showing that hypoxia (*131*) or *Vh*l deletion (*77*) and the associated switch to glycolysis in macrophages promotes their maturation. However, these studies were done with BM-derived macrophages whose progenitors are differentiated in normoxia or macrophage cell lines, exposed to normoxia for several passages. Thus, we cannot discard the possibility that VHL/HIF axis plays a different role in the maturation process of long-lived tissue-resident AMs.

To further prove that VHL regulates AM terminal maturation, we analyzed their transcriptional profile, focusing on those gene sets that define lung AM identity (*118*). The expression of most of the genes comprised in lung AM-related module 296 was upregulated in VHL-deficient AMs compared to control WT cells, including its associated transcription factors. In contrast, when we compared the expression of transcription factors specifically upregulated in lung AMs, we found 9 of them downregulated in the absence of VHL, including *Baz1a*, *Wwtr1* and *Lmo4*, whose expression was also decreased in PPARγ-deficient AMs, compared to control *Pparγ*$^{fl/fl}$ AMs (*44*). We then compared the expression of genes selectively upregulated in lung AM

compared to other tissue-resident macrophages ("signature-up" genes). VHL-deficient AMs expressed decreased mRNA levels of the maturation marker *Siglec5*, *Car4*, associated with mature AM identity (*29*) and *Epcam*, implicated in cell adhesion. In addition, from those genes specifically downregulated in lung AMs ("signature-down" genes), we only detected 4 genes whose expression was increased in AMs lacking VHL, being *Apoe* and *Abca9* implicated in lipid import and metabolism (*132*). Thus, the expression of most of the genes comprised in this "signature-down" gene set, was even decreased in VHL-deficient AMs. This observation could be also extrapolated to the "signature-up" gene set and the module 296, where at least half of total genes was even upregulated in AMs lacking VHL, compared to control WT AMs. Strikingly, this suggests that despite of their immature phenotype, part of the transcriptional program associated with lung mature AM identity is potentiated in AMs lacking VHL.

Parabiosis in mice ruled out that the phenotypic and transcriptional changes observed in VHL-deficient AM population were due to incoming monocytes that could have accessed the alveolar niche, arguing that their phenotype is cell-intrinsic. BM chimeras further demonstrated the intrinsic nature of VHL-deficient AM phenotype and the decreased ability of VHL-deficient AMs to reconstitute the alveolar niche in a context of competence. Correlating with these results, PHD3-deficient AMs also showed an immature-like phenotype and a reduced potential to occupy the alveolar space in bone marrow chimeras (*133*). Moreover, we found that HIF-1 or HIF-2 were able to restrain AM phenotypic maturation in the absence of VHL. Each isoform differentially affected the expression of the surface markers analyzed, mostly at the mRNA level, indicating an independent regulation. This result could be reflecting different kinetics of HIF-1 and HIF-2 regulation in AMs after birth (*61, 66*). Notably, deletion of both *Hif1α* and *Hif2α* fully restored the expression of surface markers to the levels found on WT AMs, in agreement with the stabilization of both subunits in hypoxic environments (*61, 66*). These results thus demonstrate that HIF regulation is required for the terminal maturation of AMs. However, whether the immature phenotype of VHL-deficient AMs is driven by HIF/glycolysis- mediated epigenetic changes (*129*) requires further investigation.

4. HIF regulation by VHL is required for AM self-renewal.

Functional analysis of transcriptomes predicted the inactivation of several pathways related to cell-cycle in the absence of VHL. We confirmed the decreased expression of several genes involved in cell-cycle progression, such as *Cdk1* and cyclins *Ccnb1* and *Ccnb2*. In addition, "NRF2-mediated oxidative stress response" pathway was predicted to be inactive in VHL-deficient AMs, correlating with a decreased mitochondrial activity and thus reduced DNA oxidative damage along with a shift in energy production by glycolysis (*134*). This correlated with the similar expression of *Tp53* and *Cdkn1a* in VHL-deficient and WT AMs. According to *in silico* analysis,

Discussion

VHL-deficient AMs expressed less Ki67 than control WT AMs, and incorporated less BrdU *in vivo*, indicating a decreased turnover rate. Moreover, this defect was reproduced upon *in vitro* stimulation of VHL-deficient AMs with M-CSF and GM-CSF (*31*).

The immature-like phenotype of VHL-deficient AMs and their decreased proliferative potential were at least partially akin to the phenotype found in arrested PPARγ-deficient pre-AMs, in which the expression of genes encoding for *Hif1*α and some HIF-target genes involved in glycolysis was upregulated compared to control WT AMs (*22*). This suggested that VHL could regulate GM-CSF signaling. However, we did not find significant differences in STAT5 phosphorylation upon *in vitro* GM-CSF simulation between VHL-deficient and control WT AMs. Moreover, downstream STAT5, the expression of *Pparγ* and its target genes *Cd36* and *Fabp4* was upregulated, pointing to the active status of the transcription factor (*125*) and correlating with its induced expression by HIF-1 in some cell types (*105*). These results suggest that VHL is required to sustain AM terminal maturation, despite of the increased *Pparγ* expression in AMs lacking VHL. Regarding self-renewal regulation, a recent report proposed that GM-CSF/mTORC1-dependent induction of glycolysis and lipogenesis might be required for AM self-renewal, since Raptor-deficient AMs showed an impaired proliferative capacity coupled to a decreased expression of genes involved in glycolysis upon GM-CSF stimulation (*33*). This contrasts with our data showing that, independently of their mTORC1 activation status, AMs lacking VHL are defective in their proliferation capacity and have a more glycolytic metabolism compared to control AMs, suggesting that the regulation of AM self-renewal capacity by mTORC1 might be independent of the HIF-induced switch to glycolysis. In agreement, a later report showed that mTORC1 activity was essential for AM accumulation in the adult lung by promoting lipid synthesis (anabolism) in a Srebp1/2-dependent and HIF-1-independent manner (*27*).

We found that self-renewal capacity was only restored when both *Hif1*α and *Hif2*α were deleted in VHL-deficient AMs. In fact, Ki67 staining evidenced that deletion of *Hif1*α or *Hif2*α did not restore, not even partially, the proliferation capacity of AMs lacking VHL, suggesting its independence of the metabolic status of AMs. Together with the intact phosphorylation of STAT5 upon GM-CSF stimulation of VHL-deficient AMs, and their incapacity to proliferate independently of the stimuli used *in vitro*, these results indicate that this defect might be downstream sensing of growth factors. At the level of HIF-dependent modulation of chromatin accessibility, it would be interesting to explore whether HIF is acting by displacing Myc from promoters of genes involved in cell-cycle progression (*121*), or rather directly inhibiting MCM DNA Helicases (*122*). Interestingly, while some tumor cells have developed the ability to overcome HIF-dependent mechanisms of cell cycle arrest (*135-137*), this is not the case in HSCs, in which hypoxia and HIF proteins usually promote quiescence (*95, 96, 138*). Notably, hypoxia also prevented proliferation

of WT AMs stimulated with M-CSF or GM-CSF. Thus, at the level of self-renewal regulation, AM resemble stem cells rather than tumor cells, in agreement with a recent work (*32*).

Strikingly, despite the reduced turnover of VHL-deficient AMs, total lung AM cell number was similar in control CD11c-cre *Vhl*$^{fl/fl}$ and CD11cΔ*Vhl* mice. Since parabiosis ruled out that monocytes contribute to VHL-deficient AM population, these results suggest a longer lifespan of AMs lacking VHL compared to control WT AMs. This would agree with the increased PHD3-deficient neutrophil survival (*84, 85*) or the decreased cell death of BM-derived macrophages with enhanced glycolysis upon exposure to hypoxia (*131*). Supporting this notion, we found that after 1.5 months of intratracheal inoculation of a fixed number of cells into *Csfr2b*$^{-/-}$ mice, the same total numbers of AMs were counted in lungs from mice transferred with VHL-deficient AMs and control WT counterparts.

In addition, experiments with BM chimeras showed that VHL-deficient AMs were less efficient to reconstitute the AM niche compared to WT AMs. This result correlated with the decreased expression of Ki67 by CD11cΔ*Vhl* AMs, consistent with the cell-intrinsic nature of this defect. These results suggest that the absence of VHL impair AM differentiation from monocyte precursors and self-renewal. Both features could thus explain that VHL-deficient AMs are overcome by WT AMs in a context of cell competence.

In summary, our results suggest that in the absence of VHL, HIF activity prevents AM terminal phenotypic maturation and proliferation. However, these defects could be likely compensated by a longer lifespan of VHL-deficient AMs compared to WT AMs, and thus translate into similar lung total numbers.

5. HIF-2 decreases AM capacity to remove lung surfactant.

Hypoxia can promote macrophage lipid uptake through the induction of expression of lipid transporters (*101*) and the increase in FA synthesis by inducing sterol regulatory-element binding protein (SREBP)-1 activation and FA synthase (FASN) in a HIF-1-dependent manner (*102*). In addition, HIF-1 can directly induce lipid storage (*103, 104, 125*) and these mechanisms could thus converge in the formation of foam cells (*100*). Staining with Oil-Red O revealed that more AMs accumulated lipids in the absence of VHL, although we did not observe a foam cell phenotype. Moreover, LXR nuclear receptor signaling, implicated in intracellular lipid sensing (*132*), was predicted to be more active in AMs lacking VHL. LXR signaling is also induced in immature AM-like cells from patients with proteinosis and from *Csf2*$^{-/-}$ mice, as well as in PPAR*γ*-deficient AMs (*43, 139*), suggesting that these nuclear sensors are also activated upon pathologic accumulation of lipids in AMs.

Discussion

VHL-deficient AMs showed a significant decreased capacity to oxidize fatty acids (FA) *in vitro*, in agreement with the previously described role of HIF-1 inhibiting mitochondrial FA oxidation (*106-109*). *In vivo*, this result correlated with a reduced therapeutic capacity of AMs lacking VHL to remove surfactant excess upon intratracheal inoculation within lungs of *Csfr2b*$^{-/-}$ mice, which spontaneously develop lung proteinosis.

Since HIF can potentially regulate lipid homeostasis affecting several pathways, we compared the transcriptional expression of genes associated to these processes. While we found a dysregulated expression of genes involved in lipid biosynthesis, the expression of most genes involved in lipid beta-oxidation was induced in VHL-deficient AMs compared to control cells, including carnitine palmitoyltransferase I (*Cpt1a*), which facilitates FA import into mitochondria, the rate-limiting step of mitochondrial lipid oxidation. This gene expression pattern could be due to a compensatory response upon the increased accumulation of lipids in VHL-deficient AMs (*140*).

Notably, the expression of most of the genes involved in lipid import was upregulated in the absence of VHL, including *Fabps* and *Cidec,* and the expression of genes involved in cholesterol synthesis and esterification was downregulated in VHL-deficient AMs, which resembled the expression profile found in foamy PPAR*γ*-deficient AMs (*44*).

The impairment in surfactant elimination by VHL-deficient AMs was rescued following *Hif2*α deletion. In hepatocytes, HIF-2 suppresses *Cpt-1* and acyl-CoA synthase long-chain family member 1 (*Acsl1*) expression, thus decreasing FA import and oxidation in mitochondria and leading to severe hepatic steatosis (*108*). However, since the expression of both genes was upregulated in VHL-deficient AMs compared to control AMs, the decreased lipid oxidation capacity of VHL-deficient AMs seems to be mediated by mechanisms different from the direct inhibition of mitochondrial beta-oxidation enzymes. Finally, deletion of *Hif2*α did not restore aerobic respiration or WT glycolytic levels in VHL-deficient AMs in the presence of pyruvate and glucose, contrasting with the partial restoration observed upon *Hif1*α deletion. Thus, this observation could also imply a differential role of HIF-1 and HIF-2 in the regulation of AM mitochondrial oxidation activity depending on the substrate.

In summary, VHL-deficient AMs show a relative accumulation of intracellular lipids that translates into an altered transcriptional profile. The induced expression of genes involved in lipid import together with their decreased lipid oxidative capacity might contribute to this phenotype. Notably, this increased expression of genes implicated in lipid import, the decreased expression of genes involved in cholesterols biosynthesis and the activation of LXRs were features also found in AMs from CD11c-Cre *Ppar*$\gamma^{fl/fl}$ mice (*22, 44*), which develop proteinosis. Indeed, VHL-deficient AMs were unable to restore homeostasis as efficiently as control AMs upon intratracheal

transference into *Csfr2b*$^{-/-}$ mice, and deletion of *Hif2*α in VHL-deficient AMs restored this defect. However, the finding that VHL-deficient AMs show a defect in surfactant excess removal *in vivo*, contrasts with the absence of foam cell development, the lack of lung proteinosis and the same AM numbers found in 8-week-old CD11cΔ*Vhl* mice. Although we cannot rule out that elder mice develop proteinosis, these results suggest that contrasting with other mouse models, the defect in AM lipid metabolism in the absence of VHL is not acute enough to lead to lung pathology (*22, 27-29*). Interestingly, this in turn suggests that even mild defects in the lipid oxidation capacity of AMs are inked with an immature phenotype. Therefore, the decreased lipid oxidation and surfactant removal capacity found in VHL-deficient AMs could be reflecting the slower metabolism of surfactant found in the lungs of pre-terms and newborns compared to adults, rather than causing lung pathology (*141*).

Conclusions

Conclusions

1. The expression of genes involved in glycolysis and adaptation to hypoxia, including HIF-target genes is downregulated during alveolar macrophage (AM) maturation after birth.
2. The absence of VHL switches AM metabolism towards glycolysis in a HIF-1 dependent fashion.
3. VHL-deficient AMs show an intrinsic immature-like phenotype, dependent on both HIF-1 and HIF-2.
4. VHL-dependent regulation of both HIF-1 and HIF-2 is required to restore full AM self-renewal.
5. VHL-deficient AMs have a decreased lipid oxidation capacity.
6. HIF-2 restrains the therapeutic potential of VHL-deficient AMs in the removal of surfactant excess in the lung.

Conclusiones

Conclusiones

1. La expresión de genes con funciones en glicolisis y adaptación a hipoxia, incluyendo genes diana de HIF, disminuye durante la diferenciación de macrófagos alveolares (MAs) de pulmón tras el nacimiento.
2. La inducción de glicolisis en MAs deficientes en VHL está mediada principalmente por HIF-
3. Los MAs deficientes en VHL muestran un fenotipo inmaduro intrínseco, dependiente de HIF-1 y HIF-2.
4. HIF-1 y HIF-2 inhiben la proliferación de MAs de pulmón de forma similar.
5. La ausencia de VHL afecta la capacidad de oxidar lípidos de los MA de pulmón.
6. La actividad de HIF-2 disminuye la capacidad terapeútica de los MA deficientes en VHL, de eliminar el exceso de surfactante pulmonar.

Bibliography

Bibliography

1. F. Ginhoux, S. Jung, Monocytes and macrophages: developmental pathways and tissue homeostasis. *Nat Rev Immunol* **14**, 392-404 (2014).

2. R. van Furth, Z. A. Cohn, The origin and kinetics of mononuclear phagocytes. *J Exp Med* **128**, 415-435 (1968).

3. M. Merad *et al.*, Langerhans cells renew in the skin throughout life under steady-state conditions. *Nat Immunol* **3**, 1135-1141 (2002).

4. B. Ajami, J. L. Bennett, C. Krieger, W. Tetzlaff, F. M. Rossi, Local self-renewal can sustain CNS microglia maintenance and function throughout adult life. *Nat Neurosci* **10**, 1538-1543 (2007).

5. F. Ginhoux *et al.*, Fate mapping analysis reveals that adult microglia derive from primitive macrophages. *Science* **330**, 841-845 (2010).

6. M. Guilliams *et al.*, Alveolar macrophages develop from fetal monocytes that differentiate into long-lived cells in the first week of life via GM-CSF. *J Exp Med* **210**, 1977-1992 (2013).

7. C. Jakubzick *et al.*, Minimal differentiation of classical monocytes as they survey steady-state tissues and transport antigen to lymph nodes. *Immunity* **39**, 599-610 (2013).

8. S. Tamoutounour *et al.*, Origins and Functional Specialization of Macrophages and of Conventional and Monocyte-Derived Dendritic Cells in Mouse Skin. *Immunity* **39**, 925-938 (2013).

9. S. Epelman *et al.*, Embryonic and adult-derived resident cardiac macrophages are maintained through distinct mechanisms at steady state and during inflammation. *Immunity* **40**, 91-104 (2014).

10. K. Molawi *et al.*, Progressive replacement of embryo-derived cardiac macrophages with age. *J Exp Med* **211**, 2151-2158 (2014).

11. C. C. Bain *et al.*, Constant replenishment from circulating monocytes maintains the macrophage pool in the intestine of adult mice. *Nat Immunol* **15**, 929-937 (2014).

12. S. Yona *et al.*, Fate mapping reveals origins and dynamics of monocytes and tissue macrophages under homeostasis. *Immunity* **38**, 79-91 (2013).

13. D. P. Schafer *et al.*, Microglia sculpt postnatal neural circuits in an activity and complement-dependent manner. *Neuron* **74**, 691-705 (2012).

14. A. Chow *et al.*, CD169(+) macrophages provide a niche promoting erythropoiesis under homeostasis and stress. *Nat Med* **19**, 429-436 (2013).

15. Y. Okabe, R. Medzhitov, Tissue-specific signals control reversible program of localization and functional polarization of macrophages. *Cell* **157**, 832-844 (2014).

16. B. C. Trapnell, J. A. Whitsett, K. Nakata, Pulmonary alveolar proteinosis. *N Engl J Med* **349**, 2527-2539 (2003).

17. S. Ghisletti *et al.*, Identification and characterization of enhancers controlling the inflammatory gene expression program in macrophages. *Immunity* **32**, 317-328 (2010).

18. M. Garber *et al.*, A high-throughput chromatin immunoprecipitation approach reveals principles of dynamic gene regulation in mammals. *Mol Cell* **47**, 810-822 (2012).

19. Y. Lavin *et al.*, Tissue-resident macrophage enhancer landscapes are shaped by the local microenvironment. *Cell* **159**, 1312-1326 (2014).

Bibliography

20. A. Aziz, E. Soucie, S. Sarrazin, M. H. Sieweke, MafB/c-Maf deficiency enables self-renewal of differentiated functional macrophages. *Science* **326**, 867-871 (2009).

21. L. M. Kelly, U. Englmeier, I. Lafon, M. H. Sieweke, T. Graf, MafB is an inducer of monocytic differentiation. *EMBO J* **19**, 1987-1997 (2000).

22. C. Schneider *et al.*, Induction of the nuclear receptor PPAR-gamma by the cytokine GM-CSF is critical for the differentiation of fetal monocytes into alveolar macrophages. *Nat Immunol* **15**, 1026-1037 (2014).

23. M. Haldar, K. M. Murphy, Origin, development, and homeostasis of tissue-resident macrophages. *Immunol Rev* **262**, 25-35 (2014).

24. D. Gosselin *et al.*, Environment drives selection and function of enhancers controlling tissue-specific macrophage identities. *Cell* **159**, 1327-1340 (2014).

25. Y. M. Lee *et al.*, Determination of hypoxic region by hypoxia marker in developing mouse embryos in vivo: a possible signal for vessel development. *Dev Dyn* **220**, 175-186 (2001).

26. Y. Shibata *et al.*, GM-CSF regulates alveolar macrophage differentiation and innate immunity in the lung through PU.1. *Immunity* **15**, 557-567 (2001).

27. C. Sinclair *et al.*, mTOR regulates metabolic adaptation of APCs in the lung and controls the outcome of allergic inflammation. *Science* **357**, 1014-1021 (2017).

28. A. Nakamura *et al.*, Transcription repressor Bach2 is required for pulmonary surfactant homeostasis and alveolar macrophage function. *J Exp Med* **210**, 2191-2204 (2013).

29. X. Yu *et al.*, The Cytokine TGF-beta Promotes the Development and Homeostasis of Alveolar Macrophages. *Immunity* **47**, 903-912 e904 (2017).

30. M. H. Sieweke, J. E. Allen, Beyond stem cells: self-renewal of differentiated macrophages. *Science* **342**, 1242974 (2013).

31. D. Hashimoto *et al.*, Tissue-resident macrophages self-maintain locally throughout adult life with minimal contribution from circulating monocytes. *Immunity* **38**, 792-804 (2013).

32. E. L. Soucie *et al.*, Lineage-specific enhancers activate self-renewal genes in macrophages and embryonic stem cells. *Science* **351**, aad5510 (2016).

33. W. Deng *et al.*, Essential Role of mTORC1 in Self-Renewal of Murine Alveolar Macrophages. *J Immunol* **198**, 492-504 (2017).

34. F. Imperatore *et al.*, SIRT1 regulates macrophage self-renewal. *EMBO J* **36**, 2353-2372 (2017).

35. P. G. Holt *et al.*, Downregulation of the antigen presenting cell function(s) of pulmonary dendritic cells in vivo by resident alveolar macrophages. *J Exp Med* **177**, 397-407 (1993).

36. T. Thepen, N. Van Rooijen, G. Kraal, Alveolar macrophage elimination in vivo is associated with an increase in pulmonary immune response in mice. *J Exp Med* **170**, 499-509 (1989).

37. P. Soroosh *et al.*, Lung-resident tissue macrophages generate Foxp3+ regulatory T cells and promote airway tolerance. *J Exp Med* **210**, 775-788 (2013).

38. R. J. Snelgrove *et al.*, A critical function for CD200 in lung immune homeostasis and the severity of influenza infection. *Nat Immunol* **9**, 1074-1083 (2008).

39. K. Westphalen *et al.*, Sessile alveolar macrophages communicate with alveolar epithelium to modulate immunity. *Nature* **506**, 503-506 (2014).

40. S. Saluzzo *et al.*, First-Breath-Induced Type 2 Pathways Shape the Lung Immune Environment. *Cell Rep* **18**, 1893-1905 (2017).

41. E. Stanley *et al.*, Granulocyte/macrophage colony-stimulating factor-deficient mice show no major perturbation of hematopoiesis but develop a characteristic pulmonary pathology. *Proc Natl Acad Sci U S A* **91**, 5592-5596 (1994).

42. L. Robb *et al.*, Hematopoietic and lung abnormalities in mice with a null mutation of the common beta subunit of the receptors for granulocyte-macrophage colony-stimulating factor and interleukins 3 and 5. *Proc Natl Acad Sci U S A* **92**, 9565-9569 (1995).

43. A. D. Baker *et al.*, Targeted PPAR{gamma} deficiency in alveolar macrophages disrupts surfactant catabolism. *J Lipid Res* **51**, 1325-1331 (2010).

44. E. L. Gautier *et al.*, Systemic analysis of PPARgamma in mouse macrophage populations reveals marked diversity in expression with critical roles in resolution of inflammation and airway immunity. *J Immunol* **189**, 2614-2624 (2012).

45. B. C. Trapnell, J. A. Whitsett, Gm-CSF regulates pulmonary surfactant homeostasis and alveolar macrophage-mediated innate host defense. *Annu Rev Physiol* **64**, 775-802 (2002).

46. C. Happle *et al.*, Pulmonary transplantation of macrophage progenitors as effective and long-lasting therapy for hereditary pulmonary alveolar proteinosis. *Sci Transl Med* **6**, 250ra113 (2014).

47. T. Suzuki *et al.*, Pulmonary macrophage transplantation therapy. *Nature* **514**, 450-454 (2014).

48. M. Y. Koh, G. Powis, Passing the baton: the HIF switch. *Trends Biochem Sci* **37**, 364-372 (2012).

49. S. L. Dunwoodie, The role of hypoxia in development of the Mammalian embryo. *Dev Cell* **17**, 755-773 (2009).

50. M. C. Simon, B. Keith, The role of oxygen availability in embryonic development and stem cell function. *Nat Rev Mol Cell Biol* **9**, 285-296 (2008).

51. J. Pouyssegur, F. Dayan, N. M. Mazure, Hypoxia signalling in cancer and approaches to enforce tumour regression. *Nature* **441**, 437-443 (2006).

52. Q. Ke, M. Costa, Hypoxia-inducible factor-1 (HIF-1). *Mol Pharmacol* **70**, 1469-1480 (2006).

53. H. Tian, S. L. McKnight, D. W. Russell, Endothelial PAS domain protein 1 (EPAS1), a transcription factor selectively expressed in endothelial cells. *Genes Dev* **11**, 72-82 (1997).

54. I. Flamme *et al.*, HRF, a putative basic helix-loop-helix-PAS-domain transcription factor is closely related to hypoxia-inducible factor-1 alpha and developmentally expressed in blood vessels. *Mech Dev* **63**, 51-60 (1997).

55. Y. Makino, A. Kanopka, W. J. Wilson, H. Tanaka, L. Poellinger, Inhibitory PAS domain protein (IPAS) is a hypoxia-inducible splicing variant of the hypoxia-inducible factor-3alpha locus. *J Biol Chem* **277**, 32405-32408 (2002).

56. W. G. Kaelin, Proline hydroxylation and gene expression. *Annu Rev Biochem* **74**, 115-128 (2005).

57. C. J. Schofield, P. J. Ratcliffe, Oxygen sensing by HIF hydroxylases. *Nat Rev Mol Cell Biol* **5**, 343-354 (2004).

58. H. Okuda *et al.*, Direct interaction of the beta-domain of VHL tumor suppressor protein with the regulatory domain of atypical PKC isotypes. *Biochem Biophys Res Commun* **263**, 491-497 (1999).

59. A. V. Kuznetsova *et al.*, von Hippel-Lindau protein binds hyperphosphorylated large subunit of RNA polymerase II through a proline hydroxylation motif and targets it for ubiquitination. *Proc Natl Acad Sci U S A* **100**, 2706-2711 (2003).

60. L. Gossage, T. Eisen, E. R. Maher, VHL, the story of a tumour suppressor gene. *Nat Rev Cancer* **15**, 55-64 (2015).

61. M. Y. Koh, R. Lemos, Jr., X. Liu, G. Powis, The hypoxia-associated factor switches cells from HIF-1alpha- to HIF-2alpha-dependent signaling promoting stem cell characteristics, aggressive tumor growth and invasion. *Cancer Res* **71**, 4015-4027 (2011).

62. W. Luo *et al.*, Hsp70 and CHIP selectively mediate ubiquitination and degradation of hypoxia-inducible factor (HIF)-1alpha but Not HIF-2alpha. *J Biol Chem* **285**, 3651-3663 (2010).

63. Y. V. Liu, G. L. Semenza, RACK1 vs. HSP90: competition for HIF-1 alpha degradation vs. stabilization. *Cell Cycle* **6**, 656-659 (2007).

64. R. Ravi *et al.*, Regulation of tumor angiogenesis by p53-induced degradation of hypoxia-inducible factor 1alpha. *Genes Dev* **14**, 34-44 (2000).

65. A. Palazon, A. W. Goldrath, V. Nizet, R. S. Johnson, HIF transcription factors, inflammation, and immunity. *Immunity* **41**, 518-528 (2014).

66. L. Holmquist-Mengelbier *et al.*, Recruitment of HIF-1alpha and HIF-2alpha to common target genes is differentially regulated in neuroblastoma: HIF-2alpha promotes an aggressive phenotype. *Cancer Cell* **10**, 413-423 (2006).

67. J. Brugarolas *et al.*, Regulation of mTOR function in response to hypoxia by REDD1 and the TSC1/TSC2 tumor suppressor complex. *Genes Dev* **18**, 2893-2904 (2004).

68. B. G. Wouters, M. Koritzinsky, Hypoxia signalling through mTOR and the unfolded protein response in cancer. *Nat Rev Cancer* **8**, 851-864 (2008).

69. M. S. Nakazawa, B. Keith, M. C. Simon, Oxygen availability and metabolic adaptations. *Nat Rev Cancer* **16**, 663-673 (2016).

70. C. Chen, N. Pore, A. Behrooz, F. Ismail-Beigi, A. Maity, Regulation of glut1 mRNA by hypoxia-inducible factor-1. Interaction between H-ras and hypoxia. *J Biol Chem* **276**, 9519-9525 (2001).

71. J. D. Firth, B. L. Ebert, P. J. Ratcliffe, Hypoxic regulation of lactate dehydrogenase A. Interaction between hypoxia-inducible factor 1 and cAMP response elements. *J Biol Chem* **270**, 21021-21027 (1995).

72. M. Obach *et al.*, 6-Phosphofructo-2-kinase (pfkfb3) gene promoter contains hypoxia-inducible factor-1 binding sites necessary for transactivation in response to hypoxia. *J Biol Chem* **279**, 53562-53570 (2004).

73. G. L. Semenza *et al.*, Hypoxia response elements in the aldolase A, enolase 1, and lactate dehydrogenase A gene promoters contain essential binding sites for hypoxia-inducible factor 1. *J Biol Chem* **271**, 32529-32537 (1996).

74. J. W. Kim, I. Tchernyshyov, G. L. Semenza, C. V. Dang, HIF-1-mediated expression of pyruvate dehydrogenase kinase: a metabolic switch required for cellular adaptation to hypoxia. *Cell Metab* **3**, 177-185 (2006).

75. I. Papandreou, R. A. Cairns, L. Fontana, A. L. Lim, N. C. Denko, HIF-1 mediates adaptation to hypoxia by actively downregulating mitochondrial oxygen consumption. *Cell Metab* **3**, 187-197 (2006).

76. N. Takeda *et al.*, Differential activation and antagonistic function of HIF-{alpha} isoforms in macrophages are essential for NO homeostasis. *Genes Dev* **24**, 491-501 (2010).

77. C. Peyssonnaux *et al.*, HIF-1alpha expression regulates the bactericidal capacity of phagocytes. *J Clin Invest* **115**, 1806-1815 (2005).

78. H. Z. Imtiyaz *et al.*, Hypoxia-inducible factor 2alpha regulates macrophage function in mouse models of acute and tumor inflammation. *J Clin Invest* **120**, 2699-2714 (2010).

79. T. Bhandari, J. Olson, R. S. Johnson, V. Nizet, HIF-1alpha influences myeloid cell antigen presentation and response to subcutaneous OVA vaccination. *J Mol Med (Berl)* **91**, 1199-1205 (2013).

80. L. E. Crotty Alexander *et al.*, Myeloid cell HIF-1alpha regulates asthma airway resistance and eosinophil function. *J Mol Med (Berl)* **91**, 637-644 (2013).

81. T. Cramer *et al.*, HIF-1alpha is essential for myeloid cell-mediated inflammation. *Cell* **112**, 645-657 (2003).

82. M. Brandes, F. Klauschen, S. Kuchen, R. N. Germain, A systems analysis identifies a feedforward inflammatory circuit leading to lethal influenza infection. *Cell* **154**, 197-212 (2013).

83. A. Hammami, T. Charpentier, M. Smans, S. Stager, IRF-5-Mediated Inflammation Limits CD8+ T Cell Expansion by Inducing HIF-1alpha and Impairing Dendritic Cell Functions during Leishmania Infection. *PLoS Pathog* **11**, e1004938 (2015).

84. S. R. Walmsley *et al.*, Hypoxia-induced neutrophil survival is mediated by HIF-1alpha-dependent NF-kappaB activity. *J Exp Med* **201**, 105-115 (2005).

85. S. R. Walmsley *et al.*, Prolyl hydroxylase 3 (PHD3) is essential for hypoxic regulation of neutrophilic inflammation in humans and mice. *J Clin Invest* **121**, 1053-1063 (2011).

86. W. J. Janssen *et al.*, Fas determines differential fates of resident and recruited macrophages during resolution of acute lung injury. *Am J Respir Crit Care Med* **184**, 547-560 (2011).

87. K. Ito, T. Suda, Metabolic requirements for the maintenance of self-renewing stem cells. *Nat Rev Mol Cell Biol* **15**, 243-256 (2014).

88. C. Nombela-Arrieta *et al.*, Quantitative imaging of haematopoietic stem and progenitor cell localization and hypoxic status in the bone marrow microenvironment. *Nat Cell Biol* **15**, 533-543 (2013).

89. T. Simsek *et al.*, The distinct metabolic profile of hematopoietic stem cells reflects their location in a hypoxic niche. *Cell Stem Cell* **7**, 380-390 (2010).

90. K. Takubo *et al.*, Regulation of glycolysis by Pdk functions as a metabolic checkpoint for cell cycle quiescence in hematopoietic stem cells. *Cell Stem Cell* **12**, 49-61 (2013).

91. W. M. Yu *et al.*, Metabolic regulation by the mitochondrial phosphatase PTPMT1 is required for hematopoietic stem cell differentiation. *Cell Stem Cell* **12**, 62-74 (2013).

92. K. Rouault-Pierre *et al.*, HIF-2alpha protects human hematopoietic stem/progenitors and acute myeloid leukemic cells from apoptosis induced by endoplasmic reticulum stress. *Cell Stem Cell* **13**, 549-563 (2013).

93. C. Chen *et al.*, TSC-mTOR maintains quiescence and function of hematopoietic stem cells by repressing mitochondrial biogenesis and reactive oxygen species. *J Exp Med* **205**, 2397-2408 (2008).

94. V. M. Renault *et al.*, FoxO3 regulates neural stem cell homeostasis. *Cell Stem Cell* **5**, 527-539 (2009).

95. P. Eliasson *et al.*, Hypoxia mediates low cell-cycle activity and increases the proportion of long-term-reconstituting hematopoietic stem cells during in vitro culture. *Exp Hematol* **38**, 301-310 e302 (2010).

96. J. Du *et al.*, HIF-1alpha deletion partially rescues defects of hematopoietic stem cell quiescence caused by Cited2 deficiency. *Blood* **119**, 2789-2798 (2012).

97. G. Santilli *et al.*, Mild hypoxia enhances proliferation and multipotency of human neural stem cells. *PLoS One* **5**, e8575 (2010).

98. K. Jin *et al.*, Vascular endothelial growth factor (VEGF) stimulates neurogenesis in vitro and in vivo. *Proc Natl Acad Sci U S A* **99**, 11946-11950 (2002).

99. T. Y. Na *et al.*, Positive cross-talk between hypoxia inducible factor-1alpha and liver X receptor alpha induces formation of triglyceride-loaded foam cells. *Arterioscler Thromb Vasc Biol* **31**, 2949-2956 (2011).

100. P. Bostrom *et al.*, Hypoxia converts human macrophages into triglyceride-loaded foam cells. *Arterioscler Thromb Vasc Biol* **26**, 1871-1876 (2006).

101. M. Crucet *et al.*, Hypoxia enhances lipid uptake in macrophages: role of the scavenger receptors Lox1, SRA, and CD36. *Atherosclerosis* **229**, 110-117 (2013).

102. E. Furuta *et al.*, Fatty acid synthase gene is up-regulated by hypoxia via activation of Akt and sterol regulatory element binding protein-1. *Cancer Res* **68**, 1003-1011 (2008).

103. I. Mylonis *et al.*, Hypoxia causes triglyceride accumulation by HIF-1-mediated stimulation of lipin 1 expression. *J Cell Sci* **125**, 3485-3493 (2012).

104. T. Gimm *et al.*, Hypoxia-inducible protein 2 is a novel lipid droplet protein and a specific target gene of hypoxia-inducible factor-1. *FASEB J* **24**, 4443-4458 (2010).

105. J. Krishnan *et al.*, Activation of a HIF1alpha-PPARgamma axis underlies the integration of glycolytic and lipid anabolic pathways in pathologic cardiac hypertrophy. *Cell Metab* **9**, 512-524 (2009).

106. J. M. Huss, F. H. Levy, D. P. Kelly, Hypoxia inhibits the peroxisome proliferator-activated receptor alpha/retinoid X receptor gene regulatory pathway in cardiac myocytes: a mechanism for O2-dependent modulation of mitochondrial fatty acid oxidation. *J Biol Chem* **276**, 27605-27612 (2001).

107. W. Du *et al.*, HIF drives lipid deposition and cancer in ccRCC via repression of fatty acid metabolism. *Nat Commun* **8**, 1769 (2017).

108. E. B. Rankin *et al.*, Hypoxia-inducible factor 2 regulates hepatic lipid metabolism. *Mol Cell Biol* **29**, 4527-4538 (2009).

109. Huang *et al.*, HIF-1-mediated suppression of acyl-CoA dehydrogenases and fatty acid oxidation is critical for cancer progression. *Cell Rep* **8**, 1930-1942 (2014).

110. I. Menendez-Montes *et al.*, Myocardial VHL-HIF Signaling Controls an Embryonic Metabolic Switch Essential for Cardiac Maturation. *Dev Cell* **39**, 724-739 (2016).

111. V. H. Haase, J. N. Glickman, M. Socolovsky, R. Jaenisch, Vascular tumors in livers with targeted inactivation of the von Hippel-Lindau tumor suppressor. *Proc Natl Acad Sci U S A* **98**, 1583-1588 (2001).

112. M. L. Caton, M. R. Smith-Raska, B. Reizis, Notch-RBP-J signaling controls the homeostasis of CD8- dendritic cells in the spleen. *J Exp Med* **204**, 1653-1664 (2007).

Bibliography

113. D. Legland, I. Arganda-Carreras, P. Andrey, MorphoLibJ: integrated library and plugins for mathematical morphology with ImageJ. *Bioinformatics* **32**, 3532-3534 (2016).

114. X. Jiang *et al.*, Skin infection generates non-migratory memory CD8+ T(RM) cells providing global skin immunity. *Nature* **483**, 227-231 (2012).

115. S. Babicki *et al.*, Heatmapper: web-enabled heat mapping for all. *Nucleic Acids Res* **44**, W147-153 (2016).

116. B. Li, C. N. Dewey, RSEM: accurate transcript quantification from RNA-Seq data with or without a reference genome. *BMC Bioinformatics* **12**, 323 (2011).

117. M. D. Robinson, D. J. McCarthy, G. K. Smyth, edgeR: a Bioconductor package for differential expression analysis of digital gene expression data. *Bioinformatics* **26**, 139-140 (2010).

118. E. L. Gautier *et al.*, Gene-expression profiles and transcriptional regulatory pathways that underlie the identity and diversity of mouse tissue macrophages. *Nat Immunol* **13**, 1118-1128 (2012).

119. H. Chanteux, A. C. Guisset, C. Pilette, Y. Sibille, LPS induces IL-10 production by human alveolar macrophages via MAPKinases- and Sp1-dependent mechanisms. *Respir Res* **8**, 71 (2007).

120. L. Stokes, A. Surprenant, Purinergic P2Y2 receptors induce increased MCP-1/CCL2 synthesis and release from rat alveolar and peritoneal macrophages. *J Immunol* **179**, 6016-6023 (2007).

121. M. Koshiji *et al.*, HIF-1alpha induces cell cycle arrest by functionally counteracting Myc. *EMBO J* **23**, 1949-1956 (2004).

122. M. E. Hubbi *et al.*, A nontranscriptional role for HIF-1alpha as a direct inhibitor of DNA replication. *Sci Signal* **6**, ra10 (2013).

123. G. Hoeffel *et al.*, C-Myb(+) erythro-myeloid progenitor-derived fetal monocytes give rise to adult tissue-resident macrophages. *Immunity* **42**, 665-678 (2015).

124. L. van de Laar *et al.*, Yolk Sac Macrophages, Fetal Liver, and Adult Monocytes Can Colonize an Empty Niche and Develop into Functional Tissue-Resident Macrophages. *Immunity* **44**, 755-768 (2016).

125. K. Bensaad *et al.*, Fatty acid uptake and lipid storage induced by HIF-1alpha contribute to cell growth and survival after hypoxia-reoxygenation. *Cell Rep* **9**, 349-365 (2014).

126. J. S. Roe, H. D. Youn, The positive regulation of p53 by the tumor suppressor VHL. *Cell Cycle* **5**, 2054-2056 (2006).

127. A. Hergovich, J. Lisztwan, R. Barry, P. Ballschmieter, W. Krek, Regulation of microtubule stability by the von Hippel-Lindau tumour suppressor protein pVHL. *Nat Cell Biol* **5**, 64-70 (2003).

128. M. P. Lolkema *et al.*, The von Hippel-Lindau tumor suppressor protein influences microtubule dynamics at the cell periphery. *Exp Cell Res* **301**, 139-146 (2004).

129. Q. Li *et al.*, E3 Ligase VHL Promotes Group 2 Innate Lymphoid Cell Maturation and Function via Glycolysis Inhibition and Induction of Interleukin-33 Receptor. *Immunity* **48**, 258-270 e255 (2018).

130. G. L. Semenza, HIF-1 mediates metabolic responses to intratumoral hypoxia and oncogenic mutations. *J Clin Invest* **123**, 3664-3671 (2013).

131. J. Roiniotis *et al.*, Hypoxia prolongs monocyte/macrophage survival and enhanced glycolysis is associated with their maturation under aerobic conditions. *J Immunol* **182**, 7974-7981 (2009).

132. P. Tontonoz, D. J. Mangelsdorf, Liver X receptor signaling pathways in cardiovascular disease. *Mol Endocrinol* **17**, 985-993 (2003).

133. S. J. Tavernier *et al.*, Opposing regulation and roles for PHD3 in lung dendritic cells and alveolar macrophages. *J Leukoc Biol* **102**, 1115-1126 (2017).

134. B. N. Puente *et al.*, The oxygen-rich postnatal environment induces cardiomyocyte cell-cycle arrest through DNA damage response. *Cell* **157**, 565-579 (2014).

135. M. E. Hubbi *et al.*, Cyclin-dependent kinases regulate lysosomal degradation of hypoxia-inducible factor 1alpha to promote cell-cycle progression. *Proc Natl Acad Sci U S A* **111**, E3325-3334 (2014).

136. J. D. Gordan *et al.*, HIF-alpha effects on c-Myc distinguish two subtypes of sporadic VHL-deficient clear cell renal carcinoma. *Cancer Cell* **14**, 435-446 (2008).

137. M. E. Hubbi, W. Luo, J. H. Baek, G. L. Semenza, MCM proteins are negative regulators of hypoxia-inducible factor 1. *Mol Cell* **42**, 700-712 (2011).

138. M. V. Gustafsson *et al.*, Hypoxia requires notch signaling to maintain the undifferentiated cell state. *Dev Cell* **9**, 617-628 (2005).

139. M. J. Thomassen *et al.*, ABCG1 is deficient in alveolar macrophages of GM-CSF knockout mice and patients with pulmonary alveolar proteinosis. *J Lipid Res* **48**, 2762-2768 (2007).

140. H. J. Renaud, J. Y. Cui, H. Lu, C. D. Klaassen, Effect of diet on expression of genes involved in lipid metabolism, oxidative stress, and inflammation in mouse liver-insights into mechanisms of hepatic steatosis. *PLoS One* **9**, e88584 (2014).

141. P. O. Nkadi, T. A. Merritt, D. A. Pillers, An overview of pulmonary surfactant in the neonate: genetics, metabolism, and the role of surfactant in health and disease. *Mol Genet Metab* **97**, 95-101 (2009).

Appendix

Appendix

Publication derived from this memory:

Helena M. Izquierdo, Paola Brandi, Manuel-José Gómez, Ruth Conde-Garrosa, Elena Priego, Michel Enamorado, Sarai Martínez-Cano, Iria Sánchez, Laura Conejero, Daniel Jiménez-Carretero, Silvia Martín-Puig, Martin Guilliams and David Sancho. Von Hippel-Lindau protein is required for optimal alveolar macrophage terminal differentiation, self-renewal and function. *Cell Reports* 2018 (accepted).

Other publications during PhD training:

Conejero L, Khouili SC, Martínez S, **Izquierdo HM**, Brandi P and Sancho D. Lung CD103+ dendritic cells restrain allergic airway inflammation by promoting Th1 immunity. *JCI Insight* 2017 May 18;2(10).

Iborra S, Martínez-López M, Cueto FJ, Conde-Garrosa R, Del Fresno C, **Izquierdo HM**, Abram CL, Mori D, Campos-Martín Y, Reguera RM, Kemp B, Yamasaki S, Robinson MJ, Soto M, Lowell CA and Sancho D. Leishmania uses Mincle to Target an Inhibitory ITAM Signaling Pathway in Dendritic Cells that Dampens Adaptive Immunity to Infection. *Immunity* 2016 Oct 18; 45(4): 788-801.

Escolano A, Martínez-Martínez S, Alfranca A, Urso K, **Izquierdo HM**, Delgado M, Martín F, Sabio G, Sancho D, Gómez-del Arco P, Redondo JM. Specific calcineurin targeting in macrophages confers resistance to inflammation via MKP-1 and p38. *EMBO Journal*. 2014 May 16; 33(10): 1117-33.

Iborra S, **Izquierdo HM**, Martínez-López M, Blanco-Menéndez N, Reis e Sousa C, Sancho D. The DC receptor DNGR-1 mediates cross-priming of CTLs during vaccinia virus infection in mice. *Journal of Clinical Investigation* 2012 May 1; 122 (5):1628-43.

Von Hippel-Lindau protein is required for optimal alveolar macrophage terminal differentiation, self-renewal and function

Authors: Helena M. Izquierdo[1], Paola Brandi[1], Manuel-José Gómez[1], Ruth Conde-Garrosa[1], Elena Priego[1], Michel Enamorado[1], Sarai Martínez-Cano[1], Iria Sánchez[1], Laura Conejero[1], Daniel Jimenez-Carretero[1], Silvia Martín-Puig[1], Martin Guilliams[2] and David Sancho[1,*]

[1] Centro Nacional de Investigaciones Cardiovasculares Carlos III (CNIC), Myocardial Pathophysiology Department. Madrid 28029, Spain.

[2] Laboratory of Myeloid Cell Ontogeny and Functional Specialisation, VIB-UGhent Centre for Inflammation Research; and the Department of Biomedical Molecular Biology, Ghent University. Ghent 9052, Belgium.

*Lead Contact. Correspondence to David Sancho: dsancho@cnic.es

L. Conejero's present address is: Inmunotek, Alcalá de Henares 28805, Spain.

Abbreviations used: AM, alveolar macrophage; BAL, bronchoalveolar lavage; GSEA: gene set enrichment analysis. SP-D, surfactant protein D; VHL, Von Hippel-Lindau; BM, bone marrow.

Summary

The rapid transit from hypoxia to normoxia in the lung that follows the first breath in newborn mice coincides with alveolar macrophage (AM) differentiation. However, whether sensing of oxygen is required for AM maturation and function has not been previously explored. We have generated mice whose AMs show a deficient ability to sense oxygen after birth by deleting VHL, the master negative regulator of HIF transcription factors, in the CD11c compartment (CD11cΔ*Vhl* mice). VHL-deficient AMs show an immature-like phenotype and an impaired self-renewal capacity *in vivo*. VHL-deficient phenotype is intrinsic to targeted AMs, as demonstrated by mixed bone marrow chimeras, and persists upon culture *ex vivo*. Unlike AMs transplanted from control $Vhl^{fl/fl}$ mice, AMs from CD11cΔ*Vhl* mice do not reverse pulmonary alveolar proteinosis when transplanted into $Csf2rb^{-/-}$ mice, demonstrating that VHL contributes to AM-mediated surfactant clearance. Thus, our results suggest that optimal AM terminal differentiation, self-renewal, and homeostatic function may be influenced by their oxygen sensing capacity.

Introduction

Tissue resident macrophages are essential for tissue homeostasis, and it is of great interest deciphering the network of factors that in turn modulate macrophage phenotype and function in each tissue. Alveolar macrophages (AMs) are resident in the lung and show a high capacity to self-maintain by local proliferation (Sieweke and Allen, 2013), with little contribution to the repopulation of the alveolar niche by blood circulating monocytes in steady-state (Guilliams et al., 2013; Hashimoto et al., 2013). The mechanisms regulating AM self-renewal ability are a focus of current research (Deng et al., 2017; Imperatore et al., 2017; Soucie et al., 2016). Mature AMs regulate surfactant levels in the lung (Baker et al., 2010; Guilliams et al., 2013; Robb et al., 1995; Schneider et al., 2014; Stanley et al., 1994). GM-CSF signaling is essential for AM development, and factors including GM-CSF (*Csf2*$^{-/-}$) and GM-CSF receptor (*Csf2rb*$^{-/-}$) (Robb et al., 1995; Stanley et al., 1994), the transcription factors PU.1 (Shibata et al., 2001) and PPAR-γ (Schneider et al., 2014) and mTOR (Sinclair et al., 2017) are therefore required to prevent surfactant accumulation in the lung. However, additional factors can affect AM lipid handling, including the transcriptional repressor Bach2 (Nakamura et al., 2013) and TGF-β (Yu et al., 2017), which are required for AM functional maturation independently of GM-CSF.

Initial lung development occurs in a relatively hypoxic environment beginning in mice on embryonic day 9 (E9) (Lee et al., 2001). Fetal monocytes colonize the developing lung around E12.5 and E16.5 and only differentiate into mature AMs after birth (Guilliams et al., 2013). Epithelial cell-derived GM-CSF is essential for the early commitment of AM precursors in the postnatal lung (Guilliams et al., 2013; Schneider et al., 2014). In addition, IL-33 production by lung epithelial cells upon the first breath leads to IL-13 secretion by type 2 innate lymphoid cells that contributes to AM polarization to an anti-inflammatory phenotype (Saluzzo et al., 2017). However, it remains unknown whether AM adaptation to increased oxygen concentrations in the postnatal lung is relevant to AM maturation and function.

We hypothesized that sensing of increased oxygen concentrations just after birth might be important for post-natal AM maturation. The hypoxia-inducible transcription factor (HIF) response is a master regulator of oxygen sensing. Under normoxia, HIF-α subunits are hydroxylated and bind to the Von Hippel-Lindau tumor suppressor protein (VHL), which acts as a ubiquitin ligase, targeting HIF-α subunits for proteasomal degradation (Nakazawa et al., 2016). Indeed, HIF conditional knockouts have revealed the relevance of the HIF oxygen-sensing pathway for myeloid cell compartment (Bhandari et al., 2013; Brandes et al., 2013) and particularly for macrophage (Imtiyaz et al., 2010; Li et al., 2018; Peyssonnaux et al., 2005), eosinophil (Crotty Alexander et al., 2013), neutrophil (Cramer et al., 2003) and dendritic cell function (Hammami et al., 2015). VHL is thus essential for HIF-α degradation upon oxygen sensing and VHL depletion induces normoxic expression of HIF-target genes (Cramer et al., 2003; Peyssonnaux et al., 2005). Here, we deleted VHL in the CD11c^{+} compartment (CD11cΔ*Vhl*) in order to desensitize AMs to oxygen after birth. VHL deletion induced the expression of HIF target genes and altered the AM metabolic profile. VHL-deficient AMs showed an immature-like phenotype and a decreased self-renewal capacity that were intrinsic, as demonstrated using mixed bone marrow (BM) chimeras. In addition, VHL contributed to AM-mediated surfactant clearance in a model of alveolar proteinosis. Our results therefore support the notion that oxygen sensing is required for AM terminal differentiation, self-renewal, and function.

Results and discussion

Downregulation of hypoxia and glycolysis during postnatal AM maturation

To explore whether oxygen sensing by AMs could be linked to their maturation, we analyzed a publicly available microarray data (Schneider et al., 2014) containing the transcriptional profile of AMs from pups at postnatal days 2 and 11 and from 8-12-week-old adult mice. Gene set enrichment analysis (GSEA) was performed on the gene expression profiles using the hallmark collection of the Molecular Signatures Database (MSigDB). Results showed significant upregulation of both hypoxia and glycolysis gene sets in immature AMs from 2-day-old pups compared with mature AMs from adults (Figure 1A). In addition, the gene expression of these two enriched hallmark gene sets was gradually downregulated during AM maturation (Figure 1B), suggesting postnatal adaptation of AMs to oxygen. Both gene sets included well-known HIF targets such as Slc2a1, Hk2, Pdk1 and Slc2a3 (Figure 1B and 1C, genes marked in red). Analysis of other classical HIF target genes in most cases revealed the same expression dynamics (Figure 1C and 1D). The mean expression of all HIF target genes was thus significantly higher in immature AMs (Day 2) than in mature AMs from adult mice, whereas no significant changes where found between postnatal day 11 and adulthood (Figure 1E), correlating with AM terminal differentiation around postnatal day 7 (Guilliams et al., 2013). These results suggest that downregulation of HIF activity in AMs upon exposure to high oxygen tension after birth may be important for AM terminal differentiation, concurring with the HIF-1-independent role of mTOR in AM development after birth (Sinclair et al. Science 2017).

Depletion of VHL alters AM metabolic profile and phenotype

To dissect the effects on AMs of preventing HIF degradation in response to high postnatal oxygen pressure, we generated CD11c-Cre $Vhl^{fl/fl}$ mice. Compared to the LysM(*Lyz2*)-Cre, the CD11c-Cre driver specifically targets postnatal AMs (Guilliams et al., 2013), and does not affect neutrophils or eosinophils (Cramer et al., 2003; Swain et al., 2014; Walmsley et al., 2011; Walmsley et al., 2005). VHL depletion leads to an increased glycolytic activity of macrophages under basal conditions (Cramer et al., 2003). Sorted BAL AMs from CD11c-Cre^{+} $Vhl^{fl/fl}$ (CD11cΔ*Vhl*) mice showed decreased *Vhl* mRNA levels relative to AMs from CD11c-Cre^{-} $Vhl^{fl/fl}$ littermates (control $Vhl^{fl/fl}$) (Figure 2A). VHL depletion in AMs resulted in increased expression of HIF-1 targets such as *Ldha* (Lactate dehydrogenase) (Semenza et al., 1996), HIF-2 targets such as *Arg1* (Arginase 1) (Takeda et al., 2010), and common HIF-1 and HIF-2 targets such as *Slc2a1* (Glucose transporter 1) (Chen et al., 2001) (Figure 2B). To explore the functional consequences of *Vhl* deletion in AMs, we conducted an RNA sequencing analysis to compare the transcriptome of BAL AMs isolated from CD11cΔ*Vhl* and control $Vhl^{fl/fl}$ mice. GSEA showed significant upregulation of hypoxia and glycolysis gene sets from the hallmark collection in the absence of VHL (Figure 2C), resembling the comparison of day 2 postnatal versus adult AMs (Figure 1A) and indicating that, at a transcriptional level, the absence of VHL affects the ability of AMs to detect oxygen. In order to address this functionally, we measured real-time metabolic profile of VHL-deficient AMs from BAL. The absence of VHL in AMs significantly decreased their basal respiratory rate (BRR) (Figure 1D and 1E), while increasing their basal extracellular acidification rate (Figure 1F). These results indicate that depletion of VHL in AMs induces the expression of HIF-1 and HIF-2 target genes and alters their basal metabolic profile.

Altered AM terminal differentiation can lead to the development of AM-like cells with a distorted phenotype (Schneider et al., 2014). We found that VHL-deficient AMs from BAL were smaller and

unable to acquire the fusiform morphology of control *Vhl*$^{fl/fl}$ AMs after culture *ex vivo* for five days, instead maintaining a rounded shape similar to precursor cells or monocytes (Figure 2G-2I) (Guilliams et al., 2013). Since altered maturation can affect AM phenotype (Schneider et al., 2014), we measured the expression of canonical surface markers on BAL AMs *ex vivo*. VHL-deficient AMs slightly reduced mRNA for *Itgax* (CD11c), without affecting membrane receptor expression (Figure 2J-2L). Notably, VHL-deficient AMs showed decreased mRNA and protein for *Siglec5* (Siglec-F) and *Fcgr1a* (CD64), whereas *Itgam* (CD11b) was increased (Figure 2J-2L). This phenotype is linked to an immature AM state (Guilliams et al., 2013; Schneider et al., 2014).

Although access to the alveolar niche is restricted in steady-state conditions, blood monocytes can access the lung alveoli and differentiate into AMs under specific conditions (Hashimoto et al., 2013). Thus, the immature like-phenotype of VHL-deficient AMs could be either intrinsic or caused by increased infiltration of monocytes in CD11cΔ*Vhl* mice. To investigate this, we performed surgical parabiosis of CD45.1 WT mice with either CD45.2 control *Vhl*$^{fl/fl}$ or CD11cΔ*Vhl* mice (Figure S1A). After 30 days, analysis of peripheral blood in CD45.2 parabionts revealed equivalent frequencies of CD45.1^{+} neutrophils and also Ly6C^{hi} monocytes, found at the same level than those exchanged after longer protocols of parabiosis in the steady-state (Hashimoto et al., 2013) (Figure S1B and S1C). Lung CD45.1^{+} Ly6C^{hi} monocytes and BAL AMs frequencies were similar in both genotypes (Figure S1D and S1E). These results suggest that the immature-like phenotype of VHL-deficient AMs is intrinsic and not a consequence of differential lung infiltration by monocytes.

VHL-deficient AMs have an altered gene expression profile

RNAseq identified 2531 differentially expressed genes in CD11cΔ*Vhl* AMs relative to control *Vhl*$^{fl/fl}$ and control CD11cCre^{+} AMs (Figure S2A). Clustering of these genes with Ingenuity Pathway Analysis software revealed several pathways altered by the absence of VHL in AMs (Figure S2B). We validated the expression of selected genes in pathways related to relevant features of AM physiology, such as cell cycle and LXR/RXR activation, implicated in intracellular lipid sensing (Figure S2C and S2D). The absence of VHL in AMs resulted in reduced expression of genes implicated in cell cycle progression, such as those encoding cyclin B1 (*Ccnb1*), cyclin B2 (*Ccnb2)*, CDK1 (*Cdk1*), CD25c (*Cd25c*) and PLK3 (*Plk3*) (Figure S2C, upper panel) and cell cycle control, including BRCA1 (*Brca1*), CHEK1 (*Chek1*), and CHEK2 (*Chek2*), but showing similar expression of the cell cycle master regulators p53 (*Tp53*) and p21 (*Cdkn1a*) (Figure S2C, lower panel). Among those genes clustered in the "LXR/RXR activation" pathway, we confirmed upregulated transcript expression of LXRα (*Nr1h3*) and LXRβ (*Nr1h2*) (Figure S2D). Accordingly, we confirmed increased expression of genes involved in cholesterol efflux, such as the transporters ABCG1 (*Abcg1*) and apolipoprotein E (*ApoE*) and the lipoprotein remodeling enzyme PLTP (*Pltp*) (Figure S2D). These results suggest that crucial distinctive features of AMs, such as proliferation and lipid handling, are affected by the absence of VHL.

AM self-renewal requires VHL

We next investigated whether the absence of VHL affected AM self-renewal capacity. We measured BrdU incorporation in BAL AMs cultured *in vitro* in the absence or presence of M-CSF and GM-CSF, tissue-derived cytokines that contribute to the maintenance and proliferation of mature AMs

(Hashimoto et al., 2013; Hoeffel et al., 2015). Unstimulated AMs retained very low proliferative capacity, and GM-CSF was more potent than M-CSF at inducing AM proliferation, coinciding with a recent report (Deng et al., 2017). VHL-deficient AMs proliferated significantly less than control $Vhl^{fl/fl}$ AMs in the absence or presence of these cytokines (Figure 3A).

To further investigate the potential role of VHL in AM self-renewal, we analyzed BAL AMs *ex vivo*. These experiments revealed significantly reduced Ki67 staining in VHL-deficient AMs than in control $Vhl^{fl/fl}$ AMs (Figure 3B and 3C), suggesting impaired proliferation. We next tracked self-renewal *in vivo* by injecting BrdU intraperitoneally every day for three consecutive weeks. One day after the last pulse, VHL-deficient AMs from BAL showed lower BrdU incorporation than control $Vhl^{fl/fl}$ AMs (Figure 3D and 3E), indicative of decreased replication rate. In contrast, 21d after the last pulse, BrdU labeling was similar in both genotypes (Figure 3D and 3E), which translated into a lower fold dilution of the incorporated BrdU in the absence of VHL (Figure 3F, right). Despite the reduced turnover in VHL-deficient AMs, total lung AM numbers were similar in both genotypes (Figure 3F). Since parabiosis experiments ruled out an increased incoming of monocytes in the lung of CD11cΔ*Vhl* mice (Figure S1), our data suggest that VHL-deficient AMs have a longer lifespan. Consistent with this, previous results show increased primary macrophage survival under hypoxia (Roiniotis et al., 2009) and reduced apoptosis in $PHD3^{-/-}$ BM-Macrophages (Swain et al., 2014). Moreover, the HIF/NF-kB axis mediates the survival response of human blood neutrophils under hypoxia (Walmsley et al., 2005).

AMs are replaced by bone-marrow-derived blood monocytes in lethal irradiation chimeras (Hashimoto et al., 2013; Yona et al., 2013). Therefore, we next asked whether VHL depletion could also affect the replenishment of AMs after irradiation-induced cytoablation. We generated chimeric mice by intravenous adoptive transfer of a mixture of BM cells from WT $CD45.2^+$ DsRed mice ($DsRed^+$) mixed at 1:1 ratio with either $DsRed^-$ $CD45.2^+$ CD11cΔ*Vhl* mice (WT:CD11cΔ*Vhl*) or $DsRed^-$ $CD45.2^+$ control $Vhl^{fl/fl}$ (WT:control $Vhl^{fl/fl}$) into lethally irradiated $CD45.1^+$ WT recipient mice (Figure 3G-K). After 47 days, AMs frequency was analyzed. Most BAL and lung AMs (after BAL) were of donor origin ($CD45.2^+$) in both types of chimeras at this time point (Figure S3A,B), in agreement with previous results on reconstitution of AMs from blood precursors after lethal irradiation (Hashimoto et al., 2013). Notably, the frequency of CD11cΔ*Vhl* AMs in the BAL (Figure 3G) and the lung (Figure S3C) of chimeric mice was significantly lower compared with control $Vhl^{fl/fl}$ AMs. This result correlated with a significantly decreased proliferative capacity of BAL CD11cΔ*Vhl* AMs compared with WT AMs from co-transferred BM (Figure 3H and 3I). As a control, no differences were found in the potential of reconstitution of lung eosinophils from the different donors (Figure S3D). Moreover, CD11cΔ*Vhl* AMs also showed an immature-like phenotype compared with WT AM counterparts (Figure 3J and 3K). Monocytic AM precursors only differentiate phenotypically into mature AMs once they reach the lung (Guilliams et al., 2013; Schneider et al., 2014; van de Laar et al., 2016). Therefore, these results suggest that the absence of VHL driven by CD11c induction during AM differentiation, intrinsically prevents their terminal phenotypic maturation and restrains their self-renewal capacity, decreasing the reconstitution of the alveolar niche in a context of competition with WT AMs. Since AM precursors come from oxygen-rich arterial blood, this result also supports that VHL-mediated oxygen sensing is required but not sufficient for AM terminal differentiation.

VHL contributes to surfactant handling by AMs

Several reports link hypoxia and HIF stabilization to dysregulation of lipid transport and beta-oxidation (Bensaad et al., 2014; Huang et al., 2014; Na et al., 2011). Mice deficient for *Csf2* (GM-CSF) or *Csf2r* or with *Pparg* depletion in AMs show impaired AM maturation, resulting in low numbers of lung immature AMs that accumulate lipids intracellularly (Robb et al., 1995; Schneider et al., 2014; Stanley

et al., 1994). Interestingly, immature AM-like cells from patients with surfactant accumulation and *Csf2*$^{-/-}$ mice, as well as *Pparg*-deficient AMs, show an induction of LXR signaling (Baker et al., 2010; Thomassen et al., 2007). These findings correlate with the LXR pathway activation predicted by our RNA-Seq analysis (Figure S2B) and with the increased expression of LXR-target genes implicated in lipid efflux in VHL-deficient AMs (Figure S2D).

In order to quantify the lipid β-oxidation capacity of AMs, we measured the oxygen consumption rate of BAL AMs in the presence of palmytoyl-CoA as a carbon source (Figure 4A). The basal respiration rate was significantly lower in AMs lacking VHL, indicating a reduced lipid oxidation capacity (Figure 4B), whereas the basal extracellular acidification rate was unaltered (Figure 4C). Unlike other models of impaired AM function, 3-month-old CD11cΔ*Vhl* mice did not show increased accumulation of total protein in bronchoalveolar lavage (BAL) supernatants (Figure 4D).

To determine whether the decreased ability to oxidize lipids of VHL-deficient AMs affected their therapeutic potential to degrade surfactant excess *in vivo*, we transplanted a limited amount of AMs from BAL of CD11cΔ*Vhl* or control *Vhl*$^{fl/fl}$ mice into *Csf2rb*$^{-/-}$ mice, which lack mature AMs and spontaneously develop lung proteinosis (Figure 4E-4G) (Robb et al., 1995). As a marker of disease severity, we measured total protein and surfactant protein D concentrations in BAL supernatants at 1.5 months after pulmonary macrophage transplantation (Figure 4E), a time point at which transferred WT AMs had removed surfactant nearly to the levels found in healthy mice (Figure 4G) (Happle et al., 2014; Suzuki et al., 2014). Consistent with our earlier results (Figure 3F), AM engraftment in the lung was similar in both genotypes (Figure 4F). Transplanted AMs from CD11cΔ*Vhl* mice were less efficient than control *Vhl*$^{fl/fl}$ mice at reversing surfactant accumulation in *Csf2rb*$^{-/-}$ recipient mice BAL (Figure 4G). These results indicate that VHL contributes to the ability of AMs to oxidize lipids and to clear pulmonary surfactant *in vivo*.

In conclusion, we investigate whether alveolar macrophage (AM) adaptation to increased oxygen concentrations in the postnatal lung is relevant for AM function. Deletion of VHL in AMs induces HIF target gene expression and alters AM metabolic profile, leading to partial desensitization of AMs to oxygen. VHL-deficient AMs resemble immature-like AMs in terms of morphology and expression of maturation markers, and have a limited self-renewal potential. Experiments with BM chimeras indicate that the phenotype is intrinsic and reproduced in AMs differentiated from monocyte precursors coming from oxygen-rich arterial blood. This result suggests that besides lung tissue-specific factors, oxygen sensing is also needed for AM terminal differentiation. Functionally, VHL-deficient AMs show defective therapeutic capacity to clear surfactant excess *in vivo*. Our results therefore suggest that oxygen sensing is a requirement for AM terminal differentiation, self-renewal capacity, and function.

MATERIALS AND METHODS

Mouse strains

C57BL/6J-Crl mice (Charles River), *Csf2rb*$^{-/-}$ mice (Robb et al., 1995), *Vhl*$^{fl/fl}$ mice (Haase et al., 2001; Menendez-Montes et al., 2016) mated with CD11c-Cre BAC transgenic mice (Caton et al., 2007) were used. B6/SJL (Ptprca Pepcb/BoyJ) mice expressing the CD45.1 allele and DsRed (Actb-DsRed.T3) mice expressing the red fluorescent protein DsRed.MST, were both from The Jackson Laboratory (Bar Harbor, ME, USA). Mice were bred at CNIC under specific pathogen-free conditions. Except where indicated, we used 8- to 12-week-old age-matched animals (males or females) for all experiments. The local ethics committee approved all animal studies. All animal procedures were reviewed and approved by Animal Ethics Committee at the CNIC, Madrid Autonomous University Ethics Committee, and the Community of Madrid authority. All animal procedures were compliant with the EU Directive 2010/63/EU and Recommendation 2007/526/EC regarding the protection of animals used for experimental and other scientific purposes, enforced by the Spanish law under Real Decreto 1201/2005. Mice were allocated randomly in the different experimental procedures.

Parabiosis

Parabiosis was performed as previously described (Jiang et al., 2012). Sex- and age-matched CD11c-Cre^{+} *Vhl*$^{fl/fl}$ and CD11c-Cre^{-} *Vhl*$^{fl/fl}$ littermates were joined with B6/SJL, expressing the CD45.1 congenic marker to facilitate cell tracking in blood and lung after one month of parabiosis.

BM chimeras

B6/SJL mice expressing the CD45.1 congenic marker were lethally irradiated (12 Gy) and were reconstituted intravenously with 5x10^{6} cells of a 1:1 mixture of CD45.2^{+} wild-type DsRed^{+} BM cells and CD45.2^{+} CD11cΔ*Vhl* BM cells, or CD45.2^{+} wild-type DsRed^{+} BM cells and CD45.2^{+} control *Vhl*$^{fl/fl}$ BM cells. Mice were analyzed 47 days after reconstitution and blood was harvested one day before sacrifize.

Alveolar macrophage (AM) isolation and culture

Mice were sacrificed with a lethal dose of pentobarbital (Dolethal, Vetoquinol). In order to obtain an enriched AM population for cell culture, ten bronchoalveolar lavages (BALs) per mouse were performed with a blunt fill needle (18G x 1 ½; 1.2mmx40mm, BD Safety products), with 1ml of phosphate-buffered saline (PBS), 2.5 mM EDTA, 2% fetal bovine serum (FBS, HyClone) (flow cytometry buffer) at 37ºC. Samples were kept on ice until further processing. Red blood cell lysis was performed at room temperature (RT) for 3 min (RBC Lysis Buffer, Sigma-Aldrich). Cells were counted with a Neubauer chamber, and then cultured in RPMI 1640 (Gibco) supplemented with 10% FBS, plus 100 U/ml penicillin and 2 mM L-glutamine (complete RPMI) at 37ºC and 5% CO_2.

- For *BrdU in vitro Assay*, 2x10^{5} BAL AMs from pools of mice were plated in triplicates (RPMI, M-CSF and rGM-CSF) in non-tissue cultured treated 24well-plates (Falcon) in 1.5 ml per well of complete RPMI. 2-3h after plating, rM-CSF and rGM-CSF (both from Peprotech) were added to stimulate cell proliferation at a final concentration of 1 ng/ml and 10 pg/ml, respectively. After 10-12h in the presence of cytokines, first pulse of BrdU (BD Pharmingen) was added to the cultures at 10μM. Since cells are not synchronized, a second pulse of BrdU was added to the cultures 24h later, in order to detect all proliferating AMs. 24h after the second pulse, cells were washed once with PBS to remove remaining FBS and incubated with accutase (StemCell Technologies) at 37ºC. After 15-20 min, cells were carefully detached by pipetting. In order to avoid losing semi-adherent cells, RPMI supernatant and PBS from washes were saved and mixed for each well. After centrifugation, cells were counted and the same cell number per condition and genotype was stained for surface markers and BrdU.

- For *Cell morphology analysis*, 2x10^{5} AMs from individual mice were cultured on crystals previously sterilized with a cycle of UV radiation, placed in 24well-plates in complete RPMI at 37ºC and 5% CO_2. After 5 days,

supernatant was carefully removed and cells were fixed for 10 min with paraformaldehyde (PFA) 4% (Thermo Fisher) at RT. Then, cells were washed twice with PBS and crystals stained with Hematoxylin and Eosin.

Cell image acquisition & analysis

Cells were examined with a Leica DM 2500 light microscope and images captured with a Leica DFC 420 digital camera. At least 3 images of different fields of a single mouse were acquired and further analyzed. Image processing and quantification of AM size and circularity were developed as a macro in Fiji (ImageJ 1.50e x64). A first preprocessing step converts the 10X color image into grayscale, applies a gaussian blurring (sigma=3), and normalizes it in order to reduce noise and standardize the intensity values. An initial segmentation of objects is done using a marker-controlled watershed algorithm (Legland et al., 2016) trying to maximize the differential detection of cells closely situated or clustered, without over-segmenting elongated cells as multiple objects. "Marker" and "mask" images used to that end were created by automatic thresholding using Minimum and Otsu implementations respectively, followed by morphological operations in order to condense the segmented objects and discard noisy elements (hole filling, closing, area opening, and removal of objects partially detected in the boundaries). The stricter first threshold allows a proper definition of seed locations ("marker") and the more permissive Otsu method achieves robust and accurate segmentation of complete macrophages ("mask"). Objects segmented in "mask" image and split by the explained watershed strategy are later filtered to discard mistakes (dirtiness and shadows typical of the image modality), by removing those ones where the ratio between mean intensity inside the object and its 10-pixel outer-ring is lower than 120% and with dimensions very far from the typical values. Circularity (4π*area/perimeter^2) and size are measured for each final detected cell and mean values are reported for each individual image. Statistical analysis was performed comparing average of the mean values obtained from groups of at least 5 mice per genotype and/or condition.

RNA isolation and quantitative-qPCR

Cell lysis was performed with buffer RLT (Qiagen), containing 10µ/ml β-mercaptoethanol and RNA was isolated with RNeasy Plus Mini Kit (Qiagen). RNA concentration and integrity were determined with an Agilent 2100 Bioanalyzer (Caliper Life Science). Samples with RNA integrity values > 8 were further processed. cDNA was prepared using the High Capacity cDNA reverse transcription kit (Applied Biosystems, Foster City, CA). Quantitative PCR was performed in a 7900-FAST-384 instrument (Applied Biosystems) by using the GoTaq qPCR master mix from Promega (Madison, WI). Primers used in this work (synthetized by Sigma) were as follows:

β-actin Fw: 5′-GGCTGTATTCCCCTCCATCG-3′, *β-actin* Rv: 5′-CCAGTTGGTAACAATGCCATGT-3′, *Vhl* Fw: 5′-TGTGCCATCCCTCAATGTCG-3′, *Vhl* Rv: 5′-CTTCCGCACACTGGGTAGT-3′, *Slc2a1*Fw: 5′-GGGCATGTGCTTCCAGTATGT-3′, *Slc2a1* Rv: 5′-ACGAGGAGCACCGTGAAGAT-3′, *Ldha* Fw: 5′-TGTCTCCAGCAAAGACTACTGT-3′, *Ldha* Rv: 5′-GACTGTACTTGACAATGTTGGGA-3′, *Arg1* Fw: 5′-CTCCAAGCCAAAGTCCTTAGAG-3′ , *Arg1* Rv: 5′-AGGAGCTGTCATTAGGGACATC-3′, *Itgax* Fw: 5′-AGTGCTAGGGGACGTGAATG-3′, *Itgax* Rv: 5′-TCTGGGATGCTGAAATCCTC-3′ , *Siglec5* Fw: 5′-TTACCTGGCACTGGTGTTACTG-3′, *Siglec5* Rv: 5′-ATCTGCAGAGATGCTCCACTC-3′, *Fcgr1* Fw: 5′-GACAGTGGCGAATACAGGTGT-3′, *Fcgr1* Rv: 5′-ATGGCGACCTCCGAATCTGA-3′, *Itgam* Fw: 5′-ATGGACGCTGATGGCAATACC-3′, *Itgam* Rv: 5′-TCCCCATTCACGTCTCCCA-3′, *Ccnb1* Fw: 5′-AAGGTGCCTGTGTGTGAACC-3′, *Ccnb1* Rv: 5′-GTCAGCCCCATCATCTGCG-3′, *Ccnb2* Fw: 5′-GCCAAGAGCCATGTGACTATC-3′, *Ccnb2* Rv: 5′-CAGAGCTGGTACTTTGGTGTTC-3′, *Cdk1* Fw: 5′-AGAAGGTACTTACGGTGTGGT-3′, *Cdk1* Rv: 5′-GAGAGATTTCCCGAATTGCAGT-3′, *Cd25c* Fw: 5′-AGCGTAGCACATCTGCACATA-3′, *Cd25c* Rv: 5′-AGGAACCGTAGTAATGGGACTG-3′, *Plk3* Fw: 5′-GCACATCCATCGGTCATCCAG-3′, *Plk3* Rv: 5′-GCCACAGTCAAACCTTCTTCAA-3′, *Brca1* Fw: 5′-AGGAGGCGTCGATCATCCA-3′, *Brca1* Rv: 5′-ACAGATTTCTTTCGAGGTTGGG-3′ , *Chek1* Fw: 5′-TTCCACCAACTCATGGCAGG-3′, *Chek1* Rv: 5′-GCGTTCACGATTATTATGCCGAA-3′, *Chek2* Fw: 5′-GATCATTAGCAAGCGGAGGTT-3′, *Chek2* Rv: 5′-CACCACCCGGTCAAATAGTTC-3′, *Tp53* Fw: 5′-CTCTCCCCCGCAAAAGAAAAA-3′, *Tp53* Rv: 5′-CGGAACATCTCGAAGCGTTTA-3′, *Cdkn1a* Fw: 5′-CCTGGTGATGTCCGACCTG-3′, *Cdkn1a* Rv: 5′-CCATGAGCGCATCGCAATC-3′, *Nr1h3* Fw: 5′-

CTCAATGCCTGATGTTTCTCCT-3′, *Nr1h3* Rv: 5′-TCCAACCCTATCCCTAAAGCAA-3′, *Nr1h2* Fw: 5′-CGTGGTCATCTTAGAGCCAGA-3′

Nr1h2 Rv: 5′-GCTGAGCACGTTGTAGTGGAA-3′, *Abcg1* Fw: 5′-CTTTCCTACTCTGTACCCGAGG-3′, *Abcg1* Rv: 5′-CGGGGCATTCCATTGATAAGG-3′, *Apoe* Fw: 5′-CTGACAGGATGCCTAGCCG-3′, *Apoe* Rv: 5′-CGCAGGTAATCCCAGAAGC-3′, *Pltp* Fw: 5′-CGCAAAGGGCCACTTTTACTA-3′, *Pltp* Rv: 5′-GCCCCCATCATATAAGAACCAG-3′. mRNA levels are shown as relative expression to β-actin (ΔΔCt) as indicated in figure legends.

Metabolic measurements

Real-time oxygen-consumption rate (OCR) and extracellular acidification rate (ECAR) in AMs were determined with an XF-96 Extracellular Flux Analyzer (Seahorse Bioscience). The assay was performed in DMEM supplemented with 2mM L-glutamine, 100 µg/ml streptomycin, phenol red and 25mM glucose + 1mM pyruvate or 5mM L-carnitine + 50 µM palmitoyl-CoA. The pH was adjusted to 7.4 with KOH. Three consecutive measurements were performed under basal conditions and after the sequential addition of the following mitochondrial electron transport chain (mETC) inhibitors: 1µM oligomycin. 1µM carbonyl cyanide m-chlorophenyl (CCCP), 1µM rotenone and 1µM antimycin A (Sigma-Aldrich). Basal respiration rate (BRR) was defined as OCR in the absence of any inhibitor. Basal ECAR (B. ECAR) was measured in the absence of drugs. AMs newly obtained from BAL were pooled from 5 to 10 mice per genotype. After red blood cell lysis, AMs were counted, washed once with Seahorse media, and $2.5x10^5$ AMs were plated in 180µl of seahorse media per well in 3 to 10 wells (replicates). After spin down, plates were incubated at 37ºC without CO_2 for 30 min before seahorse assay was run.

BrdU proliferation *in vivo*

Four groups of mice (2 groups of each genotype) were daily injected with 1mg BrdU (Sigma-Aldrich) for 2 weeks. One day and 21 days after the last injection, two groups (one of each genotype) were sacrificed and BAL AMs were analyzed for BrdU incorporation (Hashimoto et al., 2013). The ratio of frequencies of $BrdU^+$ AMs at day 21 and day 1 was calculated as a measurement of BrdU dilution during 21 days.

Pulmonary macrophage transplantation

Csf2rb$^{-/-}$ mice were pulmonary transplanted with $5x10^4$ AMs newly obtained from BAL pools of control *Vhl*$^{fl/fl}$ and CD11cΔ*Vhl* mice. Before transplantation, receptor mice were anesthetized with Ketamine (Imalgene, Merial) and Xylacine (Rompun, Bayer). When fully unconscious, a small incision was done to partially expose trachea. Then, animals were carefully intubated orotracheally with an I.V. catheter (22 GA, 0.9x25 mm; BD Insyte). Cells were inoculated with a pipette in 30µl of PBS. Next, mice were extubated and the incision sutured. Mice were finally injected with anesthesia reversor (Medeson, Urano) and kept in a warm plaque until full recovery. AMs viability was higher than 90% after the last transplantation. Six weeks after transplantation, we performed BAL of transferred mice with 1ml of PBS. In order to get rid of debris, BAL was centrifuged at 1700rpm for 5 min at RT, and BAL supernatant was used to measure total protein content in BAL and surfactant protein D (SP-D) concentration. Cell engraftment was compared by flow cytometry of total lung cells.

BCA protein measurement

Total protein concentration was determined using Pierce BCA Protein Assay Kit (Thermo Scientific) according to the manufacturer's instruction. Albumin (Thermo scientific) was used as standard.

ELISA surfactant protein D

SP-D DUO ELISA kit and capture/detection antibodies were from R&D Systems. It was used according to manufacturer's instructions. Detection antibody was biotinylated and labeled with streptavidin-conjugated horseradish peroxidase (HRP) and visualized by incubation with 5,5′-tetramethylbenzidine solution (TMB, KPL). Reaction was stopped with TMB-stop solution (KPL). Recombinant SP-D served as standard and was included

in the kit. Optical density was determined using a microplate reader (Benchmark Plus, Bio-Rad) set to 450 nm subtracting absorbance at 570 nm (wavelength correction).

Lung cell suspension preparation

Adult lungs were collected in RPMI, cut into small pieces, and enzyme digested at 37ºC with Liberase TM (Sigma-Aldrich) for 30 min. Cells were passed through a 70µm cell strainer (Falcon) and washed with flow cytometry buffer. After red blood cell lysis, cells were centrifuged and resuspended in 1ml of cold flow cytometry buffer. Cells were counted with CASYton cell counter (Roche Innovatis) and stained for flow cytometry analysis.

Flow cytometry

Stainings were performed at 4ºC with the appropriate antibody (Ab) cocktail in cold flow cytometry buffer. Samples were processed with a Spectral Analyzer flow cytometer (SP6800, SONY), and data were analyzed with FlowJo software (Tree Star). CD16/CD32 (TONBO bioscience, San Diego, CA) was used to reduce non-specific binding. The following Abs were used for the analysis of *AM surface expression profile*: anti-CD11c-Brilliant Violet 510 (HL3, BD Biosciences), anti-Siglec-F-PE, anti-Siglec-F-PerCP-Cy5.5, anti-Siglec-F-BV421 or anti-Siglec-F-Alexa Fluor 647 (All of them: clone E50-2440, BD Biosciences), anti-CD64-APC (X54-5/7.1, BD Biosciences), anti-CD11b-PE-Cy7 (M1/70, BD Biosciences), anti-CD115-biotin (AFS98, eBiosciences), Streptavidin-APC (eBiosciences). During the analysis, we realized that control *Vhl*$^{fl/fl}$ and CD11cΔ*Vhl* AMs had a distinct intrinsic autofluorescence (AUF), thus, we used Spectral analyzer software to normalize GMOF for each fluorochrome based on genotype-specific AUF. The following Abs were used for *lung staining*: anti-CD45-PerCP-Cy5.5 (30-F11, eBiosciences) or anti-CD45-BV570 (30-F11, Biolegend), anti-CD45.1-APC (A20, eBiosciences), anti-F4/80 biotin (BM8, Life Technologies), anti-CD11c, anti-Siglec-F, anti-CD11b, anti-I-A/I-E-FITC (2G9, BD Biosciences) or anti-I-A/I-E-APC (M5/114.15.2, BD Biosciences), anti-Ly6G-APC or anti-Ly6G-PE (1A8, BD Pharmingen), and anti-Ly6C-FITC (AL-21, BD Biosciences). The following Abs were used for *blood staining*: anti-CD45.1-APC, anti-Ly6G-PE, anti-Ly6C-FITC and anti-CD11b-PerCP-Cy5.5 (M1/70, eBiosciences). Hoechst 33258 (Invitrogen) was used at 0.1µM as a counterstain to exclude dead cells. Lung AM population was defined as: CD45^{+}, F4/80^{+}, CD11c^{+}, Siglec-F^{+}, CD11b$^{-/mid}$, I-A/I-E^{lo}. Blood and lung monocytes were defined as: CD45^{+}, CD11b^{hi}, Ly6G^{-}, Ly6C^{hi}. For *intracellular Ki67 staining*, same AM number were stained for surface markers, washed twice and mixed with unstained thymocytes, used as a cell carrier. Just after, cells were fixed and permeabilized using the FoxP3 staining buffer set (eBiosciences), and then stained with anti-Ki67-eFluor 660 (SolA15, eBiosciences) or isotype control Rat IgG2aκ (eBR2a, eBiosciences). For intracellular BrdU staining, AMs were stained and mixed with carrier cells as explained above, and then fixed and permeabilized using the BrdU staining set (BD Pharmingen). Then, cells were treated with DNAse and stained with anti-BrdU Ab (BD Pharmingen).

Bioinformatics Analysis

GSE60249 array data (Schneider et al., 2014)

Array data (CEL files) were downloaded from GEO and imported into the R software environment with functions provided by packages GEOquery and oligo. RMA (affy package) was used for data processing, normalization and calculation of log2 transformed expression values. The corresponding array annotation database (mogene11sttranscriptcluster.db) was used to map expression values with their associated Ensembl gene IDs, by selecting the associated transcript clusters with the higher median value across all samples.

Gene Set Enrichment Analysis tool from the Molecular Signature Database MSigDB (http://software.broadinstitute.org/gsea/msigdb/collections.jsp), was used to identify enriched gene sets, using the Hallmark gene sets. Enriched gene sets, having up-regulated and down-regulated genes, were identified using weighted enrichment statistic and a log2 ratio metric for ranking genes. Significance was defined by FDR q value < 0.25, obtained after one thousand phenotype permutations.

Heatmaps were generated with Heatmapper (Babicki et al., 2016), using no clustering method and Euclidean as distance measurement method.

RNA Seq

BAL AMs were pooled from 5-7 mice per genotype and further purified by positive selection with anti-CD11c-microbeads (Miltenyi Biotec), following manufacturer's instructions. A total of 3 pools per genotype were used for RNA Seq.

Differential expression analysis.

Sequencing reads were pre-processed by means of a pipeline that used FastQC (www.bioinformatics.babraham.ac.uk/projects/fastqc) to assess read quality, and Cutadapt v1.6 (http://journal.embnet.org/index.php/embnetjournal/article/view/200) to trim sequencing reads, eliminate Illumina adaptor remains, and to discard reads that were shorter than 30 base pairs. The resulting reads were mapped against the mouse transcriptome (GRCm38 assembly, Ensembl release 76) and quantified using RSEM v1.2.3 (Li and Dewey, 2011). Raw expression counts were then processed with an analysis pipeline that used the Bioconductor package EdgeR (Robinson et al., 2010) for normalization (using TMM method) and differential expression testing. Only genes expressed at a minimal level of 1 count per million, in at least 3 samples, were considered for differential expression analysis. Changes in gene expression were considered significant if associated to a Benjamini and Hochberg adjusted p-value < 0.05.

Functional analysis. Collections of differentially expressed genes were analyzed with Ingenuity Pathway Analysis (IPA) (https://www.qiagenbioinformatics.com/products/ingenuity-pathway-analysis) to determine significant associations to canonical pathways, biological functions and upstream transcriptional regulators; significance was defined by a Benjamini and Hochberg adjusted p-value < 0.05. GOrilla and ReViGO were used to identify and summarize Gene Ontology terms enriched in the collections of differentially expressed genes; significance was defined by FDR q value < 0.05. Venn diagram was generated by term lists comparison with Venny (http://bioinfogp.cnb.csic.es/tools/venny/index.html) to identify and visualize specific and shared elements. Circular plots representing the association between genes and enriched functional categories were generated with GOplot. GSEA was used to identify enriched gene sets, from the Hallmark collection of MSigDB, having up-regulated and down-regulated genes, using a weighted enrichment statistic and a log2 ratio metric for ranking genes. Significance was defined by FDR q value < 0.25, obtained after one thousand phenotype permutations.

Statistical Analysis

Statistical comparisons were made with Prism v7 (GraphPad Software, La Jolla, CA). Statistical tests are detailed in figure legends. p-values: ns, not significant; *p < 0.05; **p < 0.01; ***p < 0.001.

ACKNOWLEDGMENTS

We are grateful to the members of the D.S. lab for discussions and critical reading of the manuscript. We are grateful to Andrés Hidalgo for providing DsRed mice, to Stefanie K. Wculek for helping in BM transplantation and to Natalia Pietrosemoli for support in the *in silico* analysis. We thank the CNIC facilities and personnel for technical support and S. Bartlett for editorial assistance. H.M.I. was funded by the Spanish Ministry of Economy, Industry and Competitiveness (MINECO, BFU). Work in the D.S. laboratory is funded by the CNIC and grant SAF2016-79040-R from MEIC, Agencia Estatal de Investigación and FEDER; B2017/BMD-3733 Immunothercan-CM from Comunidad de Madrid; RD16/0015/0018-REEM from FIS-Instituto de Salud Carlos III, MEIC and FEDER; Acteria Foundation; Constantes y Vitales prize (Atresmedia); La Marató de TV3 Foundation (201723); the European Commission (635122-PROCROP H2020) and the European Research Council (ERC-2016-Consolidator Grant 725091). The CNIC is supported by the MEIC and the Pro-CNIC Foundation, and is a Severo Ochoa Center of Excellence (SEV-2015-0505).

The authors have no conflicting financial interests.

Author contributions: H.M.I. and D.S. conceived and designed the project. H.M.I., P.B., R.C., E.P., M.E., S.M.-C., I.S., and L.C. performed the experiments. H.M.I., R.C. and P.B. acquired the data. H.M.I. and D.S. analyzed and interpreted the data. M.J.G analyzed *in silico* data. D.J.-C. analyzed microscopy images. R.C., S.M.-C, I.S., S.M.-P., and M.G. contributed with technical, material, intellectual and administrative support. All the authors discussed the results and the manuscript. H.M.I. and D.S. wrote the manuscript. D.S. supervised the study.

REFERENCES

Babicki, S., Arndt, D., Marcu, A., Liang, Y., Grant, J.R., Maciejewski, A., and Wishart, D.S. (2016). Heatmapper: web-enabled heat mapping for all. Nucleic Acids Res 44, W147-153.

Baker, A.D., Malur, A., Barna, B.P., Ghosh, S., Kavuru, M.S., Malur, A.G., and Thomassen, M.J. (2010). Targeted PPAR{gamma} deficiency in alveolar macrophages disrupts surfactant catabolism. J Lipid Res 51, 1325-1331.

Bensaad, K., Favaro, E., Lewis, C.A., Peck, B., Lord, S., Collins, J.M., Pinnick, K.E., Wigfield, S., Buffa, F.M., Li, J.L., et al. (2014). Fatty acid uptake and lipid storage induced by HIF-1alpha contribute to cell growth and survival after hypoxia-reoxygenation. Cell Rep 9, 349-365.

Bhandari, T., Olson, J., Johnson, R.S., and Nizet, V. (2013). HIF-1alpha influences myeloid cell antigen presentation and response to subcutaneous OVA vaccination. J Mol Med 91, 1199-1205.

Brandes, M., Klauschen, F., Kuchen, S., and Germain, R.N. (2013). A systems analysis identifies a feedforward inflammatory circuit leading to lethal influenza infection. Cell 154, 197-212.

Caton, M.L., Smith-Raska, M.R., and Reizis, B. (2007). Notch-RBP-J signaling controls the homeostasis of CD8- dendritic cells in the spleen. J Exp Med 204, 1653-1664.

Chen, C., Pore, N., Behrooz, A., Ismail-Beigi, F., and Maity, A. (2001). Regulation of glut1 mRNA by hypoxia-inducible factor-1. Interaction between H-ras and hypoxia. J Biol Chem 276, 9519-9525.

Cramer, T., Yamanishi, Y., Clausen, B.E., Förster, I., Pawlinski, R., Mackman, N., Haase, V.H., Jaenisch, R., Corr, M., Nizet, V., et al. (2003). HIF-1alpha is essential for myeloid cell-mediated inflammation. Cell 112, 645-657.

Crotty Alexander, L.E., Akong-Moore, K., Feldstein, S., Johansson, P., Nguyen, A., McEachern, E.K., Nicatia, S., Cowburn, A.S., Olson, J., Cho, J.Y., et al. (2013). Myeloid cell HIF-1α regulates asthma airway resistance and eosinophil function. Journal of molecular medicine (Berlin, Germany) 91, 637-644.

Deng, W., Yang, J., Lin, X., Shin, J., Gao, J., and Zhong, X.P. (2017). Essential Role of mTORC1 in Self-Renewal of Murine Alveolar Macrophages. J Immunol 198, 492-504.

Guilliams, M., De Kleer, I., Henri, S., Post, S., Vanhoutte, L., De Prijck, S., Deswarte, K., Malissen, B., Hammad, H., and Lambrecht, B.N. (2013). Alveolar macrophages develop from fetal monocytes that differentiate into long-lived cells in the first week of life via GM-CSF. J Exp Med 210, 1977-1992.

Haase, V.H., Glickman, J.N., Socolovsky, M., and Jaenisch, R. (2001). Vascular tumors in livers with targeted inactivation of the von Hippel-Lindau tumor suppressor. Proc Natl Acad Sci U S A 98, 1583-1588.

Hammami, A., Charpentier, T., Smans, M., and Stäger, S. (2015). IRF-5-Mediated Inflammation Limits CD8+ T Cell Expansion by Inducing HIF-1α and Impairing Dendritic Cell Functions during Leishmania Infection. PLoS Pathogens 11, e1004938.

Happle, C., Lachmann, N., Skuljec, J., Wetzke, M., Ackermann, M., Brennig, S., Mucci, A., Jirmo, A.C., Groos, S., Mirenska, A., et al. (2014). Pulmonary transplantation of macrophage progenitors as effective and long-lasting therapy for hereditary pulmonary alveolar proteinosis. Sci Transl Med 6, 250ra113.

Hashimoto, D., Chow, A., Noizat, C., Teo, P., Beasley, M.B., Leboeuf, M., Becker, C.D., See, P., Price, J., Lucas, D., et al. (2013). Tissue-Resident Macrophages Self-Maintain Locally throughout Adult Life with Minimal Contribution from Circulating Monocytes. Immunity 38, 792-804.

Hoeffel, G., Chen, J., Lavin, Y., Low, D., Almeida, F.F., See, P., Beaudin, A.E., Lum, J., Low, I., Forsberg, E.C., et al. (2015). C-Myb(+) erythro-myeloid progenitor-derived fetal monocytes give rise to adult tissue-resident macrophages. Immunity 42, 665-678.

Huang, D., Li, T., Li, X., Zhang, L., Sun, L., He, X., Zhong, X., Jia, D., Song, L., Semenza, G.L., et al. (2014). HIF-1-mediated suppression of acyl-CoA dehydrogenases and fatty acid oxidation is critical for cancer progression. Cell Rep 8, 1930-1942.

Imperatore, F., Maurizio, J., Vargas Aguilar, S., Busch, C.J., Favret, J., Kowenz-Leutz, E., Cathou, W., Gentek, R., Perrin, P., Leutz, A., et al. (2017). SIRT1 regulates macrophage self-renewal. EMBO J 36, 2353-2372.

Imtiyaz, H.Z., Williams, E.P., Hickey, M.M., Patel, S.A., Durham, A.C., Yuan, L.J., Hammond, R., Gimotty, P.A., Keith, B., and Simon, M.C. (2010). Hypoxia-inducible factor 2alpha regulates macrophage function in mouse models of acute and tumor inflammation. J Clin Invest 120, 2699-2714.

Jiang, X., Clark, R.A., Liu, L., Wagers, A.J., Fuhlbrigge, R.C., and Kupper, T.S. (2012). Skin infection generates non-migratory memory CD8+ T(RM) cells providing global skin immunity. Nature 483, 227-231.

Lee, Y.M., Jeong, C.H., Koo, S.Y., Son, M.J., Song, H.S., Bae, S.K., Raleigh, J.A., Chung, H.Y., Yoo, M.A., and Kim, K.W. (2001). Determination of hypoxic region by hypoxia marker in developing mouse embryos in vivo: a possible signal for vessel development. Dev Dyn 220, 175-186.

Legland, D., Arganda-Carreras, I., and Andrey, P. (2016). MorphoLibJ: integrated library and plugins for mathematical morphology with ImageJ. Bioinformatics 32, 3532-3534.

Li, B., and Dewey, C.N. (2011). RSEM: accurate transcript quantification from RNA-Seq data with or without a reference genome. BMC Bioinformatics 12, 323.

Li, C., Wang, Y., Li, Y., Yu, Q., Jin, X., Wang, X., Jia, A., Hu, Y., Han, L., Wang, J., et al. (2018). HIF1alpha-dependent glycolysis promotes macrophage functional activities in protecting against bacterial and fungal infection. Sci Rep 8, 3603.

Menendez-Montes, I., Escobar, B., Palacios, B., Gomez, M.J., Izquierdo-Garcia, J.L., Flores, L., Jimenez-Borreguero, L.J., Aragones, J., Ruiz-Cabello, J., Torres, M., et al. (2016). Myocardial VHL-HIF Signaling Controls an Embryonic Metabolic Switch Essential for Cardiac Maturation. Dev Cell 39, 724-739.

Na, T.Y., Lee, H.J., Oh, H.J., Huh, S., Lee, I.K., and Lee, M.O. (2011). Positive cross-talk between hypoxia inducible factor-1alpha and liver X receptor alpha induces formation of triglyceride-loaded foam cells. Arterioscler Thromb Vasc Biol 31, 2949-2956.

Nakamura, A., Ebina-Shibuya, R., Itoh-Nakadai, A., Muto, A., Shima, H., Saigusa, D., Aoki, J., Ebina, M., Nukiwa, T., and Igarashi, K. (2013). Transcription repressor Bach2 is required for pulmonary surfactant homeostasis and alveolar macrophage function. J Exp Med 210, 2191-2204.

Nakazawa, M.S., Keith, B., and Simon, M.C. (2016). Oxygen availability and metabolic adaptations. Nat Rev Cancer 16, 663-673.

Peyssonnaux, C., Datta, V., Cramer, T., Doedens, A., Theodorakis, E.A., Gallo, R.L., Hurtado-Ziola, N., Nizet, V., and Johnson, R.S. (2005). HIF-1alpha expression regulates the bactericidal capacity of phagocytes. J Clin Invest 115, 1806-1815.

Robb, L., Drinkwater, C.C., Metcalf, D., Li, R., Kontgen, F., Nicola, N.A., and Begley, C.G. (1995). Hematopoietic and lung abnormalities in mice with a null mutation of the common beta subunit of the receptors for granulocyte-macrophage colony-stimulating factor and interleukins 3 and 5. Proc Natl Acad Sci U S A 92, 9565-9569.

Robinson, M.D., McCarthy, D.J., and Smyth, G.K. (2010). edgeR: a Bioconductor package for differential expression analysis of digital gene expression data. Bioinformatics 26, 139-140.

Roiniotis, J., Dinh, H., Masendycz, P., Turner, A., Elsegood, C.L., Scholz, G.M., and Hamilton, J.A. (2009). Hypoxia prolongs monocyte/macrophage survival and enhanced glycolysis is associated with their maturation under aerobic conditions. J Immunol 182, 7974-7981.

Saluzzo, S., Gorki, A.D., Rana, B.M., Martins, R., Scanlon, S., Starkl, P., Lakovits, K., Hladik, A., Korosec, A., Sharif, O., et al. (2017). First-Breath-Induced Type 2 Pathways Shape the Lung Immune Environment. Cell Rep 18, 1893-1905.

Schneider, C., Nobs, S.P., Kurrer, M., Rehrauer, H., Thiele, C., and Kopf, M. (2014). Induction of the nuclear receptor PPAR-gamma by the cytokine GM-CSF is critical for the differentiation of fetal monocytes into alveolar macrophages. Nat Immunol 15, 1026-1037.

Semenza, G.L., Jiang, B.H., Leung, S.W., Passantino, R., Concordet, J.P., Maire, P., and Giallongo, A. (1996). Hypoxia response elements in the aldolase A, enolase 1, and lactate dehydrogenase A gene promoters contain essential binding sites for hypoxia-inducible factor 1. J Biol Chem 271, 32529-32537.

Shibata, Y., Berclaz, P.Y., Chroneos, Z.C., Yoshida, M., Whitsett, J.A., and Trapnell, B.C. (2001). GM-CSF regulates alveolar macrophage differentiation and innate immunity in the lung through PU.1. Immunity 15, 557-567.

Sieweke, M.H., and Allen, J.E. (2013). Beyond stem cells: self-renewal of differentiated macrophages. Science 342, 1242974.

Sinclair, C., Bommakanti, G., Gardinassi, L., Loebbermann, J., Johnson, M.J., Hakimpour, P., Hagan, T., Benitez, L., Todor, A., Machiah, D., et al. (2017). mTOR regulates metabolic adaptation of APCs in the lung and controls the outcome of allergic inflammation. Science 357, 6355.

Soucie, E.L., Weng, Z., Geirsdottir, L., Molawi, K., Maurizio, J., Fenouil, R., Mossadegh-Keller, N., Gimenez, G., VanHille, L., Beniazza, M., et al. (2016). Lineage-specific enhancers activate self-renewal genes in macrophages and embryonic stem cells. Science 351, aad5510.

Stanley, E., Lieschke, G.J., Grail, D., Metcalf, D., Hodgson, G., Gall, J.A., Maher, D.W., Cebon, J., Sinickas, V., and Dunn, A.R. (1994). Granulocyte/macrophage colony-stimulating factor-deficient mice show no major perturbation of hematopoiesis but develop a characteristic pulmonary pathology. Proc Natl Acad Sci U S A 91, 5592-5596.

Suzuki, T., Arumugam, P., Sakagami, T., Lachmann, N., Chalk, C., Sallese, A., Abe, S., Trapnell, C., Carey, B., Moritz, T., et al. (2014). Pulmonary macrophage transplantation therapy. Nature 514, 450-454.

Swain, L., Wottawa, M., Hillemann, A., Beneke, A., Odagiri, H., Terada, K., Endo, M., Oike, Y., Farhat, K., and Katschinski, D.M. (2014). Prolyl-4-hydroxylase domain 3 (PHD3) is a critical terminator for cell survival of macrophages under stress conditions. J Leukoc Biol 96, 365-375.

Takeda, N., O'Dea, E.L., Doedens, A., Kim, J.W., Weidemann, A., Stockmann, C., Asagiri, M., Simon, M.C., Hoffmann, A., and Johnson, R.S. (2010). Differential activation and antagonistic function of HIF-{alpha} isoforms in macrophages are essential for NO homeostasis. Genes Dev 24, 491-501.

Thomassen, M.J., Barna, B.P., Malur, A.G., Bonfield, T.L., Farver, C.F., Malur, A., Dalrymple, H., Kavuru, M.S., and Febbraio, M. (2007). ABCG1 is deficient in alveolar macrophages of GM-CSF knockout mice and patients with pulmonary alveolar proteinosis. J Lipid Res 48, 2762-2768.

van de Laar, L., Saelens, W., De Prijck, S., Martens, L., Scott, C.L., Van Isterdael, G., Hoffmann, E., Beyaert, R., Saeys, Y., Lambrecht, B.N., et al. (2016). Yolk Sac Macrophages, Fetal Liver, and Adult Monocytes Can Colonize an Empty Niche and Develop into Functional Tissue-Resident Macrophages. Immunity 44, 755-768.

Walmsley, S.R., Chilvers, E.R., Thompson, A.A., Vaughan, K., Marriott, H.M., Parker, L.C., Shaw, G., Parmar, S., Schneider, M., Sabroe, I., et al. (2011). Prolyl hydroxylase 3 (PHD3) is essential for hypoxic regulation of neutrophilic inflammation in humans and mice. J Clin Invest 121, 1053-1063.

Walmsley, S.R., Print, C., Farahi, N., Peyssonnaux, C., Johnson, R.S., Cramer, T., Sobolewski, A., Condliffe, A.M., Cowburn, A.S., Johnson, N., et al. (2005). Hypoxia-induced neutrophil survival is mediated by HIF-1alpha-dependent NF-kappaB activity. J Exp Med 201, 105-115.

Yona, S., Kim, K.W., Wolf, Y., Mildner, A., Varol, D., Breker, M., Strauss-Ayali, D., Viukov, S., Guilliams, M., Misharin, A., et al. (2013). Fate mapping reveals origins and dynamics of monocytes and tissue macrophages under homeostasis. Immunity 38, 79-91.

Yu, X., Buttgereit, A., Lelios, I., Utz, S.G., Cansever, D., Becher, B., and Greter, M. (2017). The Cytokine TGF-beta Promotes the Development and Homeostasis of Alveolar Macrophages. Immunity 47, 903-912 e904.

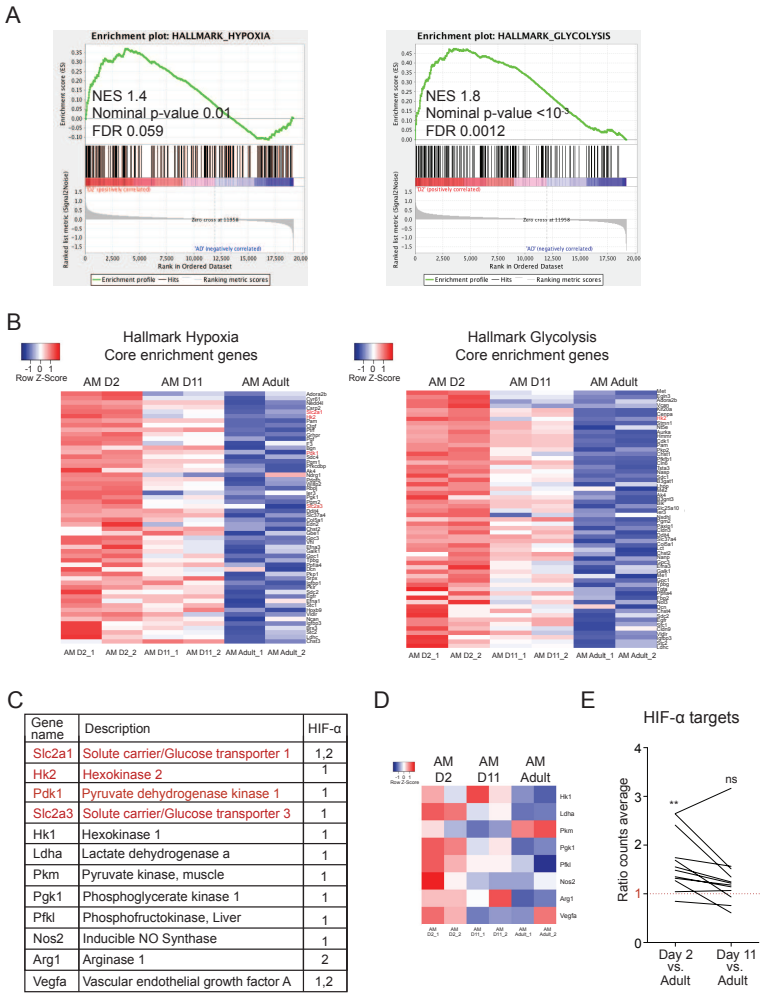

Gene name	Description	HIF-α
Slc2a1	Solute carrier/Glucose transporter 1	1,2
Hk2	Hexokinase 2	1
Pdk1	Pyruvate dehydrogenase kinase 1	1
Slc2a3	Solute carrier/Glucose transporter 3	1
Hk1	Hexokinase 1	1
Ldha	Lactate dehydrogenase a	1
Pkm	Pyruvate kinase, muscle	1
Pgk1	Phosphoglycerate kinase 1	1
Pfkl	Phosphofructokinase, Liver	1
Nos2	Inducible NO Synthase	1
Arg1	Arginase 1	2
Vegfa	Vascular endothelial growth factor A	1,2

Figure 1. Downregulation of hypoxia and glycolysis during postnatal AM maturation. (A) Enrichment plots from GSEA of postnatal day 2 (D2) compared with adult (AD) AMs using the hallmark gene set collection from the Molecular Signature Database (MSigDB). (B) mRNA expression (Log_2 of intensity) of genes from the core of the hallmark gene sets "Hypoxia" and "Glycolysis" in lung AMs from postnatal day 2 (D2), D11 and adult mice. Red squares correspond to over-expressed genes and blue squares correspond to under-expressed genes. (C) Table depicting some classic HIF target genes. Red genes are present in (B). (D) mRNA expression of HIF target genes not included in the hallmark gene sets "Hypoxia" and "Glycolysis" from table Figure 1B (marked in black), color intensity defined as in (B). (E) Mean expression of HIF target genes from (C) in D2 and D11 AMs. Expression values for each gene are shown as the ratio of mean expression on D2 or D11 to the mean expression in adult AMs. ns, not significant; **p-value< 0.01 by Column Statistics analysis, hypothetical value=1.

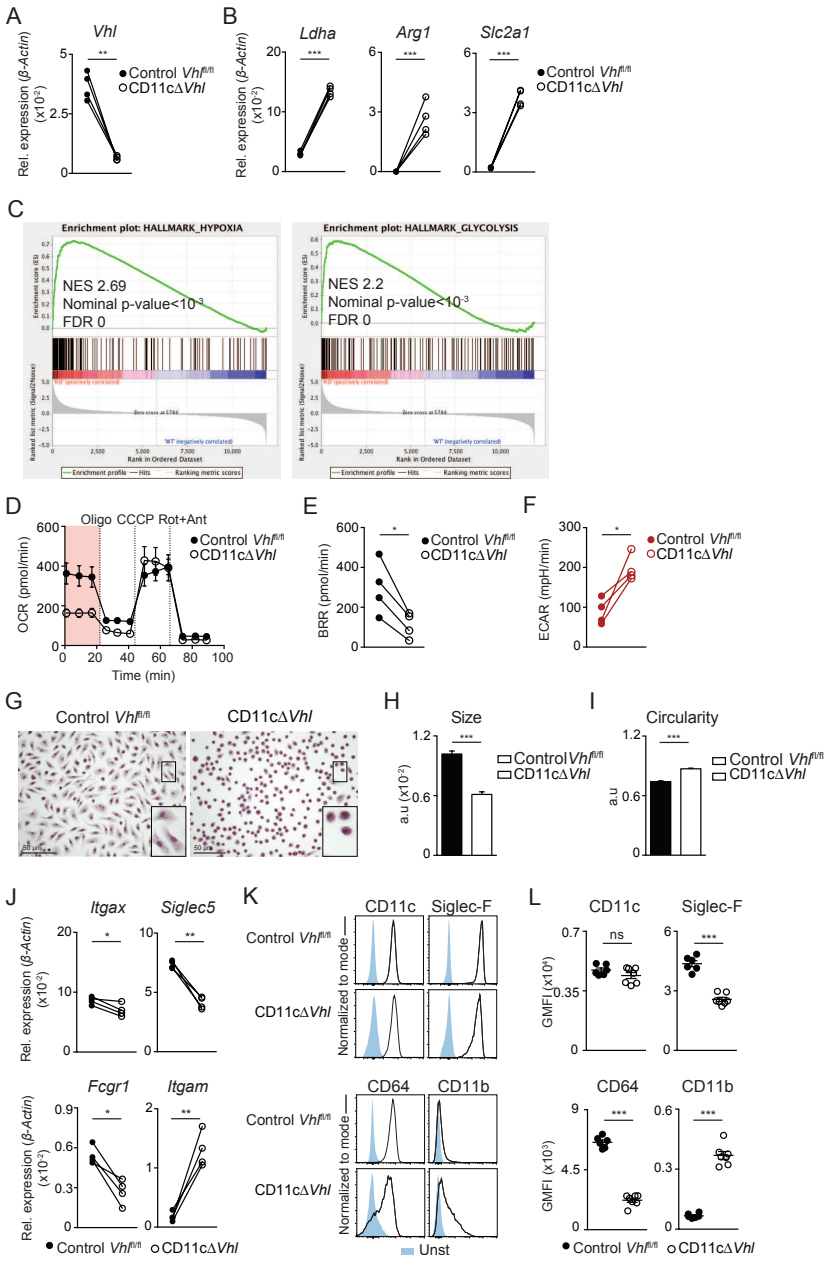

Figure 2. Depletion of VHL alters AM metabolic profile and phenotype. Quantitative PCR for the expression of *Vhl* (A), *Ldha*, *Arg1* and *Slc2a1* (B) in sorted BAL AMs from the indicated mouse genotypes. Data correspond to four pools of mice (n=4-5) represented as individual dots and corresponding to four independent experiments: **, p<0.01; ***, p<0.001 (ratio paired Student *t*-test). (C) Enrichment plots from GSEA analysis of CD11cΔ*Vhl* (KO), compared with control $Vhl^{fl/fl}$ (WT) AMs using the hallmark gene set collection from the Molecular Signature Database MSigDB for *hypoxia* and *glycolysis* gene sets. (D) Oxygen consumption rate (OCR) in the presence of glucose, glutamine and pyruvate by BAL AMs from the indicated genotypes sequentially treated with

oligomycin (Oligo), carbonyl cyanide m-chlorophenylhydrazone (CCCP) and rotenone+antimycin (Rot+Ant). Data are means ± s.d. using AMs pooled from 6-7 mice per genotype in a representative experiment of four performed. (E) Basal respiratory rate (BRR) in AMs measured as in D. (F) Basal extracellular acidification rate (ECAR) in AMs from the indicated genotypes. (E,F) Paired independent experiments (AMs pooled from 4-5 mice per experiment): *, $p<0.05$ (ratio paired Student t test). (G-I) Morphological parameters of BAL AMs after 5-day culture in complete medium. (G) Representative images of Hematoxilin & Eosin staining of BAL AMs from the indicated genotypes, bars 50μm; (H) mean AM size ± s.e.m. (I) mean AM circularity ± s.e.m. (H,I) one representative experiment showing mean± s.e.m. of 4-5 biological replicates with analysis of at least 3 images containing >100 cells per replicate. ***, $p<0.001$ (unpaired Student *t*-test). (J) Quantitative PCR for the expression of *Itgax*, *Siglec5*, *Fcgr1*, and *Itgam* in sorted BAL AMs from mice of the indicated genotypes. Individual dots correspond to four independent experiments, with AMs from 4-5 pooled mice per experiment: *, $p<0.05$; **, $p<0.01$ (ratio paired Student *t*-test). (K) Representative flow cytometry histograms for CD11c, Siglec-F, CD64, and CD11b (black line) compared with unstained samples (tinted blue) in BAL AMs from the indicated genotypes. (L) Normalized geometric mean fluorescence intensity (GMFI) for the selected markers in AMs from the indicated genotypes. Data shown as mean ± s.e.m. from one representative experiment of three performed. Each dot represents the normalized GMFI of an individual mouse (n=6-7 per genotype): ***, $p<0.001$ (unpaired Student *t*-test). See also Figure S1.

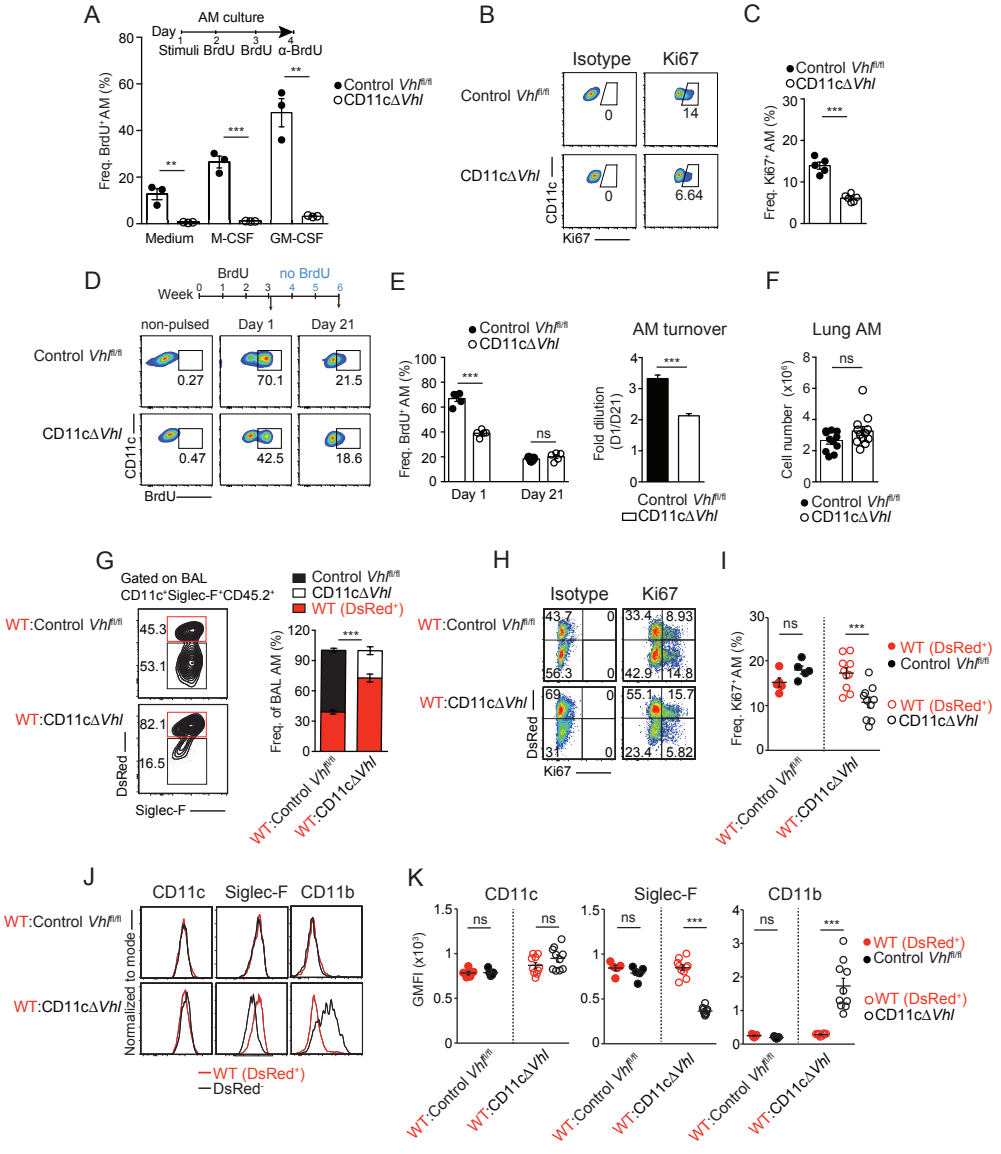

Figure 3. Cell-intrinsic VHL requirement for AM self-renewal and terminal maturation. (A) *In vitro* BrdU assay of AM pools from the indicated genotypes left unstimulated in complete RPMI (medium) or stimulated with rM-CSF (1 ng/ml) or rGM-CSF (10 pg/ml) for 4 days, as indicated. Data shown as means ± s.e.m. of one independent experiment of three performed. Each dot represents a replicate of BAL AMs pooled from 5-6 mice per condition. **, p<0.01; ***, p<0.001; (unpaired Student *t*-test). (B-C) Staining of Ki67 in *ex vivo* BAL AMs isolated from the indicated genotypes. Representative flow cytometry plots showing the positive staining for Ki67 compared with isotype control (B) and frequencies of Ki67$^+$ BAL AMs (C). (D-E) Mice were pulsed with BrdU for three weeks (1mg i.p. daily), and BrdU incorporation into BAL AMs was assessed 1 and 21 days after the last pulse. (D) Representative flow cytometry plots. (E) Frequencies of BrdU$^+$ AMs (left). AM turnover (right) calculated as the ratio of the frequency of BrdU$^+$ AMs at day 1 versus day 21. (F) Total lung AM number. (G) Representative flow cytometry plots and frequencies of DsRed$^+$ (WT) and DsRed$^-$ (Control *Vhl*$^{fl/fl}$ or CD11cΔ*Vhl*)

AMs (normalized to blood Ly6Chi monocyte frequency in each mouse and genotype) in CD45.2^{+} AMs from BM chimeras. (H-I) Staining of Ki67 in *ex vivo* BAL AMs of the indicated genotypes from BM chimeras. (H) Representative flow cytometry plots showing the positive staining for Ki67 compared with isotype control of AMs of the indicated genotypes in each chimera. (I) Frequencies of Ki67^{+} BAL AMs. (J) Representative flow cytometry histograms for CD11c, Siglec-F and CD11b (red line for WT DsRed^{+} AMs or black line for Control *Vhl*$^{fl/fl}$ or CD11cΔ*Vhl* AMs) in BAL AMs from the indicated BM chimera. (K) Normalized GMFI for the selected markers in AMs from the indicated genotypes and chimera. (A,C,E,F) Data are shown as individual data points and means ± s.e.m. of one experiment of three performed (n=4-5 mice per genotype) (A,C,E) or a pool of two experiments of four performed (n=11-12 per group) (F). (G) Data shown as mean ± s.e.m. from one representative experiment of three performed (n=5-10 per genotype). (I-K) Data shown as mean ± s.e.m. from one representative experiment of two performed. Each dot represents the frequency of Ki67+ BAL AMs (I) and the normalized GMFI of an individual mouse (J) (n=5-10 per genotype). **, $p<0.01$; ***, $p<0.001$; ns: not significant (unpaired Student *t*-test). See also Figures S2 and S3.

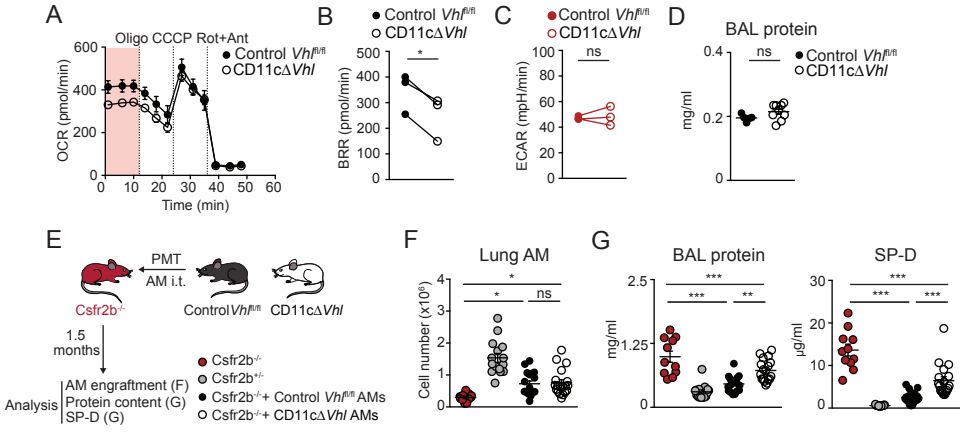

Figure 4. VHL contributes to surfactant handling by AMs. (A) Oxygen consumption rate (OCR) in the presence of palmitoyl Co-A by BAL AMs from the indicated genotypes treated as in Figure 2D. Data are means ± s.d. using AMs pooled from 6-7 mice per genotype in a representative experiment of three performed. (B) Analysis of basal respiratory rate (BRR) in AMs measured as in A. (C) Basal extracellular acidification rate (ECAR) in BAL AMs from the indicated genotypes. (B,C) Paired independent experiments (AMs pooled from 6-7 mice per experiment): *, $p<0.05$. ns, not significant (ratio paired Student t test). (D) Protein concentration in BAL in 3-month-old mice of the indicated genotypes. Data are shown as individual data points and means ± s.e.m. from one representative experiment of three performed (n=5-9). ns: not significant (unpaired Student's *t*-test). (E-G) $5x10^4$ AMs from control $Vhl^{fl/fl}$ or CD11cΔ*Vhl* AMs were transferred intratracheally (i.t.) to $Csfr2b^{-/-}$ mice. After 1.5 months, measurements were made of AM numbers in the lung (F) and of the BAL concentrations of total protein (G, left) and SP-D (G, right). Data are shown as individual data points and means ± s.e.m. of a pool of three independent experiments. Control mice ($Csfr2b^{-/-}$ and $Csfr2b^{+/-}$) are from four independent experiments (n=10-18 per group): ns, not significant; *p-value<0.05; **p-value<0.01; ***p-value<0.001 by one-way ANOVA, Bonferroni post-hoc test. Only some relevant comparisons indicated. See also Figure S2.

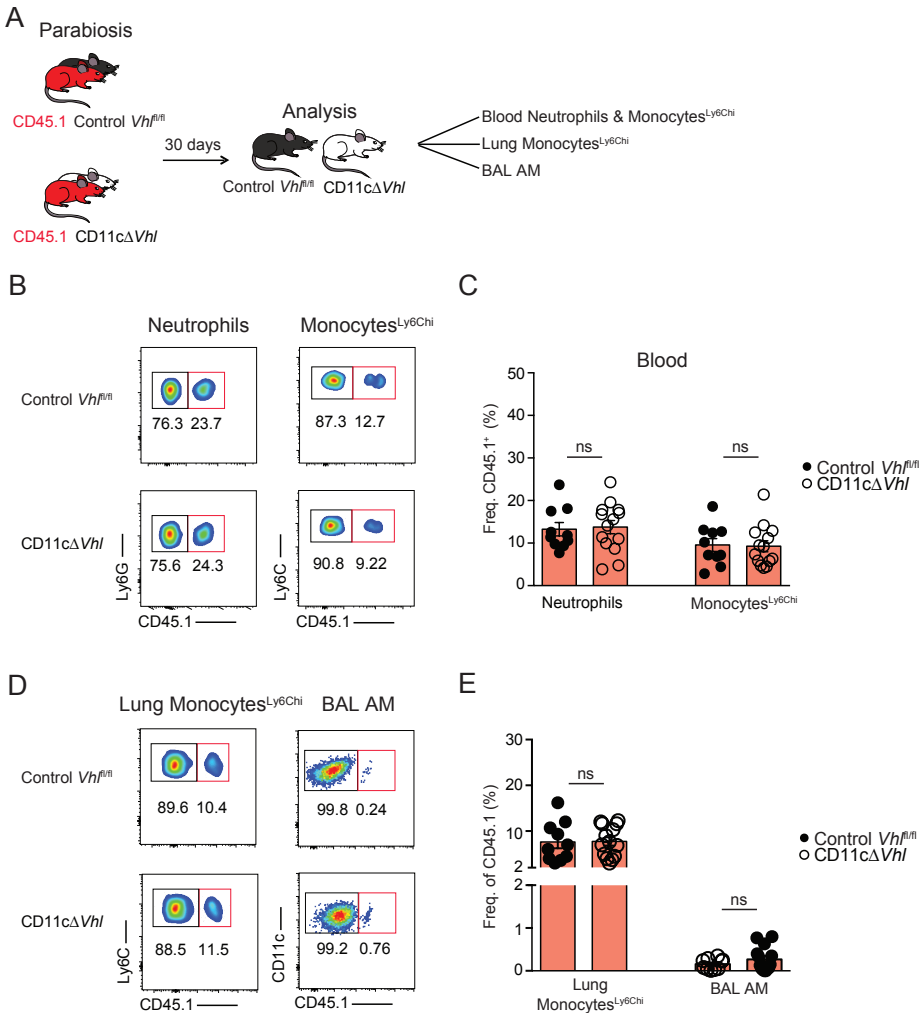

Figure S1, related to Figure 2. Circulating monocytes do not contribute to Vhl-deficient AM phenotype. CD45.2 control *Vhl*$^{fl/fl}$ and CD11cΔ*Vhl* mice were surgically joined to a CD45.1 mouse in parabiosis. Thirty days after surgery, CD45.2 parabionts were analyzed. (A) Scheme of the procedure. (B, C) Representative flow cytometry plots (B) and frequencies of CD45.1$^+$ cells (C) in neutrophils (gated on CD11b$^+$Ly6G$^+$) and Ly6C^{hi} monocytes (gated on CD11b$^+$Ly6C^{hi}) from peripheral blood. (D, E) Representative flow cytometry plots (D) and frequencies of CD45.1$^+$ cells (E) in lung Ly6C^{hi} monocytes (gated on CD45$^+$ Siglec-F$^-$ CD11b$^+$ Ly6C^{hi}) and BAL AMs (gated on Siglec-F$^+$ CD11c$^+$). (C, E) Frequencies shown as mean ± s.e.m. of a pool of three independent experiments performed, where each dot represents an individual mouse (n=10-14 per genotype): ns, not significant (unpaired Student *t*-test).

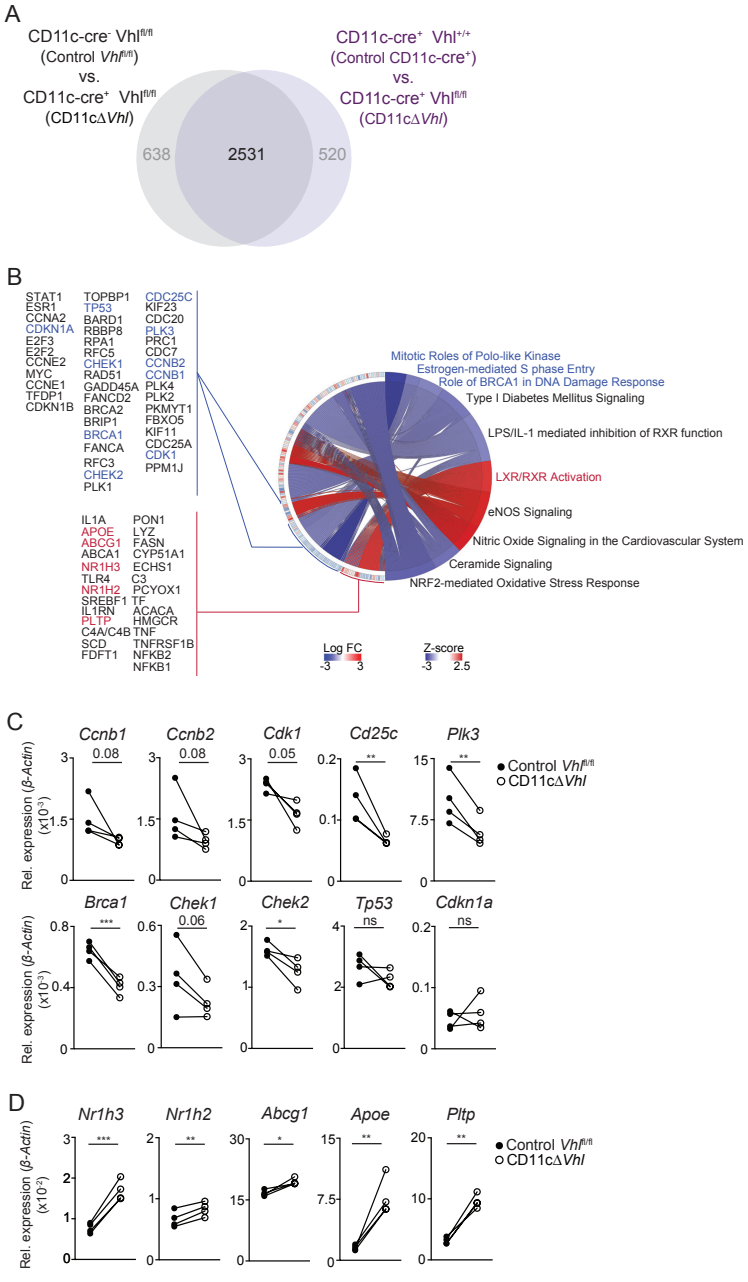

Figure S2, related to Figures 3 and 4. VHL-deficient AMs have an altered gene expression profile. (A) Venn diagram showing genes differentially expressed in CD11cΔ*Vhl* AMs versus control *Vhl*$^{fl/fl}$ AMs or control CD11c-cre^{+}. (B) Circular plot representing Ingenuity Pathway Analysis of differentially expressed genes from pathways with Z-score > |2| and p-value (-log (B-H p-value)) >2.5 in VHL-deficient AMs (CD11cΔ*Vhl*) versus control *Vhl*$^{fl/fl}$ AMs from BAL. Depicted genes correspond to cell-cycle-related (blue) and lipid-handling-related (red) pathways. (C,D) Quantitative PCR of selected differentially expressed genes related to cell cycle (C) and lipid

sensing (D), depicted in blue and red, respectively, in Figure S2B. ns, not significant; *p-value<0.05; **p-value<0.01; ***p-value<0.001 by ratio paired Student *t*-test.

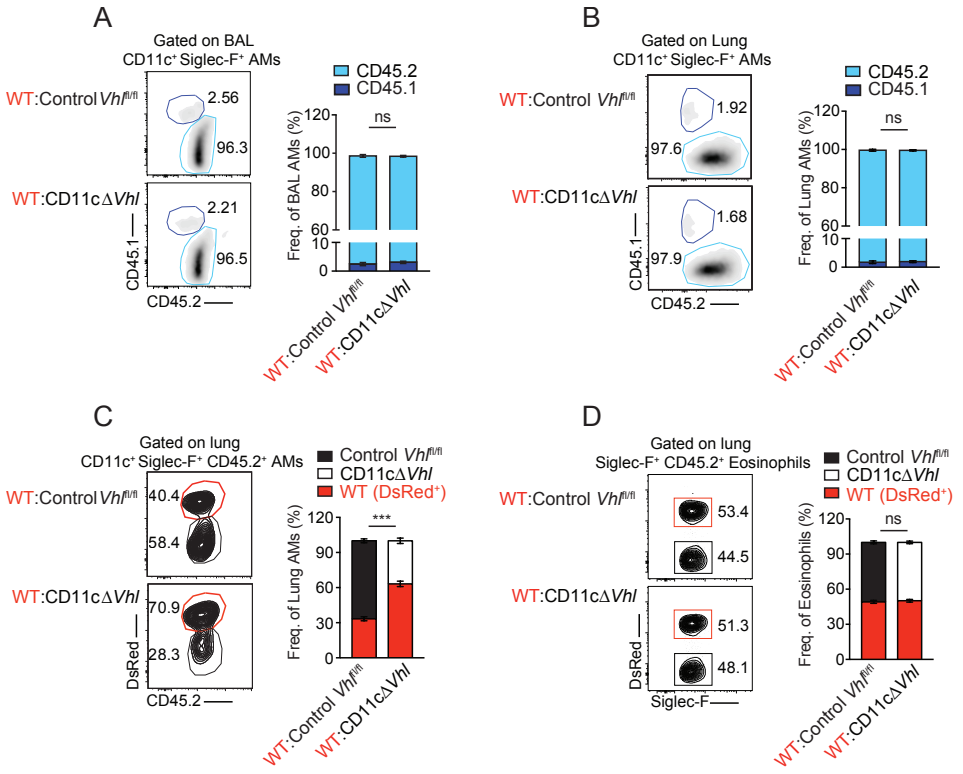

Figure S3, related to Figure 3. VHL-deficient AMs have a cell autonomous defect in lung reconstitution. (A-B) Representative flow cytometry plots and frequencies of host CD45.1$^+$ cells and donor CD45.2$^+$ cells in BAL AMs (A) and lung AMs (after BAL) (B) from BM chimeras. (C-D) Representative flow cytometry plots and frequencies of DsRed$^+$ (WT) and DsRed$^-$ (Control *Vhl*$^{fl/fl}$ or CD11cΔ*Vhl*) cells (normalized to blood Ly6Chi monocyte frequency in each mouse and genotype) in CD45.2$^+$ lung AMs (C) and lung eosinophils (D) from BM chimeras. Frequencies shown as mean ± s.e.m. of one experiment of three independent experiments performed (n=5-10 per genotype): ns, not significant; ***p-value<0.001 (ratio paired Student *t*-test)